GENERAL DECLASSIFICATION SCHEDULE

IN ACCORDANCE WITH

DOD 5200.1-R & EXECUTIVE ORDER 11652

REPORT No. 906

The Transition From A Turbulent To A Laminar Boundary Layer

JOSEPH STERNBERG

DEPARTMENT OF THE ARMY PROJECT No. 503-06-004
ORDNANCE RESEARCH AND DEVELOPMENT PROJECT No. TB3-0118

B A L L I S T I C R E S E A R C H L A B O R A T O R I E S

REPORT NO. 906

MAY 1954

THE TRANSITION FROM A TURBULENT TO A LAMINAR BOUNDARY LAYER

Joseph Sternberg

Department of the Army Project No. 503-06-004
Ordnance Research and Development Project No. TB3-0118

A B E R D E E N P R O V I N G G R O U N D, M A R Y L A N D

TABLE OF CONTENTS

[illegible] TO R[illegible] [illegible] LABORATORIES

REP[illegible] NO. [illegible]06

JSternberg/llr
Aberdeen Proving Ground, Md.
May 1954

[illegible] FROM A TURBULENT TO A LAMINAR BOUNDARY LAYER

ABSTRACT

The boundary layer on a 58° included angle cone-cylinder model has been studied over a range of supersonic speeds. Boundary layer recovery factors have been measured and shadowgraphs have been taken of the model in the wind tunnel and free flight. These measurements indicate that when the boundary layer ahead of the shoulder is turbulent, the boundary layer is laminar after the shoulder for a short distance. A theoretical model of the phenomenon has been constructed and calculations have been made using available boundary layer theory and experimental data to describe the course of the boundary layer from just ahead of the shoulder to the transition back to turbulent flow on the cylinder. Reasonably good agreement is found between the experiments and the calculations.

A distinction is made between the complete shear layer at a given position which results from the action of frictional forces all along the model surface from the model tip, and the boundary layer at the same position which may be all or only the inner portion of the complete shear layer.

A turbulence parameter analogous to Taylor's turbulence parameter for the effect of a turbulent free stream on laminar - turbulent transition, but applicable to a high speed boundary layer is obtained.

NOTATION

Re	=	Reynolds Number
r	=	$\frac{T_W - T_S}{T_0 - T_S}$ Recovery factor
r_L	=	Laminar recovery factor
r_T	=	Turbulent recovery factor
T_W	=	Wall temperature
T_S	=	Local free stream temperature
T_0	=	Stagnation temperature
P_0	=	Supply Section pressure
U	=	Mean velocity
S	=	Subscript referring to local free stream conditions
p	=	Static pressure
M	=	Mach Number
q	=	Dynamic pressure = $\frac{1}{2} \rho U^2$
ρ	=	Density
μ	=	Viscosity
ν	=	Kinematic viscosity
Pr	=	Prandtl Number
Re_{tr}	=	Transition Re defined as the beginning of the transition region

1 Refers to conditions just ahead of the corner

2 Refers to conditions just after the corner

y	=	Distance normal from the surface
δ	=	Boundary layer thickness

NOTATION

x = Coordinate in direction of motion

τ_w = Wall friction

$C_f = \frac{\tau_w}{q}$ = Local friction coefficient

$C_F = 2C_f$ = Average friction coefficient

U_τ = Friction velocity $= \sqrt{\frac{\tau_w}{\rho_w}}$

$g(M) = C_F\sqrt{\frac{Ux}{\nu}}$

u', v', w' = Root mean square turbulent fluctuation velocities in the x, y, z directions

a, b, c = Initial coordinates in the Lagrangian description

$E = \frac{u'^2}{2} + \frac{v'^2}{2} + \frac{w'^2}{2}$ = Turbulent kinetic energy

t = Time

u, v, w = Instantaneous fluctuation velocities

$\tilde{u}' = \sqrt{\frac{u'^2 + v'^2 + w'^2}{3}}$

$L_y = \int_0^\infty R_u dy$ = Integral scale of turbulence

R_u = Correlation coefficient $= \frac{\overline{u_1 u_2}}{u_1 u_2}$

$\overline{uv}$ = Time average of product of instantaneous values of u and v at a point

$\frac{\partial p'}{\partial x} = \sqrt{\left(\frac{\partial p}{\partial x}\right)^2}$ = Root mean square spatial pressure gradient

NOTATION

λ_x = Longitudinal microscale = $\left(\frac{\frac{2u'^2}{\partial u'}}{\partial x}\right)^2$

λ_y = Lateral microscale = $\left(\frac{\frac{2u'^2}{\partial u'}}{\partial y}\right)^2$

λ_η = Lagrangian microscale

$h(M)$ = $\frac{\theta}{\delta}$

θ = Boundary layer momentum thickness

U_{max} = Maximum velocity defect in a wake

y_0 = Half width of wake based on mean velocity distribution

D_{eff} = Equivalent cylinder diameter for a two-dimensional wake

Λ = Pohlhausen parameter = $\frac{-\delta^2}{\mu U}\frac{dP}{dx}$

M_{eff} = Mesh size used to produce a given isotropic turbulent flow

Re_T = Turbulence Reynolds Number defined as $Re_T = \frac{u' \times 2y_0}{\nu}$

Re_{cyl} = Equivalent cylinder Reynolds Number $\frac{U_\infty D_{eff}}{\nu}$

W = $\frac{U}{U_{t=\bar{\delta}}}$

t = Transformed y coordinate, $dt = \frac{1}{L}\frac{\rho_S}{\rho_0}dy$

$\bar{\delta}$ = Edge of boundary layer in coordinate t

υ_S = $\frac{U_S}{c}$

c = Velocity of efflux into a vacuum

s = Transformed x coordinate $ds = \frac{1}{LRe_0}\frac{P_S}{P_0}dx$

Re_0 = $\frac{Lc}{\nu}$

L = Characteristic Length of problem

FIGURES

17. Temperature Recovery Factors M = .55

Various Pres . . vels

18. Shadowgraph of New Laminar Boundary Layer

(a) on cone

(b) on cylinder

P_0 = 180 cm. - M = 3.02

19. Shadowgraph of 20° Cone Showing Wavy Laminar Boundary Layer

20. Shadowgraph of 20mm. Free Flight Cone Cylinder Model

21. Compressible Turbulent Boundary Layer Thickness

22. Effect of Corner on Turbulent Boundary Layer

23. New Laminar and Turbulent Boundary Layer Growth

24. Growth of Effective Wake

25. Effect of Corner on Laminar Boundary Layer

26. Old Shear Layer After Corner

27. Comparison of Estimated and Experimental Temperature

Recovery Factors on Cylinder

28. Low Speed Correlation Curve for Transition

by Strong Turbulence

29. Fluctuation Level Before and After Corner

30. Streamtube Contraction

31. Turbulence Levels and Microscales Along Cylinder

32. Turbulence Parameters Along Cylinder

33. Effect of Compressibility on Transition Turbulence Parameter

34. Laminar Boundary Layer within Laminar B.L.

35. Observed Boundary Layer Flows

INTRODUCTION

It has been generally believed that once a boundary layer becomes turbulent it remains turbulent. In the usual transition region, say of a boundary layer on a flat plate, an instantaneous picture might show laminar flow from the leading edge, a generally laminar region interspersed with "bursts" of turbulent fluid, and then finally, further downstream a fully developed turbulent boundary layer. In this case, the turbulent "bursts" remain turbulent as they move downstream and grow, enveloping the contiguous laminar regions. The fluid in the laminar patches between the "bursts" has been laminar from the leading edge. In this report, evidence will be presented which indicates that under suitable conditions a fully developed turbulent boundary layer can be converted into a laminar boundary layer. The transformation does not require the disappearance of the turbulent energy in the turbulent boundary layer. Rather, some of the turbulent fluid in the turbulent boundary layer becomes laminar in the same sense that some of the turbulent fluid in a wind tunnel airstream becomes laminar when there is a laminar boundary layer on the surface of a wind tunnel model.

The phenomenon of inverse transition was noticed accidentally. A 58° included angle cone-cylinder model was being used to study the effect of a sharp pressure gradient on the boundary layer temperature recovery factors. The idea was to produce reasonably well-defined laminar and turbulent boundary layers on the cone and then measure the equilibrium surface temperatures on the cylinder. We believed that the velocity and temperature distributions in the boundary layers would not be the familiar equilibrium ones and that the surface temperature would be thereby changed. It was thought that the deviation would be the greatest just after the shoulder of the model and that the usual equilibrium values would be approached asymptotically. With a smooth model surface, the boundary layer was laminar on the cone and became turbulent on the cylinder at different positions, depending on the tunnel pressure level. The surface temperatures on the cylinder were in general agreement with our expectations, rising in a normal way in the transition region on the cylinder. When transition on the cone was fixed by surface roughness, the temperatures on the cylinder followed a distinctly different

pattern. For a short distance along the cylinder, the surface temperatures were approximately constant and corresponded closely to the usual laminar levels after which the temperatures rose rapidly to values close to the usual turbulent levels.

After some unsuccessful attempts, shadowgraphs were obtained of the model. With surface roughness the fully developed turbulent boundary layer ahead of the shoulder was clearly visible. From the shoulder downstream, the turbulence that was visible in the boundary layer ahead of the shoulder seemed to disappear, or at least it was not distinguishable from the background of the picture. In the downstream region where the surface temperatures increased, a turbulent boundary layer was again visible.

This report presents the results of a study of the effects of the strong favorable pressure gradient at the shoulder of the cone-cylinder on both laminar and turbulent boundary layers.

EXPERIMENTAL ARRANGEMENT

The tests were conducted in the Ballistic Research Laboratories' Flexible Nozzle Tunnel shown in Figure 1. The tunnel is of the closed circuit variable density type so that data could be obtained over a range of Reynolds Numbers at each Mach Number as shown in the following table:

M	$\left(\frac{Re}{cm}\right)_{Max}$	$\left(\frac{Re}{cm}\right)_{Min}$
3.02	2.8×10^5	$.70 \times 10^5$
3.55	1.8×10^5	$.49 \times 10^5$

The test section at these Mach Numbers is 38 cm. wide by 33 cm. high, and the top and bottom walls of the test section are sloped to account for the boundary layer growth on the tunnel walls. The Mach Number and flow direction distributions along the axis of the tunnel, including the region used for these tests, are shown in Figure 2.

The cone cylinder model used for these tests is shown in Figure 3. Since it is necessary to know the surface Mach Number distribution in order to analyze the temperature data, a steel model with static pressure orifices along its length (see Figure 4) was tested at M = 3.02, the Mach Number at which most of the measurements were made. Figure 5 shows the comparison of the measured speed distribution along the cylinder and the surface Mach Numbers given in reference 1.

If, in calculating the recovery factor, an incorrect value for the local Mach Number is used, then the computed recovery factor will be in error. If the Mach Number used is too high, then the recovery factor will be high and vice versa. Since, at M $\approx$ 3, a .05 error is Mach Number only results in an error of .001 in r, the agreement in Figure 5 was considered good enough to use the calculations at the other test Mach Numbers. The calculated surface distribution for M = 3.55 is shown in Figure 6.

The construction of the lucite temperature recovery model is shown in Figure 3. Iron-Constantan thermocouple leads were attached to small lead plugs placed at regular intervals along the lucite body. Because the Mach Number is lower on the cone than on the cylinder, the level of the temperatures on the cone is higher than the level on the cylinder. Although the lucite is a moderately good insulator, the model thickness was reduced near the shoulder to reduce the heat transfer in the lucite from ahead of the shoulder to the cylinder. The spoked body supports, as well as the front portion of the strut, were also made of lucite. The interior of the model was filled with glass wool and the base was covered with lucite, except for a hole to take out the thermocouple leads and a vent hole to allow the internal pressure of the model to equalize with model base pressure.

The shadowgraphs were taken by placing a spark source close to the outside surface of one window at the test section, and the film against the other window. The spark source was developed by the Airflow Branch of the Exterior Ballistics Laboratory for taking free flight interferograms, and had high intensity coupled with short duration. At these high Mach Numbers,

a short duration spark is necessary since the characteristic pattern of the turbulence in the boundary layer sweeps by with almost the free stream velocity. Presumably, the shadowgraph will include the optical contribution of the turbulent boundary layers on the windows as well as the boundary layer on the model. To reduce the interference of the window boundary layers, the light source and the film were placed close to the outside of each of the test section windows as suggested by Professor L. S. G. Kovasznay of Johns Hopkins University.

TEMPERATURE RECOVERY FACTORS

Probably the most reliable information on the boundary layer recovery factors in the transition region has been obtained on cones.[25, 26] Figure 7 shows some of these data taken from two different wind tunnels at various Mach Numbers. As can be seen from the figure, the recovery factors rise from about .845 where the boundary layer is laminar, to turbulent values of about .88. The curves shown cover a wide range of transition Reynolds Numbers, presumably due to differences in the disturbance levels in the various wind tunnels. As with skin friction transition curves, when the transition starts earlier, the transition region on a logarithmic scale tends to be longer.

SMOOTH MODEL RESULTS

For the 58° cone cylinder in the smooth condition, that is with no turbulence promoters on the cone, the boundary layer was laminar on the cone and for various distances along the cylinder. Figures 8 and 9 are shadowgraphs at a supply pressure of 140 cm; the boundary layer is laminar on the cone and undergoes transition on the cylinder at about 20 cm. from the shoulder. Several features of the temperature data shown in Figure 10 are of particular interest. The temperature level for the first six plugs is approximately the same, but a systematic decrease can be observed as the shoulder is approached and the temperature just ahead of the shoulder is considerably less than the others. On the cylinder, the temperatures apparently rise towards an asymptotic value well back on the cylinder. The temperatures within one or two

centimeters of the shoulder fall above the curve that represents the most natural extrapolation upstream of the temperature data. The temperature fall off ahead of the shoulder and the higher values just behind the shoulder are believed to be the result of heat transfer in the lucite itself. since the lucite necessarily must have a continuous temperature distribution. The same data are shown as recovery factors in Figure 11. The recovery factors are lower than the normal laminar values after the shoulder, rise smoothly towards an asymptotic value, until there is an abrupt rise at the onset of transition on the cylinder. At first it was thought that heat transfer effects in the vicinity of the shoulder might be responsible for the low temperatures after the shoulder. Since the base of the cone is cooled by heat transfer to the front of the cylinder, there must be heat transfer from the boundary layer ahead of the shoulder to the cone surface. After the corner, the boundary layer would have an energy deficiency which would result in low recovery temperatures. However, if it is assumed that the heat flow can be mainly accounted for by two mechanisms; heat transfer between the model and the air, and heat flow within the shell, (heat flow to the air within the model is neglected), then, since the model is at equilibrium temperature at all points, heat flow out to the air ahead of the shoulder should be balanced by heat flow back to the air after the shoulder so that the heat flow in the lucite should not cause an energy deficiency in the boundary layer on the cylinder. The heat flow out of and back into the boundary layer would be expected to have some influence on the temperature distribution, and so the recovery temperatures. Heat flow estimates in the lucite indicate that these heat transfer effects should be negligible 2.5 cm. from the shoulder at P_0 = 140 cm.

The laminar recovery factors on the cone are in good agreement with the data shown in Figure 7. In the initial tests, a great deal of difficulty was experienced in repeating the recovery factor levels. Finally, it was noticed that when the supply temperature as measured by five thermocouples distributed over the center of the supply header, was above room temperature, the recovery temperatures were lower than expected, and vice versa. Surveys of the flow in the tunnel contraction section showed strong separation so that it was likely that the air in the center of the header was not the air that passed over the

model. The correlation with supply temperature could be explained if it was assumed that the air temperature was some value between that in the center of the header and the room temperature. Until the contraction section was rebuilt, the tests were run with the supply temperature set within 1° of the room temperature.

TRANSITION FIXED ON THE CONE

Several methods were tried for tripping the boundary layer on the cone, such as lampblack and sand. However, for ease in running alternately, in the smooth and tripped condition, easily removable single wire trips were used. In these tests the wire size necessary for causing turbulence in the vicinity of the wire was larger than has been found for low-speed measurements. For instance, at a Mach Number of 3.55, at an equivalent flat plate Reynolds Number of 2.15×10^5, a wire five times as large as the boundary layer displacement thickness at the wire did not cause transition anywhere on the cone surface. According to Dryden,[2] at low speeds at the same Reynolds Number a single roughness element .8 of the boundary layer displacement thickness would be sufficient to cause transition at the element.

The use of wire trips disclosed some very interesting variations of the boundary layer recovery temperature as influenced by the size of the wire trip used. While these variations are of interest themselves and should be the subject for another investigation, they are undesirable for this investigation and it was necessary to use wire sizes for which they were not present. Figure 12 presents surface temperature data at the same Mach Number and Reynolds Number, but for different wire sizes. Shadowgraphs for these three cases are shown in Figure 13. The smallest wire size, .025 cm., produces very limited regions of separation ahead of and behind the wire and transition occurs about halfway between the wire and the model shoulder. For the median wire size, transition starts a short distance downstream of the wire and again the separation regions ahead of and behind the wire are relatively limited. For the largest wire size, separation of the boundary layer occurs well ahead of the wire and transition occurs at the wire. There is a sharp rise in the surface temperature ahead of the wire, and a sharp decrease after the wire. If the

boundary of the model followed the shape of the separated region, the surface temperatures would be expected to vary as they do because of the changes in surface Mach Number. However, the temperatures in the fully-developed turbulent region on the cone are low, and they remain low all the way back on the cylinder, only gradually approaching the temperature data with the smaller wire trips. Static pressure measurements along the model surface for two wire trips, both of which caused transition, are compared with the smooth model static pressure distribution in Figure 14. The temperature data indicated that the .064 cm. dia. wire was too large to be satisfactory, (see Figure 12). The pressure changes in the separated region ahead of and downstream of the wire trips are consistent with the flow photographs. Of more interest is the fact that the surface pressures near the base of the cone are only slightly altered by the wire trips. However, the pressure model was also fitted with two sets of three total head tubes, one positioned near the base of the cone, and one placed well downstream on the cylinder. (See Figure 4). The total pressure tubes near the cone surface showed a loss in total pressure, presumably a result of the shock wave system associated with the flow about the wire trip. For the .025 cm. trip, the Mach Number decreased by about .06 M at the cone base, so that using the smooth cone surface Mach Number for calculating the recovery factor should have resulted in the computed r being too high by .005. The Mach Number decrease at the cone base is the largest with the .062 cm. wire trip, and as Figure 12 shows, the computed recovery factors are lowered rather than raised. The greatest Mach Number changes on the cylinder produced by the wire trips, as evaluated from the static pressure measurements along the cylinder and the total pressure measurements near the cylinder surface, would have a negligible influence on the recovery factor computations. Evidently, the Mach Number changes introduced by the large wire trips cannot account for the effect of wire size on the temperature data. Possibly, there is some redistribution or extraction of energy involved in the flow changes in the vicinity of the wire which persists for a very large number of boundary layer thicknesses. With a two-wire trip, the effect is even more pronounced. On the basis of these experiments, wire sizes were established, which as far as surface temperatures were concerned, produced equilibrium fully-developed turbulent boundary layers just ahead of the shoulder.

A comparison of the recovery factors for the smooth model, and one case where the boundary layer was turbulent ahead of the shoulder is shown in Figure 11. Shadowgraphs of the flow along the cylinder, for the latter case, show clearly that the boundary layer is turbulent from about 8 cm. from the model shoulder to the model base. See Figure 15. Also, the recovery factors in the same region are close to the normal levels. On the other hand, for about 2.5 cm. after the shoulder, the recovery factors appear to be at the laminar levels. Figure 16, which contains data for tripped boundary layers obtained over a range of Reynolds Numbers, shows that the data at various pressure levels have the same features. Similar measurements at M = 3.55 are shown in Figure 17. At P_0 = 100 cm., the recovery factors appear to conform to laminar values for about 7.5 cm. from the shoulder. The beginning of the temperature "transition" region on the cylinder is difficult to pinpoint because of the relative scarcity of the temperature measuring positions. At any rate, it would appear to be more than 2.5 cm. from the shoulder in Figures 16 and 17.

Photographic evidence proved to be difficult to obtain; Figure 18 represents the best shadowgraph obtained in the wind tunnel. The following observations can be made. The turbulence in the boundary layer ahead of the shoulder appears to disappear in the expansion at the shoulder. A diffuse white line, sometimes wavy in appearance, can be seen a short distance from the shoulder, and then turbulence in the boundary layer appears over a range of positions which agree with the region labeled "transition" based on the temperature measurements. Other wavy laminar boundary layers, just prior to transition to turbulence, have been observed under conditions where the laminar boundary layer was much thicker, as in Figure 19.

One difficulty with getting good quality wind tunnel shadowgraphs is the fact that the density in the test section is low. A "ring" was machined on the nose of a 20mm cone-cylinder model for which the free flight Reynolds Number corresponded to one of the wind tunnel Reynolds Numbers, and the model was fired in the Ballistic Research Laboratories Aerodynamic Range.* Figure 20

* The firing was carried out under the supervision of L. C. McAllister.

is a shadowgraph of the free flight model. Because of the model motion, the turbulent region ahead of the shoulder is more difficult to distinguish; however, the ring size chosen, scaled appropriately, was more than sufficient to cause transition at the ring in the wind tunnel. Just after the shoulder there is the characteristic white line of the laminar boundary layer before the appearance of turbulence. There is another feature in this photograph which suggests that the boundary layer is laminar. It has been observed in many free flight shadowgraphs that even for highly polished models, (the cylinder of the 20mm model was polished), where the boundary layer is turbulent, there is a disturbed pattern in the surrounding flow field, limited on the upstream end by the Mach wave from the beginning of the turbulent boundary layer. This disturbed pattern has been assumed to be a sound field originating from the turbulent boundary layer. In Figure 20, such a pattern is visible behind the ring on the cone, (Mach waves are also visible; they are present because the model surface between the ring and the shoulder was not polished), and in the flow field around the cylinder. The Mach wave defining the leading edge of this region, about the cylinder, extended to the model surface, clearly intersects the model downstream of the shoulder in the region identified as "transition" on the cylinder.

ANALYSIS

These experimental results can be explained in the following way.

The turbulent boundary layer is known to have a thin region near the surface, which is identified as the laminar sub-layer, where the direct viscous terms are predominant. Measurements of the turbulent velocity fluctuation level through the turbulent boundary layer show that a peak in the turbulence level is reached at the edge of the laminar sub-layer. This high disturbance level apparently prevents the laminar sub-layer from growing, so that the Reynolds Number based on the thickness of the laminar sub-layer is invariant.

The sharp pressure drop at the model shoulder produces a large increase in velocity of the boundary layer fluid. Even near the surface, the air is accelerated to supersonic speeds. The effect of the velocity increase on the turbulence level throughout the boundary layer is similar to the reduction in turbulence level accomplished by the contraction section of a wind tunnel. At the beginning of the cylinder, the air that comprised the turbulent boundary layer ahead of the shoulder is the non-uniform, fairly turbulent "free stream" for a new laminar boundary layer growing from the beginning of the cylinder. The reduction in the turbulence level of the boundary layer fluid produced by the pressure drop permits the growth of the laminar shear layer from the model surface. Compared to the usual wind tunnel flow, the turbulence level of this new "free stream" is high, and so a transition of the new laminar boundary layer to a turbulent boundary layer would be expected to occur at relatively low Reynolds Numbers based on distances along the cylinder from the shoulder. The only turbulent fluid which becomes laminar is the fluid in the new laminar boundary layer, the same process that occurs in the laminar boundary layer on a model in the usual wind tunnel, since the wind tunnel air is turbulent.

A similar acceleration takes place when there is a laminar boundary layer ahead of the corner. The laminar shear flow at the beginning of the cylinder may be considered to be a new "free stream" for a new laminar boundary layer growing from the shoulder. The evaluation of the temperature recovery factors along the cylinder must take into account the fact that the boundary layer velocity and temperature distributions differ importantly from the velocity and temperature distributions for a boundary layer on a constant pressure surface. (The gradual pressure rise along the cylinder will be neglected in the computations.)

In the following sections, estimates will be made for the boundary layer conditions on the cylinder for both a laminar and a turbulent boundary layer at the base of the cone. For the case where the boundary layer at the cone base is turbulent, the properties of the turbulence in the new "free stream" on the cylinder will be examined to see what can be established about the probable state, laminar or turbulent, of the new boundary layer starting from the beginning of the cylinder.

At a number of points in the analysis, it will be necessary to use low-speed data because of the limited nature of supersonic information.

(a) Turbulence field in supersonic boundary layer.

Recently, Kovasznay[3] has made exploratory velocity and temperature fluctuation level measurements in a supersonic boundary layer. He found, in addition to the velocity fluctuation field, that adjacent fluid masses in the boundary layer have unequal stagnation temperatures; i.e. a "turbulent" temperature field in an Eulerian system. The more voluminous low-speed data are used in the analysis, but a comparison of Kovasznay's fluctuation levels and the fluctuation levels obtained from the low-speed measurements will be made.

(b) Mean and turbulent properties of two-dimensional supersonic wakes.

The author was unable to find any suitable supersonic data, so low-speed data have been used exclusively.

(c) Influence of the free stream turbulence on laminar turbulent transition at supersonic speeds.

The available information in the literature on the role of the turbulence of the free stream on the state of the boundary layer is for free streams with isotropic turbulence. When the boundary layer is turbulent at the base of the cone, the "free stream" at the beginning of the cylinder will be anisotropic. To represent the "free stream" conditions from the beginning of the cylinder, this anisotropic field will be represented by an equivalent isotropic field by using an average fluctuation level $\tilde{u}'$ and a turbulence microscale based on isotropic relations. Along the cylinder, turbulence in the "free stream" should approach isotropy. As will be seen, the interpretation of the results is not sensitive to the engineering approximations that are made.

An existing solution for the compressible laminar boundary layer will be used to estimate the effect of free stream turbulence on the laminar turbulent transition at supersonic speeds.

To avoid confusion in the calculations, the following notation will be adopted. The free stream Mach number distribution along the cone-cylinder corresponding to the static pressure distribution will be designated as M_S. The recovery factor r is the recovery factor computed using the measured surface temperature T_S, the Mach number M_S, and the wind tunnel stagnation temperature T_0, as follows.

$$r = 1 - \frac{T_0 - T_S}{T_0}\left[\frac{1 + .2M_S^2}{.2M_S^2}\right]$$

As a new boundary layer grows along the cylinder, its edge at any axial position is at some Mach Number less than M_S. At any axial position the value of this "effective" free stream Mach Number will depend on the new boundary layer thickness at that position and the properties of the "free stream" flow. Primes will be used to identify the conditions at the edge of the "new" boundary layers. Hence, r' would be obtained as follows.

$$r' = 1 - \frac{T_0' - T_S}{T_0'}\left[\frac{1 + .2M_S'^2}{.2M_S'^2}\right]$$

T_0' = stagnation temperature of flow at edge of "new" boundary layer

M_S' = Mach Number at edge of "new" boundary layer

T_S = Surface temperature

r_L' = Laminar recovery factor = .85

r_T' = Turbulent recovery factor = .88

While T_0' and M_S' are insufficient to establish properly the temperature recovery factors along the cylinder, the above expression is considered to be a useful approximation.

As shown in Figures 16 and 17, the temperature data at different pressure levels all had the same general characteristics. The numerical calculations that are made in the following sections are for a supply pressure P_0 = 180 cm. at M = 3.02, which is considered to be a representative test condition. Data for a turbulent boundary layer at the cone base are for a .041 cm. boundary layer trip.

TURBULENT BOUNDARY LAYER AT BASE OF CONE

The shadowgraphs indicate that the boundary layer with the .041 cm. trip is turbulent for about 40 boundary layer thicknesses before it reaches the cone base. At low speeds, Klebanoff and Diehl[4] found that badly disturbed turbulent boundary layers had re-established the equilibrium or constant pressure surface velocity profiles and turbulent fields after traveling $\approx$ 30 boundary layer thicknesses. Further evidence that equilibrium conditions are closely approached, if not reached, at the cone base is the fact that the temperature recovery measurements near the cone base correspond to those shown in Figure 7. Available measurements indicate that the velocity profiles in supersonic boundary layers are similar to those in low-speed boundary layers, provided the Reynolds Numbers are comparable. It is therefore assumed that the boundary layer velocity can be represented as:

$$\frac{U}{U_S} = \left(\frac{Y}{\delta}\right)^{1/7}$$

Since transition is produced by a roughness element, it is not possible to compute the boundary layer thickness at the cone base. The shadowgraphs show, as would be expected, different apparent boundary layer thicknesses for different size roughness elements, at different pressure levels, and different Mach Numbers.

A large fraction of the turbulent boundary layer has an intermittent character, which is three-dimensional in nature. Low-speed measurements[5,6] show that there is a sharp boundary between the turbulent fluid in the boundary layer near the wall and the main flow. This boundary is irregular and in

a typical case may extend from $\frac{y}{\delta} = .4$ to $\frac{y}{\delta} = 1.2$, with a mean position at $\frac{y}{\delta} = .78$, where δ is the conventionally defined boundary layer thickness. In one case, a wave length from peak to peak of the turbulent boundary of 2δ was observed using hot-wire equipment.

The shadowgraphs at high speed of turbulent boundary layers and wakes show the same sharp boundary between the turbulent and apparently non-turbulent fluid. The strong optical effect is presumed to be due to the temperature spottiness of the turbulent fluid. Since the path length of the light rays in the boundary layer is usually several boundary layer thicknesses, the shadowgraphs do not show the large variations in the position of the edge of the turbulent boundary layer that are found in the low-speed measurements. However, the boundary has a sharply irregular appearance. If the path length of the light through the boundary layer was very large compared to δ, then it could be argued that the boundary in the shadowgraph should represent 1.2δ. This requirement is not fulfilled for the test model, and since peak excursions of the turbulent fluid may not be at the top cone element, it is difficult to establish, with any precision, the boundary layer thicknesses from the shadowgraphs. On the other hand, it seems reasonable to believe that the photographic boundary lies somewhere between $.78\delta$ and 1.2δ. The simplest assumption is to set the apparent thickness on the photographs equal to δ.

An appropriate picture of the boundary layer velocity and temperature profiles can be obtained by relating the local friction coefficient to the boundary layer thickness. For a compressible boundary layer with zero axial pressure gradient, we have $\tau_w = \rho_s U_s^2 \frac{d\theta}{dx}$ or $\frac{C_{f_c}}{2} = \frac{d\theta}{dx}$ where C_{f_c} is the local friction coefficient.

Now, for incompressible fluids, in the range of Reynolds Numbers where the velocity profile can be represented by a 1/7th power law, we can express the local friction coefficient in terms of the length Reynolds Number as follows:

$$C_f = \frac{.0577}{Re_x^{1/5}}$$

Recently, a number of experiments have been performed at supersonic speeds, in which the local friction coefficient has been compared with the incompressible local friction coefficient at the same Reynolds Number. The compressible local friction coefficient can be represented as follows:

$$C_{f_c} = \frac{.0577}{Re_x^{1/5}} \quad f(M)$$

where f(M) is given, for instance, in NACA TN 2305, p. 29.

Then $\frac{d\theta}{dx} = \frac{.0288}{Re_x^{1/5}} f(M)$ or $\frac{\theta}{x} = \frac{.036}{Re_x^{1/5}} f(M)$

To compare $\frac{\delta_c}{x}$ compressible and $\frac{\delta_{inc}}{x}$ incompressible at the same x Reynolds Number, the ration $\frac{\theta}{\delta}$ is required. Assuming the Prandtl Number equals 1, and no heat transfer at the surface, it can be shown that

$$\frac{\theta}{\delta} \int_0^1 \frac{F(\eta)\left[1 - F(\eta)\right]}{1 + \frac{\gamma-1}{2} M_S^2 \left[1 - F^2(\eta)\right]} d\eta \qquad F(\eta) = \frac{U}{U_S}$$

Convenient tabulations of the value of this ratio for various Mach Numbers and various power law representations of the velocity distribution are given in NACA TN 2337. If $\frac{\theta}{\delta} = G(M)$

then $\frac{\delta_c}{x} = \frac{\delta_{inc}}{x} \quad \frac{G(M=0)}{G(M)} f(M)$

The factor $\frac{G(M=0)}{G(M)} f(M)$ is shown in Figure 21, and it appears that for a given free stream Reynolds Number, the ration $\frac{\delta}{x}$ varies less than 5% with Mach Number. Approximately, then $\delta_c = \delta_{inc}$, and

$$C_{f_c} = \frac{.045\ f(M)}{Re_{\delta_c}^{1/4}}$$

Measurement of the shadow graph gives δ = .08 cm. at the base of the cone, so that $Re_\delta = 1.9 \times 10^4$ $\quad C_f(M_S = 1.89) = 2.9 \times 10^{-3}$

Using the measured wall temperatures, $\frac{T_W}{T_S} = 1.63$

so that $U_\tau = 2.43 \times 10^3$ cm/sec

where $U_\tau = \sqrt{\frac{\tau_w}{\rho_w}}$ the friction velocity.
Finally, at the wall $\left(\frac{\partial U}{\partial y}\right)_w = 1.20 \text{ sec}^{-1}$

The extent of the laminar sub-layer is a matter of definition. Some authors choose $\frac{U_\tau y}{\nu} = 10$ as the edge of the layer since that is where the direct viscous stress and the turbulent shear stress are approximately equal. Others choose $\frac{U_\tau y}{\nu} = 30$, where the direct viscous stress is negligible and the mean velocity profile starts to follow the logarithmic law. From the wall to $\frac{U_\tau y}{\nu} = 10$ the velocity profile is linear and the region $\frac{U_\tau y}{\nu} = 10$ to $\frac{U_\tau y}{\nu} = 30$ represents a transition region to a logarithmic mean velocity profile. The construction of the desired velocity profile was simplified as follows: $U = ky$ near the wall where $\left(\frac{\partial U}{\partial y}\right)_w = 1.20 \text{ sec}^{-1}$ $\frac{U}{U_S} = \left(\frac{y}{\delta}\right)^{1/7}$ for the rest of the boundary layer.

The linear variation of U with y was continued until the profile based on the 1/7th power law was intersected so that no attempt was made to introduce the correct distribution for the intermediate region where the laminar shearing stresses and the turbulent shearing stresses are both important. Figure 22 shows the Mach Number distribution assuming Pr = 1. (Because of this assumption, the Mach Numbers near the wall are a few per cent in error.)

The fact that the acceleration of the flow around the corner occurs in a relatively short distance makes possible a simple computation of the boundary layer profile after the expansion. The momentum equation for the x direction of the low-speed turbulent boundary layer may be written as

$$\rho\left(U\frac{\partial U}{\partial x} + V\frac{\partial U}{\partial y}\right) = \frac{\partial}{\partial y}\left[\mu\frac{\partial U}{\partial y} + \rho\overline{uv}\right] - \frac{\partial P_S}{\partial x}$$

where $\mu\frac{\partial U}{\partial y}$ is the laminar shearing stress and $\rho\overline{uv}$ is the Reynolds shear stress, and the forces are expressed as forces per unit mass of the fluid. The shear stress is a maximum at the wall, and decreases steadily through the boundary layer to close to zero at $y = \delta$.

Then, approximately, the viscous force per unit mass of the boundary layer fluid is $\frac{\tau_W}{\rho\delta}$. In a typical turbulent boundary layer $\delta \frac{\overline{uv}}{u'v'} \approx .5$ from the wall to $\frac{y}{\delta} \approx .8$, falling off rapidly to zero between $\frac{y}{\delta} = .8$ and $\frac{y}{\delta} = 1.2$ (the maximum extent of the turbulent spikes). The effect of the acceleration at the corner on the correlation coefficient $\frac{\overline{uv}}{u'v'}$ is not known. It will develop in a later section that the product u'v' after the corner is reduced to about .42 of its value ahead of the corner, so that even if $\frac{\overline{uv}}{u'v'}$ after the corner was increased to the maximum possible value of one, the average $\overline{uv}$ would be reduced in the pressure drop at the shoulder. Since the turbulent boundary layer thickness increases almost by a factor of 3, (See Page 28) it appears that $\frac{\tau_W}{\rho\delta}$ throughout the turbulent boundary layer will be a maximum just before the acceleration.

Referring to the x momentum equation for the boundary layer, for a very rapid and substantial acceleration the term $\frac{1}{\rho}\frac{\partial P_S}{\partial x}$, which is the pressure force per unit mass of the boundary layer fluid, may be very large compared to $\frac{\tau_W}{\rho\delta}$. If $\frac{\tau_W}{\rho\delta}$ can be neglected compared with $\frac{1}{\rho}\frac{\partial P_S}{\partial x}$, then the Mach number profile after the corner can be obtained in a simple way. The relative influence of the viscous and pressure terms can be evaluated by considering their contribution to the change in kinetic energy per unit mass of the boundary layer fluid in the acceleration at the shoulder. The acceleration length is greatest for the outer streamlines, where it may be from 5 to 10 δ, but small for the inner regions, where it should be of the order of δ. Taking the acceleration length as δ, Δ K.E.$_V$ due to Viscous Forces $\approx \frac{\tau_W}{\rho\delta} \times \delta \approx \frac{\tau_W}{\rho}$

$$\Delta \text{ K.E.}_P \text{ due to Pressure Forces} \approx \frac{\Delta P_S}{\rho}$$

For an increase in Mach number from 1.89 to 3.13

$$\frac{\Delta P_S}{q_{M=1.89}} \approx .34 \quad \text{so} \quad \frac{\Delta \text{K.E.}_V}{\Delta \text{K.E.}_P} \approx 3 \left(\frac{\tau_W}{q}\right)_{M=1.89}$$

But $\frac{\tau_w}{q} = C_f \approx 3 \times 10^{-3}$ so that over most of the boundary layer the viscous forces can be neglected.

The Mach Number for each streamtube after the expansion can then be easily computed from the Mach Number of the streamtube ahead of the corner, assuming that the flow in each streamtube goes isentropically from P_{S_1} to P_{S_2}. The dependence of the Mach Number on the distance from the wall after the acceleration is obtained by a numerical step by step calculation for the boundary layer mass flow from the wall. Figure 22 shows the results of these computations. The air that was almost stationary ahead of the shoulder, adjacent to the wall, is accelerated to almost M = 2 after the shoulder. Of course the conditions right in the vicinity of the wall are not properly represented by the approximation, since the viscous forces there cannot be neglected. At the wall, the momentum equation reduces to $\frac{\partial P_S}{\partial x} = \frac{\partial}{\partial y}\left[\mu \frac{\partial U}{\partial y}\right]$ and for the real flow the Mach Number will drop rapidly to zero in a narrow region near the wall.

The expansion of the streamtubes results in an increase of the boundary layer thickness δ from δ = .08 cm. to δ = .23 cm.

The boundary layer fluid at the beginning of the cylinder can be viewed as a "new" free stream for the development of a new boundary layer downstream from the shoulder. Its Mach Number ranges from M = 2 at the wall, to M = 3.13 at δ = .23 cm., beyond which distance the free stream is approximately uniform. This "new" free stream should not retain the Mach Number distribution which has been calculated for the start of the cylinder. Turbulent mixing should alter the Mach Number distribution and should cause a spread of the mixing region into the uniform outer flow. If the shear along the cylinder surface were zero, then the turbulent mixing region would correspond to half of a two-dimensional turbulent wake. Presumably, the Mach Number distribution which has been computed for the flow after the corner would approach the equilibrium distribution for a turbulent wake. In the real flow, the existence of shear at the wall requires the growth of a new shear layer starting at the shoulder which could be either a new laminar boundary layer or a new turbulent boundary layer. The

growth and properties, such as temperature distribution, of either of these new boundary layers is complicated by (a) the variable Mach Number distribution of the free stream, and (b) the variable stagnation enthalpy of the free stream.

There is a redistribution of the stagnation enthalpy in the boundary layer fluid ahead of the corner, with a decrease near the wall and a compensating increase in the outer region of the boundary layer. The mixing after the turn may cause a further change in the enthalpy distribution. The new boundary layer growth will be estimated in two different "free streams".

1. The boundary layer Mach Number distribution as calculated for the beginning of the cylinder. (See Figure 22.) This "free stream" will remain unchanged along the cylinder.

2. A two-dimensional wake with the model surface corresponding to the center. The wake width will increase and the speed defect near the surface will decrease with increasing distance along the cylinder.

EQUIVALENT TWO-DIMENSIONAL WAKE

First it will be assumed that friction at the model surface is zero, so that the model surface corresponds to the wake center. The influence of friction at the wall can be separately evaluated. The asymptotic representation for the mean velocity distribution in a two-dimensional wake[7] is $\frac{U}{U_{max}} = \left[1 - \left(\frac{y}{y_0}\right)^{3/2}\right]^2$ where U_{max} is the maximum velocity deflect occuring at the wake center and y_0 equals half of the wake width as defined by the above equation.

The two conditions necessary to obtain U_{max} and y_0 at the beginning of the cylinder are chosen so that the wake and the boundary layer are equivalent. Since the momentum of a wake does not vary with distance downstream, the momentum defect of the wake is set equal to the momentum defect of the boundary layer,

$$\rho_S U_S^2 \theta_{B.L.} = \rho_S U_S^2 \theta_W \qquad \left(\frac{\theta}{\delta}\right)_{B.L.} = .029$$

$$\left(\frac{\theta}{y_0}\right)_W = \frac{U_{max}}{U_S} \times .45$$

It also seems reasonable to set the total mass of fluid in the equivalent wake equal to the mass of fluid in the boundary layer,

$$\rho_S U_S \left[\delta_{B.L.} - \delta^*_{B.L.}\right] = \rho_S U_S \left[y_{0_W} - y_{0_W}^*\right] \qquad \left(\frac{\delta^*}{\delta}\right)_{B.L.} = .153$$

$$\left(\frac{y_0^*}{y_0}\right)_W = \frac{U_{max}}{U_S} \times .45 \ .$$

The equation for the displacement thickness δ^*, for $P_r = 1$ and zero heat transfer is

$$\frac{\delta^*}{\delta} = \int_0^1 \left\{1 - \frac{F(\eta)}{1 + \frac{\gamma-1}{2} M_S^2 \left[1 - F^2(\eta)\right]}\right\} .$$

Using these two equations, and numerically evaluating the integrals for θ_W and δ^*_W, $\frac{U_{max}}{U_S}$ and y_0 can be found in terms of $\theta_{B.L.}$ and $\delta^*_{B.L.}$.

For the equivalent wake at the beginning of the cylinder,

$$\frac{U_{max}}{U_0} = .084 \quad \text{and} \quad y_0 = .99\ \delta_{B.L.}$$

To calculate the downstream development of this equivalent wake it is necessary to obtain an effective starting distance. From Goldstein,[7]

$$\frac{U_{max}}{U_S} = \frac{1}{7.7 \times 10^{-1}} \times \frac{y_0}{x}$$

Hence, an effective starting distance is x = 3.5 cm. along an equivalent cylinder.

Townsend[8] has measured the turbulence in a low-speed two-dimensional wake and has found that the turbulence Reynolds Number $Re_T \approx \frac{1}{3} Re_{cyl}$ where $Re_{cyl} = \frac{U_S D_{eff}}{\nu}$ D_{eff} = cylinder diameter and $Re_T = \frac{u' \times 2y_0}{\nu}$

For a distance from the cylinder of about 100 cylinder diameters, $\frac{u}{U_{max}} \approx .3$ independent of the Reynolds Number. Setting $Re_x = \frac{1}{3} Re_{cyl}$ results in $D_{eff} = 3.4 \times 10^{-2}$ cm. or $\frac{x}{D_{eff}} \approx 100$ diameters. These calculations suggest that the flow would not closely approach the wake distribution in one or two cm. Hence, the mean flow distribution probably lies between the boundary layer distribution at the beginning of the cylinder and the wake profile.

The effective wake width would increase, proceeding downstream, proportional to $x^{1/2}$, where x = 3.5 cm. plus the distance from the shoulder.

GROWTH OF NEW LAMINAR BOUNDARY LAYER

The supersonic laminar boundary layer on a flat plate grows according to the following law.

$$\frac{d\delta}{dx} = \frac{1}{\delta} \quad \frac{g^2(M_S)}{\frac{U_S}{\nu_S} h^2(M_S)\delta} \qquad \text{where } \frac{\theta}{\delta} = h(M_S) \qquad \text{and } C_F\sqrt{\frac{U_S x}{\nu_S}} = g(M_S)$$

As an engineering approximation, the boundary layer growth was numerically computed, step by step, using appropriate values of $g(M_S')^2$ and $h(M_S')$ at each step of the process, for the Mach Number distribution of the boundary layer after the corner and for the equivalent wake Mach Number distribution along the cylinder.

There was little difference between the results for the boundary layer and wake distributions, so that apparently a knowledge of the exact Mach Number distribution of the "free stream" is not necessary. The new laminar boundary layer growth in the equivalent wake is shown in Figure 23.

The estimates for the development of the wake "free stream" along the cylinder have been made with the friction at the surface of the cylinder set equal to zero. As a new laminar or turbulent boundary layer grows from the beginning of the cylinder, the "free stream" fluid is consumed so that the

momentum defect of the wake "free stream" is steadily decreased and its development should be altered. The following calculations made for conditions 4.5 cm. from the shoulder indicate that as far as the calculation for the growth of the new laminar boundary layer is concerned, there is little error in using the mean velocity distribution for the wake "free stream" obtained by setting the surface friction equal to zero.

At $x = 4.5$ cm. the wake "free stream" width $y_0 = 3.45 \times 10^{-3}$ cm. and the new laminar boundary layer thickness $\delta \approx .2y_0$.

At $x = 4.5$ cm. a new equivalent wake is determined by considering the edge of the new laminar boundary layer to be the center of the new equivalent wake and by equating the momentum defect and mass flow for the new equivalent wake y_0' and the truncated wake from $y = \delta$ to $y = y_0$ (see Figure 24).

There results $y_0' + \delta \approx y_0$

so that the outer edge of the new equivalent wake is about the same as for the truncated wake.

Also, $\frac{U_{max}'}{U_S} = 4.3 \times 10^{-2}$ is very close to

$\frac{U_\delta}{U_S} = 4.6 \times 10^{-2}$, the mean velocity in the truncated wake at $y = \delta$.

GROWTH OF NEW TURBULENT BOUNDARY LAYER

It was previously shown that for a given Re_x, that $\frac{\delta}{x}$ varied very little with Mach Number, so that it is sufficient to take

$\frac{\delta}{x} = \frac{.37}{Re_x^{1/5}} = \frac{.37}{\left(\frac{U_S' x}{\nu_S'}\right)^{1/5}}$ where the primes denote the conditions in the "free stream" at the edge of the new turbulent boundary layer. As for the new laminar boundary layer, the new turbulent boundary layer growth is not sensitive to small changes in the "free stream" flow. Figure 23 shows the results for the growth of a new turbulent boundary layer from the beginning of the cylinder in the wake "free stream".

LAMINAR BOUNDARY LAYER AT BASE OF CONE

The approximation used for obtaining the effect of the pressure drop on the turbulent boundary layer mean velocity distribution should be just as valid when the boundary layer at the base of the cone is laminar. At P_c = 180 cm., M_s = 1.89, the laminar boundary layer thickness at the base of the cone is 2.5×10^{-2} cm. Figure 25 shows the computed velocity profiles before and after the corner. (For simplicity, a linear profile was used ahead of the corner.) In this case, the boundary layer thickness is not increased by as large a factor as for the turbulent case. Since a much greater extent of the laminar boundary layer ahead of the corner is subsonic, the net expansion of the streamtubes is less.

However, as compared with the turbulent case, there is an important difference. In the turbulent wake, the turbulence mechanism provides some interchange across the whole extent of the wake since there will be some eddies of a size comparable to the wake width. For the laminar shear flow, the interchange depends on the molecular transport mechanism and has a local behavior. Consider the following cases. A laminar boundary layer grows from the leading edge of a flat plate at rest. (See Figure 34.)

Between x_1 and x_2 a movable surface is inserted. Now the boundary layer growing from the beginning of the plate represents the propagation of significant information, by viscous forces, of the presence of the wall. An element of fluid at A has had a slight change in its motion because of a change in the flow potential, but it has not yet been significantly affected by viscous forces. The fact that the surface is moving, starting at x_1, propagates along some surface such as the one shown. This information should be transmitted away from the plate more rapidly by viscous forces than for the initial growth of the boundary layer from the plate leading edge because of the lower velocities near the wall. The fluid element at B has not learned of the change in boundary condition at x_1 and decreases its velocity at the same rate as if the wall condition at x_1 had been unchanged.

With the velocity distribution after the corner shown in Figure 26, the fluid elements of the new free stream should move roughly as if they belonged to another laminar boundary layer of much greater thickness. The profile after the corner is almost linear and might be imagined to be the outer reaches of a boundary layer with a linear profile growing on a surface well below the real surface.

Since the boundary layer growth decreases with boundary layer thickness, the new laminar boundary layer should engulf the old laminar layer about 2.5 cm. from the corner. Probably, some further travel downstream would be required to reach an equilibrium profile. (Since for air the temperature boundary layer is of the same order as the viscous layer, what has been said for sudden changes in shear at the surface would hold equally well for sudden changes in surface temperature.)

TEMPERATURE RECOVERY FACTORS ALONG THE CYLINDER

In the discussion of the experimental results the temperatures on the cylinder were described in relation to the "usual" laminar or "usual" turbulent levels. It is clear from the foregoing considerations that the temperature recovery factors for the new laminar or turbulent boundary layers on the cylinder would differ from the constant pressure surface levels.

Calculations will be made assuming that in terms of M_S' and T_0', $r_L' = .85$ and $r_T' = .88$. (The limitations of this assumption were previously noted.) The recovery factors, r, along the cylinder for the various cases can then be obtained in terms of M_S and T_0.

As there is heat transfer between the air and the model for about one centimeter ahead of and downstream of the model shoulder, the measured surface temperatures in the corresponding regions are not recovery temperatures. The recovery factor calculations for the boundary layers on

the cylinder will not take this heat transfer into account so that the measured temperatures in the vicinity of the shoulder should not agree with the calculations.

(a) Laminar at base of cone.

For $r_L = .85$ at the cone base $\frac{T_{w_1}}{T_0} = .937$ where $M_s = 1.89$, so that for the fluid adjacent to the wall ahead of the shoulder $T_0' = T_{w_1}$. A new laminar boundary layer at the beginning of the cylinder would have $M_s' = 1.91$ and $T_0' = .937\ T_0$ and with $r_L' = .85$, $r = .82$ based on $M_s = 3.13$ and a stagnation temperature T_0.

(b) Turbulent at base of cone.

For $r_T = .88$ at the cone base, $T_{w_1} = .95\ T_0$ so that for the fluid adjacent to the wall ahead of the shoulder $T_0' = T_{w_1}$. If the new boundary layer after the corner is laminar, then with $r_L' = .85$, $M_s' = 1.91$, and $T_0' = .95\ T_0$, - - - - $r = .834$ at the beginning of the cylinder based on $M_s = 3.13$. $1\ T_0$.

If, as previously estimated, the new laminar boundary layer engulfed the old laminar boundary layer by 2.5 cm. from the corner, then from 2.5 cm. downstream the free stream for the growing boundary layer would be that obtained from the surface pressure variation. Figure 11 shows that the recovery factor r has only reached a value of .84 by 2.5 cm. from the corner, and appears to level out at a somewhat higher value than expected. The reason for this behavior is not known; it may be that after engulfing the old boundary layer, the new laminar layer approaches the usual equilibrium temperature distribution fairly slowly. Certainly, it does not seem likely that the temperature distribution at the point of engulfment is the equilibrium distribution since the old boundary layer suffered a pronounced energy redistribution ahead of the corner, and this should effect the distribution of energy in the new boundary layer.

Kovasznay[3] found that the total enthalpy was constant within his measuring accuracy, (approximately 1%) across a supersonic boundary layer at a Mach Number of 1.75, at least between $\frac{y}{\delta} = .05$ and $\frac{y}{\delta} = 1$. The measurements covered the supersonic portion of the boundary layer. Evidently, the loss in enthalpy occurs very near the wall. $\frac{y}{\delta} = .1$ in the turbulent layer ahead of the corner corresponds to $y = 1.6 \times 10^{-2}$ cm. after the corner. The new laminar layer would have grown to this thickness within about .2 cm. from the shoulder. Therefore, except for conditions just after the shoulder, the "free stream" enthalpy would be approximately the stagnation enthalpy of the tunnel, but the "free stream" Mach Number would be reduced. Because of the reduced "free stream" Mach Number, the apparent recovery factor, r, would be greater than .85.

If the new boundary layer is turbulent, then $r_T' = .88$, $M_S' = 1.91$, $T_0' = .95\ T_0$, and $r = .85$ at the beginning of the cylinder.

The apparent recovery factor, r, along the cylinder for the turbulent boundary layer would be greater than $r = .88$. Figure 27 compares the calculated apparent recovery factors and the experimental results. A 1% difference between the actual and assumed stagnation temperatures of the "free stream", due either to a variation ahead of the corner or a redistribution after the corner, would correspond to a change of the predicted recovery factor levels for the new laminar and turbulent boundary layers of about .015.

The course of the recovery temperatures, as shown in Figures 16 and 11, and perhaps more clearly at $M = 3.55$ in Figure 17, is a rise from the shoulder flattening out at 2 - 7 cm. from the shoulder and then a fairly steep rise to much higher values.

The conclusion that the sharp rise in the experimental temperatures on the cylinder is due to a transition from a "new" laminar boundary layer to a "new" turbulent boundary layer is believed to be consistent with these approximate calculations.

TRANSITION BY STRONG TURBULENCE

At low speeds the transition from laminar to turbulent flow is known to depend on the turbulence of the wind tunnel airstream. Taylor[10] proposed a suitable parameter for correlating the transition results when the turbulence of the stream was relatively large. In the Karman-Pohlhausen method for calculating the behavior of laminar boundary layers in the presence of pressure gradients, the boundary layer profile at any position depends on the local boundary layer thickness and the local pressure gradient, and is defined in terms of a parameter Λ where

$$\Lambda = \frac{-\delta^2}{\mu w_s} \frac{dP_s}{dx}$$

(It is known that for rapid changes in pressure the local profile depends on the boundary layer history and cannot be described in this simple way.) Taylor suggested that in the presence of strong turbulence, the instantaneous pressure gradient, due to the turbulence, caused separation of the laminar boundary layer with resulting transition. Taking the Pohlhausen treatment as a useful approximation, in spite of its known limitations, and estimating the root mean square value of the spatial pressure gradient in isotropic turbulence, that is

$$\frac{\partial p'}{\partial x} = \frac{\sqrt{2}\rho\, u'^2}{\lambda_\eta} = \frac{4\rho\, u'^2}{\lambda_x}$$

λ_η = Lagrangian microscale
λ_x = Longitudinal microscale
u' = root mean square fluctuation velocity

then the Pohlhausen parameter Λ is equal to $\Lambda = -1.36 \times 10^2 \left(\frac{u'}{U}\right)^2 \frac{x}{\lambda_x}$

This can also be written as $\Lambda^{2/5} \propto \frac{u'}{U} \left(\frac{x}{L_y}\right)^{1/5} Re_x^{1/5}$

where L_y = Lateral integral scale.

The parameter $\frac{u'}{U} \left(\frac{x}{L_y}\right)^{1/5}$ is known as the "turbulence parameter". Surprisingly enough, the correlation of $\frac{u'}{U} \left(\frac{x}{L_y}\right)^{1/5}$ vs. Re_{xtr} worked very well for the existing sphere data and later $\Lambda^{2/5}$ was used to correlate flat plate transition data by Fage and Preston.[11] (Re_x transition is defined

as the beginning of the transition region.) $\Lambda = -12$ corresponds to separation in the Pohlhausen treatment; the subsonic transition data give $\Lambda = -2$. In view of the approximations involved, the absolute value of Λ probably doesn't have much significance. Figure 20 shows $\Lambda^{1/2}$ vs. Re_{xtr} where $\Lambda^{1/2} \propto \frac{u'}{U} \left(\frac{x}{\lambda_x}\right)^{1/2}$ where λ_x is the longitudinal microscale of the turbulence. (For the present problem there are some advantages in using λ_x rather than L_y.) In addition to the points of Hall and Hislop[12] (used by Fage and Preston), two values from Dryden's[13] work are shown. The scale of the turbulence for Dryden's low Reynolds Number points was not measured and was not easily estimable from the mesh size of the screen producing the turbulence. A large number of aluminum flags were tied to the downstream side of the screen to increase the turbulence level, and they may have also altered the turbulence scale. Because of the doubtful value of λ_x for these points, the curve is shown dashed. Dryden's value for the higher Reynolds Number is in good agreement with the values of Hall and Hislop.

Dryden's value was the lowest transition Reynolds Number point this author was able to find in the literature. It is naturally interesting to consider whether the same general correlation would hold for still lower transition Reynolds Numbers. In a restricted sense, the laminar sub-layer in a fully developed turbulent boundary layer can be used to extend the correlation curve to very low transition Reynolds Numbers.

Laufer[14] has shown that the fluctuation velocities, as well as the mean velocities, within and in the immediate vicinity of the laminar sub-layer when plotted as $\frac{u'}{U_\tau}$ vs $\frac{yU_\tau}{\nu}$ are independent of the Reynolds Number. Since the mean velocity for different Reynolds Numbers follows a single curve of $\frac{U}{U_\tau}$ vs $\frac{yU_\tau}{\nu}$, if a value for $\frac{yU_\tau}{\nu}$ is decided upon, then the Reynolds Number of the laminar sub-layer based on the laminar sub-layer thickness is invariant, i.e.,

$$Re_\delta = \left(\frac{U\delta}{\nu}\right) \frac{yU_\tau}{\nu} = c_1$$

For $\frac{yU_\tau}{\nu} = 30$, $Re_\delta = 375$

$\frac{yU_\tau}{\nu} = 10$, $Re_\delta = 87$

This laminar sub-layer can be thought of having originated at some distance x upstream where $x = \frac{\delta^2}{\nu}\frac{U_\delta}{34}$ $\delta = y$ and $U_\delta = U$ at $\frac{yU_\tau}{\nu} = 10$ or 30 for the flat plate laminar boundary layer. Clearly the disturbance in the turbulent boundary layer just outside of the laminar sub-layer is so intense that it prevents the laminar sub-layer from growing, that is in terms of Re_δ. The correlation of $\frac{u'}{U}\left(\frac{x}{\lambda_x}\right)^{1/2}$ vs. Re_{xtr} as given in Figure 28 can be viewed as a purely empirical result. For values of $\frac{u'}{U}\left(\frac{x}{\lambda_x}\right)^{1/2}$ below the curve, transition does not occur. The value of this same parameter can be computed, fairly crudely, for the laminar sub-layer using the measured properties of the boundary layer in the immediate vicinity of the laminar sub-layer as the "free stream". The parameter can be only loosely determined because the boundary layer turbulence is anisotropic and there are many fluctuation levels and many microscales. Taylor's value for the spatial pressure gradient was based on a Lagrangian scale $\lambda\eta$ whose relation to the Eulerian microscale was determined from one experiment in isotropic turbulence. Intuitively, the most important determining factor in a given spatial gradient would be the appropriate fluctuation component and the corresponding microscale, such as u' and λ_x.

Using u' alone and λ_x, taking the edge of the laminar sub-layer at $\frac{yU_\tau}{\nu} = 30$, and considering the "free stream" to be an average of conditions from $\frac{yU_\tau}{\nu} = 30$ to $\frac{yU_\tau}{\nu} = 60$, $\frac{u'}{U}\left(\frac{x}{\lambda_x}\right)^{1/2} = .31$ $Re_{xtr} = 4.1 \times 10^3$.

If the laminar sub-layer is defined as extending to $\frac{yU_\tau}{\nu} = 10$, then a similar calculation gives

$$\frac{u'}{U}\left(\frac{x}{\lambda_x}\right)^{1/2} = .14 \qquad \text{where } Re_{xtr} = 1.7 \times 10^2$$

The values of $\frac{u'}{U}\left(\frac{x}{\lambda_x}\right)^{1/2}$ for the laminar sub-layer are used to extend the correlation curve in Figure 28 to very low Reynolds Numbers.

TURBULENCE PARAMETERS FOR BOUNDARY LAYER ON CYLINDER

In order to compare the turbulence parameter $\frac{u'}{U}\left(\frac{x}{\lambda_x}\right)^{1/2}$ for the new laminar boundary layer along the cylinder with the correlation curve in Figure 28, the turbulence levels and microscales for the possible "free stream" flows, boundary layer or wake, are required. The turbulence level and microscale for the boundary layer free stream can be obtained by estimating the change in turbulence level and microscale of the boundary layer on traversing the corner. The turbulence level and microscale for the wake have to be based on low-speed wake measurements. If there were no turbulence production, then the boundary layer turbulence at the beginning of the cylinder would decay rapidly as for isotropic turbulence. Since there is turbulence production, the turbulence level must be higher than that obtained for isotropic decay. On the other hand, the turbulence level in a wake is limited, and asymptotically $\frac{u'}{U_{max}} \longrightarrow .2$ where U_{max} is the maximum mean speed decrement.[8] Since U_{max} decreases $\propto x^{-1/2}$, the turbulence level steadily decreases.

The parameter $\frac{u'}{U}\left(\frac{x}{\lambda_x}\right)^{1/2}$ will be computed for the following cases. (The Mach Number variation along the cylinder will be neglected.)

(a) The mean velocity distribution of Figure 22 assumed constant and the turbulence assumed to decay isotropically.

(b) The mean velocity distribution for a wake with the turbulence level and microscale based on low-speed wake data.

TURBULENCE LEVEL AND SCALE IN BOUNDARY LAYER AHEAD OF THE CORNER

Experimental studies of low-speed turbulent flows, such as boundary layers,[6] channel flow[15] and pipe flow,[14] have established the following facts:

(a) Close to the wall, out to the region where the velocity distribution follows the logarithmic law, the fluctuation levels for all of these flows substantially fall on a single curve when the data are plotted in terms of U_τ, the friction velocity, that is $\frac{u'}{U_\tau}$ vs. $\frac{yU_\tau}{\nu}$.

(b) As shown by Laufer for pipe flow, well away from the wall the friction velocity is the proper reference velocity so that a plot of $\frac{u'}{U_\tau}$ vs. $\frac{y}{\delta}$ is independent of Reynolds Number.

(c) In view of (a) and (b) it would seem reasonable to guess that a curve of $\frac{u'}{U_\tau}$ vs. $\frac{y}{\delta}$ for the boundary layer well away from the laminar sub-layer would be substantially independent of Reynolds Number. Klebanoff and Diehl[4] made fluctuation measurements in turbulent boundary layers at two different air speeds and at several different boundary layer thicknesses. While all of the data plotted in terms of $\frac{u'}{U_\tau}$ do not fall on a single curve, qualitative results are consistent with the hypothesis. Furthermore, near $\frac{y}{\delta} \approx .4$ in the boundary layer well away from the wall but not in the intermittently turbulent region, a comparison of Klebanoff's[6] boundary layer data with Laufer's[14] pipe flow data in the same region shows that the values of $\frac{u'}{U_\tau}$ are approximately the same. For these computations, the fluctuation levels $\frac{u'}{U_\tau}$ as measured by Klebanoff are used for the portion of the boundary layer where (a) does not apply.

(d) The experiments of Laufer,[15] Klebanoff and Diehl,[4] and Klebanoff,[6] show that the longitudinal integral scale of turbulence appears to be controlled by the boundary conditions so that for a given flow, say a boundary layer, the ratio of the integral scale to the boundary layer thickness, say $\frac{L_x}{\delta}$ is not a function of the Reynolds Number. For the boundary layer, $\frac{L_x}{\delta} = .4$

For isotropic turbulence the relation between the microscale of turbulence and the integral scale is[16]

$$\frac{\lambda_x}{L_x} = \frac{7}{\sqrt{N_{O_x}}} \quad \text{where } N_{O_x} = \frac{u'L_x}{\nu}$$

Since the turbulent shear flows under consideration are not isotropic, this relation between the turbulence scales would not be expected to hold. However, a check of Klebanoff's boundary layer data shows that over a fairly large portion of the flow, excluding the laminar sub-layer, the isotropic relation between λ_x and L_x holds surprisingly well. In order to obtain suitable values for the turbulence scales in these high-speed flows, the approximation that $\frac{\lambda_x}{L_x} = \frac{7}{\sqrt{N_{O_x}}}$ will be made.

At the cone base at M = 3.02, with M_s = 1.89, P_0 = 180 cm., U_r = 2.44 x 10^3 cm/sec., and λ_x = 1.15 x 10^{-2} cm. Figure 29 shows the turbulence levels $\frac{\tilde{u}'}{U}$, across the boundary layer where U is the mean velocity at any point across the boundary layer and $\tilde{u}'$ is the square root of the average of the squares of the turbulent velocity components u', v', and w'.

THE EFFECT OF THE EXPANSION AT THE SHOULDER ON THE BOUNDARY LAYER TURBULENCE

Consider a flow in which there is a vorticity distribution superimposed on a uniform mean motion. When there is an irrotational change of the mean motion, the rotational and irrotational flows will interact, so that, in general, the energy of the rotational field is changed. In connection with the design of wind tunnel contractions, Prandtl[17] showed that if the gain in energy for all of the streamlines in a contraction is the same, a condition that would realized if the pressure drop for each streamline were the same, then a longitudinal steady perturbation in velocity would be reduced. He also applied the circulation theorem to a vortex with its axis in the stream direction and showed that its energy would be increased in traversing the contraction. G. I. Taylor,[18] and more recently, Ribner and Tucker,[19] and Tucker[20] have investigated the interaction of an irrotational and a rotational flow field using the Helmholtz Equations. The Helmholtz Equations give the vorticity of a fluid element in terms of its vorticity at some initial time and the motion of the fluid element with respect to its initial coordinates, and so it is a Lagrangian representation. The modification of the vorticity distribution by viscosity is neglected so that viscous diffusion and viscous dissipation are not included. The equations are[21]

$$\frac{\xi}{\rho} = \frac{\xi_0}{\rho_0}\frac{\partial x}{\partial a} + \frac{\eta_0}{\rho_0}\frac{\partial x}{\partial b} + \frac{\zeta_0}{\rho_0}\frac{\partial x}{\partial c}$$

$$\frac{\eta}{\rho} = \frac{\xi_0}{\rho_0}\frac{\partial y}{\partial a} + \frac{\eta_0}{\rho_0}\frac{\partial y}{\partial b} + \frac{\zeta_0}{\rho_0}\frac{\partial y}{\partial c}$$

$$\frac{\zeta}{\rho} = \frac{\xi_0}{\rho_0}\frac{\partial z}{\partial a} + \frac{\eta_0}{\rho_0}\frac{\partial z}{\partial b} + \frac{\zeta_0}{\rho_0}\frac{\partial z}{\partial c}$$

where ξ_0, η_0, ζ_0, are the initial components of the vorticity vector

a, b, c, are the initial cartesian coordinates of the fluid element

ρ_0 = initial fluid element density

and they are valid for a compressible fluid. In a general case, to obtain the vorticity components at time t, all of the nine Lagrangian coordinate derivates have to be known. The above authors simplify the problem by assuming that the changes in the potential motion are large and rapid, and the rotational motion is relatively small so that the motion of a fluid element is primarily specified by the velocity changes of the potential motion. Under this restriction, six of the Lagrangian derivatives become zero and only $\frac{\partial x}{\partial a}$, $\frac{\partial y}{\partial b}$, and $\frac{\partial z}{\partial c}$ remain, so that the equations describe the alteration of a vorticity distribution by a geometrical deformation of the flow field. Any desired vorticity distribution can be represented by the superposition of elementary vorticity distributions.

These methods have been developed to deal with the problem of the changes of turbulence in a wind tunnel contraction where unfortunately in general, all of the Lagrangian coordinate derivatives are important and where the dissipation cannot be neglected.* As previously noted, in the present experiments, for a good portion of the boundary layer, the acceleration at the shoulder of the cone cylinder model occurs in a length of the order of δ so that compared to the usual wind tunnel contraction the changes in the mean motion of the turbulent boundary layer fluid occur very rapidly. The following estimates for the importance of the non-linear terms and the viscous dissipation in the expansion at the cone cylinder shoulder indicate that, in this case, the linear theory should be reasonably good.

For the turbulent boundary layer at the base of the cone $L_x = .46$ and $\frac{u'}{U} = .09$ (Average from $\frac{y}{\delta} = .1 \rightarrow \frac{y}{\delta} = .4$).

An average value of $\frac{U_2}{U_1}$ for the same region is $\frac{U_2}{U_1} = 1.43$

*See Appendix

Also, we have $U_{1_{aver}} = 3.7 \times 10^4$ cm/sec

$U_{2_{aver}} = 5.3 \times 10^4$ cm/sec

$\Delta U = 1.6 \times 10^4$ cm/sec

Suppose there is an eddy of dimension L_y and strength $\tilde{u}'$ with its axis transverse to the direction of the mean motion, then the motion of a fluid element depends on its initial y coordinate b, as follows:

$$x = U_{mean} \times \Delta t + \ell a + \frac{\delta}{L_y} \left(\frac{\tilde{u}'}{U}\right)_{mean} \times b$$

U_{mean} mean velocity in acceleration

and $\frac{\partial x}{\partial a} = \ell$, $\frac{\partial x}{\partial b} = \frac{\delta}{L_y} \left(\frac{\tilde{u}'}{U}\right)_{mean} \approx .3$

where $\ell = \frac{U_{2\ aver}}{U_{1\ aver}} \approx 1.5$ or $\frac{\partial x}{\partial b} \Big/ \frac{\partial x}{\partial a} \approx .2$

so that even for this case, the neglected derivatives are not negligible although they are smaller than the derivatives that are included, and the assumptions in the calculations are at least roughly satisfied. It is also necessary that the turbulent dissipation in the flow about the shoulder be unimportant as compared to the change in turbulent energy produced by the fluid element deformation.

The decay of the turbulence, if isotropic, would be proportional to[16]

$$\frac{d(\tilde{u}'^2)}{dt} = \frac{1}{5} \frac{\tilde{u}'^3_{mean}}{L_y}$$

The time for passage past the shoulder, assuming the acceleration length is δ is $\Delta t = \frac{\delta}{U_{mean}}$

Then the loss of turbulent kinetic energy is $(\Delta \tilde{u}')^2 = -\frac{1}{5} \frac{\tilde{u}'^3_{mean}}{L_y} \frac{\delta}{U_{mean}}$

The fraction of the turbulent energy lost is $\frac{(\Delta \tilde{u}')^2}{\tilde{u}_1'^2} = -\frac{1}{5} \frac{\tilde{u}'_{mean}}{U_{mean}} \times \frac{\delta}{L_y} \approx .06$

Now $\frac{\tilde{u}_2'^2}{\tilde{u}_1'^2} = .25$ so that $\frac{(\Delta \tilde{u}')^2}{\tilde{u}_1'^2}$ due to fluid element deformation is .75 as compared with .06 for viscous dissipation.

It has been shown that the restrictions of the linearized theory are fairly well satisfied for the rapid acceleration at the shoulder of the cone cylinder. Since the available measurements on the overall changes in turbulence intensity in wind tunnel contractions are in general agreement with the calculations, it is believed justifiable to use the theory for obtaining the overall turbulence intensity changes at the shoulder. However, certain inaccuracies are manifest. The turbulent field ahead of the corner is neither isotropic as in reference 19 nor axisymmetric as in reference 20. Furthermore, the expansion right at the model shoulder is two-dimensional rather then axisymmetric which is the case computed in the above references.

The conclusion as to the general nature of the phenomenon on the cylinder is not dependent on an accurate knowledge of the turbulence level. Since many other approximations are made, it did not seem worthwhile to attempt to evaluate the possible error due to the above differences. It is noted by Ribner and Tucker that their result is very close to the result obtained by Prandtl for a much simplified vorticity distribution. In any case, the author could not resist the pleasure of merely plucking an attenuation factor from a handy chart. Figure 29 shows the fluctuation levels after the expansion at the shoulder as obtained using reference 19.

APPLICATION TO TURBULENCE

Figure 30 shows an expansion of a turbulent flow where the change in mean velocity is large and rapid enough to permit the use of Helmholtz's Equations with G. I. Taylor's restrictions. The calculation can be described in the following terms.

At any time t, an instantaneous measurement of the velocity field, if it could be made, would establish the vorticity of the fluid elements at station A. The Helmholtz Equations can then be used to determine the change in vorticity of the fluid elements at station B. If a sufficient number of similar measurements are made randomly, the average changes in vorticity of the fluid elements can be obtained, and so the average change in energy in the rotational motion.

The turbulent energy equation represents the change in turbulent kinetic energy in a fluid element moving with the mean motion. Any particular fluid element may lose or gain turbulent energy in various ways, such as turbulent energy convection, but the fluctuation field as a whole can only have its total turbulent kinetic energy changed by losing kinetic energy to heat through viscous dissipation or by having its kinetic energy changed by interaction with the mean motion.

The interaction term, which is usually called the turbulent production term is $-\rho\overline{u_i u_j}\,\frac{\partial U_i}{\partial x_j}$ (i, j are repeating indices) and may be either positive or negative. When the mean motion is uniform, then the production term is zero. If the viscous dissipation is negligible in the section A-B, then the integration of the production term over the volume A-B must result in a change in turbulent kinetic energy equal to the change in turbulent energy calculated using the Helmholtz Equations.

The calculations of Ribner and Tucker[19] show that mean flow changes may result in either a decrease or an increase of turbulent energy. For accelerations at supersonic speeds, the fluid elements are stretched in both the

longitudinal and the lateral directions. As a result, both the longitudinal and lateral fluctuations are reduced by the deformation and the turbulent energy is thereby reduced. In a sense, the turbulent energy flows from the turbulent fluctuation field to the mean flow. This conversion of random energy into directed motion is analogous to the conversion of random thermal energy in a gas into directed motion in a supersonic nozzle. If the flow process is reversed, the turbulent energy will be increased.

STAGNATION TEMPERATURE UNEVENNESS IN THE TURBULENT BOUNDARY LAYER

Kovasznay's[3] hot-wire measurements in a supersonic boundary layer at M = 1.75 show that adjacent fluid masses vary in stagnation temperature; if a measurement is made at a fixed point in the boundary layer there is a stagnation temperature fluctuation. The magnitude of the fluctuation varies through the boundary layer and reaches a peak value of about 3% of the stagnation temperature. As Kovasznay discusses in his paper, the stagnation temperature fluctuation involves a density fluctuation but does not involve a pressure fluctuation.

However, when a field of uneven stagnation temperature is accelerated to higher speed, a vorticity field consisting of longitudinal velocity variations should be created. Corrsin[23] has derived an expression for the magnitude of the resulting velocity perturbation in terms of the initial stagnation temperature perturbation. The relation is

$$\frac{u_2'}{U_2} = \frac{1}{2}\left[1 - \left(\frac{M_1}{M_2}\right)^2\right]\frac{\vartheta_0}{T_0}$$

where ϑ_0 = stagnation temperature perturbation.

If Kovasznay's measurements are applied to the turbulent boundary layer at $M_s = 1.89$, we have, as maximum values of the root mean square fluctuations

$$\frac{\vartheta_0}{T_1} = .05 \quad \text{for} \quad \frac{\vartheta_0}{T_0} = .03$$

$$\frac{M_1}{M_2} = .6 \qquad \frac{T_1}{T_2} = 1.75$$

so that $\frac{u_2'}{U_2} = .009$.

Assuming that this specially created vorticity field would become a part of the general vorticity field after the model shoulder, the contribution to the turbulent fluctuation level would be .005. This addition to the turbulence after the shoulder will be neglected.

EFFECT OF SHOULDER EXPANSION ON TURBULENCE MICROSCALE

For isotropic turbulence, the integral scales are often considered to define a sort of average eddy size. Tucker[20] has calculated the effect of stream velocity changes on the correlation coefficients from which the integral scale is determined. He notes that in certain cases the longitudinal scale becomes negative which makes fairly dubious the identification of the integral scale as an average eddy size.

The turbulence microscale can be defined as $\lambda_x^2 = \frac{2u'^2}{\left(\frac{\partial u'}{\partial x}\right)^2}$ so that the change in λ_x is essentially determined by the stretching in the x direction, that is

$$\lambda_{x_2} = \lambda_{x_1} \times 1.42$$

1 refers to position just ahead of corner

2 refers to position just after corner

But in the expansion at the shoulder, the expansion of the fluid elements in the y direction is not equal to that in the x direction, so that with

$$\lambda_y^2 = \frac{2u'^2}{\left(\frac{\partial u'}{\partial y}\right)^2} \qquad \lambda_{y_2} = \lambda_{y_1} \times 1.66$$

At the beginning of the cylinder the "free stream" turbulence in these experiments is certainly anisotropic; even if it were isotropic ahead of the shoulder it would be anisotropic after the expansion. The flow near the center of a two-dimensional wake is roughly isotropic, so that as the "free stream" flow takes on the aspect of a wake, the turbulence field

should move towards isotropy. Since, in any case, the turbulence in the "free stream" along the cylinder will be compared with low-speed data where the free stream turbulence was isotropic, the anisotropic turbulent field at the beginning of the cylinder will be described in terms of an equivalent isotropic flow. Hence the geometrical changes in the expansion will be averaged, giving $\lambda_2 = 1.54\ \lambda_1$.

BOUNDARY LAYER "FREE STREAM"

Following are average values for the region in the boundary layer ahead of the corner, from $\frac{y}{\delta} = .2$ to $\frac{y}{\delta} = .4$

$$\tilde{u}_1' = 3.3 \times 10^3 \text{ cm/sec} \qquad \lambda_{x_1} = 1.15 \times 10^{-2} \text{ cm.}$$

After the corner,

$$\tilde{u}_2' = 2.1 \times 10^3 \text{ cm/sec} \qquad \lambda_{x_2} = 1.76 \times 10^{-2} \text{ cm.}$$

To estimate the turbulence decay in the "free stream" along the cylinder, it is necessary to establish the integral scale or an effective mesh size for the equivalent isotropic flow. This can be done as follows.

For isotropic turbulence, the decay of the turbulent energy is given by $\frac{d(\tilde{u}')^2}{dt} = -\frac{20\nu\tilde{u}'^2}{\lambda_x^2}$ which is based on the expression for the viscous dissipation W, where $W = \frac{30\mu\tilde{u}'^2}{\lambda_x^2}$

Except near the laminar sub-layer, the dissipation has been found to be reasonably well represented by the above formula. Now, from measurements behind grids of mesh size M_{eff}, it has been found that[7]

$\frac{U_S}{\tilde{u}'} = \frac{1.25\ x}{M_{eff}}$ which can be written as $\frac{d(\tilde{u}')^2}{dx} = \frac{1.25\ (\tilde{u}')^3}{M_{eff}\ U_S}$

An effective mesh size for the equivalent isotropic flow can be determined by equating the above expressions for the turbulence decay.

Then after the corner $M_{eff} = 5.8 \times 10^{-2}$ cm. and it follows that

$$\lambda_x^2 = \frac{5\nu x}{U_S} + C$$

The results of the calculations for the turbulence level and the microscale are shown in Figure 31. The resulting turbulence parameter $\frac{\tilde{u}'}{U}\left(\frac{x}{\lambda_x}\right)^{1/2}$ is shown in Figure 32. At any position along the cylinder, x, as used here, is the effective length of the new laminar boundary layer at that position, so that x is approximately equal to the distance from the beginning of the cylinder.

WAKE FREE STREAM

The only measurements of the turbulence in two-dimensional wakes that the author was able to find are those of Towsend[8] where the distributions of u' and the microscale λ_x were measured. Previously it was noted that for such flows as channel flows and boundary layers, the integral scale L_x was determined by the boundary conditions, so that $\frac{L_x}{\delta^*}$ was a constant independent of Re. It will be assumed that for a wake,* also, the integral scale is a constant fraction of the wake width, so that we assume $\frac{L_x}{y_0}$ constant.

From Townsend, for $U_S = 1.12 \times 10^3$ cm/sec.

$$\frac{\lambda_x}{L_x} = 1.30 \text{ and } \frac{\lambda_x}{y_0} = 3.18 \times 10^{-1}$$

(y_0 = half wake for mean velocity distribution)

So $$\frac{L_x}{y_0} = .244$$

Since the equivalent wake at the beginning of the cylinder has

$$\frac{U_{max}}{U_S} = .084$$

Then $\frac{u'L_x}{\nu} = 124$ and $\frac{\lambda_x}{L_x} = .63$ or $\lambda_x = 3.50 \times 10^{-2}$ cm.

*Suggested by Professor Stanley Corrsin of Johns Hopkins University

which compares with $\lambda_x = 1.76 \times 10^{-2}$ cm. for the boundary layer after the corner.

The decay as the wake width grows can be obtained using the fact that $\frac{U_{max}}{U_S} = 1.3 \frac{y_0}{x}$ where $x = x_S + x_T$

x_S Effective starting length for the wake

x_T Distance from corner

Since $Re_T = \frac{u' \times 2y_0}{\nu}$ = constant for any given wake,

and $\frac{L_x}{y_0}$ = constant, then $\frac{u'L_x}{\nu}$ = constant.

or $\lambda_x = .15\, y_0$

Also, we have $y_0 = c_1 x^{1/2}$, c_1 = constant.

The turbulence levels and microscale values are shown in Figure 31. The resulting "turbulence parameter" is shown in Figure 32. Allowance has been made for the loss of wake fluid to a new laminar boundary layer.

The start of the abrupt surface temperature rise on the cylinder is not a well defined point since the measuring points were not closely spaced. The position marked on Figure 32 as representing transition on the cylinder is 2.5 cm. from the corner.

In a low-speed wind tunnel test the free stream turbulence is of relatively large scale so that over the length of a flat plate model in the test section the changes of the turbulence level and turbulence scale are small. The turbulence parameter for the low-speed boundary layer increases steadily proportional to $x^{1/2}$ and would necessarily intersect the correlation curve. In the present case, the turbulence scale in the "free stream" along the cylinder is relatively small so that significant decay of the turbulence occurs along the run of the new laminar boundary layer. Apparently, the calculated decay is large enough so that the turbulence parameter for the boundary layer free stream, decaying isotropically, has a maximum value along the cylinder. Figure 32 shows the turbulence parameter curve just touching the correlation curve.

Actually, as has been noted previously, the turbulence level of the "free stream" should decrease more slowly than for isotropic decay because of the turbulence production taking place in the "free stream" mixing processes. At the beginning of the cylinder the turbulence level in the boundary layer "free stream" is higher than that for the equivalent wake "free stream" at the same position as shown in Figure 31. Eventually, the turbulence parameter for the wake will also reach a maximum and then decrease, but over the region of interest it increases monotonically. It appears likely that the turbulence parameter for the boundary layer on the cylinder is either on or above the turbulence parameter for the wake. But, in any case, it is clear from the curves in Figure 32 that the general nature of the turbulence parameter along the cylinder is the same for both of the "free stream" assumptions. The confluence of all of the curves in the vicinity of the experimental value of Re_{xtr} would appear to support the hypothesis concerning a laminar turbulent transition on the cylinder.

Figures 16 and 17 show that there are differences in the temperature data at different tunnel pressure levels. If the value of $\frac{u'}{U} \times \frac{1}{\lambda_x^{1/2}}$ were the same at each pressure level, then x for the beginning of transition on the cylinder would be the same at all of the pressure levels, and $Re_{xtr.}$ would increase proportional to the pressure level. At M = 3.02, this is roughly the experimental result. At M = 3.55 only the 100 cm. data has transition beginning at a significantly different position along the cylinder as compared with the data at the other pressure levels. The sizes of the wire trips used on the cone at the different pressure levels were not carefully controlled to make the boundary layer conditions at the trips "similar" as the pressure level was varied. Since the parameter $\frac{u'}{U} \times \frac{1}{\lambda_x^{1/2}}$ will depend on both the turbulent boundary layer thickness at the cone base and the tunnel pressure level, $\frac{u'}{U} \times \frac{1}{\lambda_x^{1/2}}$ would be expected to vary in a random way with tunnel pressure level.

EFFECT OF COMPRESSIBILITY

Compressibility effects have been included for that portion of the analysis involving the mean flow properties ahead of the corner and on the cylinder. The introduction of turbulence levels and turbulence scales was based on low-speed data. For this reason alone, the close agreement between the predicted value of Re_{xtr} and the experimental value of Re_{xtr} could be considered fortuitous.

The supersonic boundary layer measurements of Kovasznay can be compared with the low-speed fluctuation level measurements. Kovasznay made his measurements at the following conditions

$$M_S = 1.75 \qquad \delta = 1.27 \text{ cm.} \qquad T_0 = 300^{\circ}K \qquad P_0 = 80 \text{ cm Hg}$$

Assuming $T_W = T_R$, $\frac{T_W}{T_S} = 1.54$

Using the relations given previously

$$C_f = 1.77 \times 10^{-3}, \quad U_\tau = \sqrt{\frac{\tau_W}{\rho_W}} = 1.75 \times 10^3 \text{ cm/sec}$$

The following comparison will be made at $\frac{y}{\delta} = .5$

For Kovasznay

$$\frac{U}{\frac{y}{\delta} = .5} = 4.3 \times 10^4 \text{ cm/sec}$$

$$\left(\frac{u'}{U}\right)_{\frac{y}{\delta} = .5} = .0325 \quad \text{So} \quad u' = 1.4 \times 10^3 \text{ cm/sec.}$$

For Klebanoff

$$\left(\frac{u'}{U_\tau}\right)_{\frac{y}{\delta} = .5} = 1.32$$

So the value of u' expected on the basis of the low-speed measurements would be

$$u' = 2.3 \times 10^3 \text{ cm/sec} \quad \text{Or} \quad \frac{u'_{M = 1.75}}{u'_{M=0}} = .6$$

Also, Kovasznay finds $L_{x_{M = 1.75}} = .5\, L_{x_{M = 0}}$

If $\frac{\lambda_x}{\lambda_x} = \frac{7}{\sqrt{N_{c_x}}}$ then $\lambda_{x_{M=1.75}} = .7\lambda_{x_{M=0}}$

This change in these parameters would reduce $\frac{u'}{U}\left(\frac{x}{\lambda_x}\right)^{1/2}$ by .71 at the beginning of the cylinder. (For $T_0 = 300^{\circ}K$, the test section recovery temperature should be below room temperature, so that the wall temperature will be raised somewhat by heat transfer from the room. A higher wall temperature would increase U_τ and thereby u').

The influence of Mach Number on the "turbulence parameter" can be obtained by making use of an existing solution for high-speed boundary layers. Doridnitzen,[24] under the restrictions that the Prandtl Number equaled one and that the heat transfer is zero, developed a method for handling a compressible boundary layer analogous to the Karman-Pohlhausen method for a low-speed boundary layer.

The boundary layer profile is expressed as a fourth order polynomial

$$W = A\tau + B\tau^2 + C\tau^3 + D\tau^4$$

where $A = \left(2 + \frac{\Lambda}{6}\right)$, $B = -\frac{\Lambda}{2}$, $C = \left(\frac{\Lambda}{2} - 2\right)$

$D = \left(1 - \frac{\Lambda}{6}\right)$, $W = \frac{U}{U_{t=\bar{\delta}}}$

$\tau = \frac{t}{\bar{\delta}}$ where t is a transformed coordinate of the distance from the wall y as follows

$$dt = \frac{1}{L}\,\frac{\rho}{\rho_0}\,dy$$

$W = \frac{U}{U_{t=\bar{\delta}}} = W(\tau)$ L = characteristic length of problem

$\bar{\delta}$ = edge of boundary layer in coordinate t.

Then $\left(\frac{dW}{d\tau}\right)_{t\to 0} = 0$ gives $\Lambda = -12$ for separation as for the low-speed solution.

The parameter Λ is as follows:

$\Lambda = \frac{\bar{\delta}^2}{1 - v_S^2}\,\frac{dv_S}{ds}$, $v_S = \frac{U_S}{c}$ c = velocity of efflux into vacuum

s is a transformed x coordinate, where

$$ds = \frac{1}{L\,Re_0}\,\frac{P_S}{P_0}\,dx \qquad Re_0 = \frac{cL}{\nu}$$

P_S - local free stream pressure

So $$\frac{dU_S}{ds} = \frac{dU_S}{dx}\,\frac{dx}{ds} = \frac{dU_S}{dx}\,L\,Re_0 \times \frac{P_0}{P_S}$$

For a compressible fluid

$$U_S dU_S + \frac{dP_S}{\rho_S} = 0$$

$$\frac{dU_S}{dx} = -\frac{1}{\rho_S c^2 U_S}\,\frac{dP_S}{dx} .$$

Since

$$dy = L\,\frac{\rho_0}{\rho_S}\,dt \quad , \quad \delta = L\int_0^{\bar{\delta}} \frac{\rho_0}{\rho_S}\,dt$$

or with

$$\tau = \frac{t}{\bar{\delta}}$$

$$dt = \bar{\delta}\,d\tau$$

and

$$\delta = L\bar{\delta}\int_0^1 \frac{\rho_0}{\rho_S}\,d\tau \quad , \quad \frac{\rho_0}{\rho_S} = \left[1 + \frac{\gamma-1}{2} M_S^2\right]^{\frac{\gamma}{\gamma-1}} \left[1 - U_S^2 W^2\right] .$$

Then

$$\bar{\delta} = \frac{\delta}{L\left(1 + \frac{\gamma-1}{2} M_S^2\right)^{\frac{\gamma}{\gamma-1}} \int_0^1 \left(1 - U_S^2 W^2\right) d\tau} ,$$

Substituting for $\bar{\delta}$ and $\frac{dU_S}{ds}$ we have

$$\Lambda_c = \frac{-\delta^2}{\mu_0 U_S} H(M_S, \Lambda_c) \left(\frac{dP_S}{dx}\right)_c$$

$$H(M_S, \Lambda_0) = \left[\int_0^1 (1 - \nu_S^2 w^2)\, d\tau \right]^{-2}$$ "c" denotes compressible

This can be compared with

$\Lambda_{inc} = \frac{-\delta^2}{\mu_0 U_S} \left(\frac{dP_S}{dx}\right)_{inc}$ for an incompressible fluid

"inc" denotes incompressible

As $M_S \to 0$, $\nu_S \to 0$ so $\Lambda_{M_S} \to \Lambda_{M=0}$

Now if a turbulence field is carried along by a supersonic flow, there should be instantaneous pressure gradients analogous to those for a low-speed turbulence field.

We then have, simply assuming that the low-speed relation holds

$$\frac{\partial P'}{\partial x} = \frac{4\rho_S u'^2}{\lambda_x} \quad \text{or} \quad \Lambda_c = \frac{-\delta^2}{\mu_0 U_S} \times \frac{4\rho_S u'^2}{\lambda_x} H(M_S, \Lambda_c)$$

For a high-speed boundary layer

$$\frac{\delta^2}{\nu_S} = K(M_S) \frac{x}{U_S} \times 34 \qquad K(M_S) \to 1 \text{ for } M_S \to 0$$

Substituting for δ^2

$$\Lambda_c = -\frac{\mu_S}{\mu_0} H(M_S, \Lambda_c) K(M_S) \times 136 \left(\frac{u'}{U_S}\right)^2 \left(\frac{x}{\lambda_x}\right)$$

So

$$\Lambda_c = G^2(M_S, \Lambda_c) \Lambda_{inc}$$

If it is assumed that the same value of $\Lambda^{1/2}$, compressible or incompressible, is required for transition, then a smaller value of $\frac{u'}{U_S}\left(\frac{x}{\lambda_x}\right)^{1/2}$ is required for the compressible fluid since $G(M_S)$ is in general greater than unity. (See Figure 33. To evaluate G, Λ_c was varied from 0 to -12.) So Re_{xtr} at high speeds will be less than at low speeds for the same value of $\frac{u'}{U_S} \times \frac{1}{\lambda_x^{1/2}}$

At a Mach Number of ≈ 3, $\left[\frac{u'}{U_S}\left(\frac{x}{\Lambda_x}\right)^{1/2}\right]_{M\approx 3} \approx .6\left[\frac{u'}{U_S}\left(\frac{x}{\Lambda_x}\right)^{1/2}\right]_{M=0}$ for transition. But Kovasznay's results show $\frac{u'}{U_S \Lambda_x^{1/2}}$ reduced by a factor of .7, so that the two different effects of compressibility would approximately cancel in this experiment.

If the concept of transition being caused by the instantaneous pressure gradients due to the turbulent field has any validity, then the superposition of a steady pressure gradient of sufficient magnitude should prevent the occurrence of instantaneous adverse gradients. In Figure 32 the calculated turbulence parameters for the boundary layer flow from the beginning of the cylinder follow fairly close and almost parallel to the correlation curve. The decay of the turbulence in the "free stream" is very significant and the turbulence parameters for the new laminar boundary layer tend to level out fairly quickly. The present model actually has a small adverse pressure gradient which has been neglected in these calculations. It seems possible that a model designed with a suitable favorable pressure gradient after the shoulder might have much longer runs of new laminar flow since the favorable pressure gradient might lower the turbulence parameter curve for the boundary layer enough to avoid transition.

Nothing in the present analysis indicates that the pressure drop need be a particularly sudden one. In a gradual turn, the laminar boundary layer would grow and the turbulence level would be steadily reduced. It is necessary that the acceleration keep the turbulence parameter at any point at a respectable level. Tests on a model with a .3 cm. R at the shoulder gave the same results as for a sharp cornered model. Spreading the acceleration over a much greater length, perhaps up to one or two centimeters, may still produce a new laminar boundary layer.

SUMMARY

In this work it has been necessary to make a distinction between the boundary layer at a particular position on a model and the complete shear layer at the same position. The complete shear layer represents the results of the direct action of laminar and turbulent shearing stresses all along the model surface from the leading edge or tip. The boundary layer, as it is used here, is defined in a local sense, and may be all or only the inner portion of the complete shear layer. In the latter case, the outer portion of the shear layer is the outer flow or environment in which the boundary layer grows. As such, it may have substantial influence on the friction and heat transfer as well as the state of the boundary layer.

A laminar boundary layer is considered present when the knowledge of the surface friction at a particular position is being transmitted to the outer flow, which may be the outer part of the complete shear layer, by molecular viscous forces. For instance, in Figure 34, the velocity change of the wall is propagated out into the flow by molecular viscous forces and so the boundary layer at that position is laminar.

A turbulent boundary layer exists when the propagation of the surface friction at a particular position on the surface to the outer flow is controlled by turbulent shearing stresses. Of course, even when the boundary layer is turbulent, there is a laminar sub-layer adjacent to the wall, but some information about the shear at the wall is very rapidly communicated to the whole turbulent boundary layer. The growth of the turbulent boundary layer at any position can be described in terms of the wall friction at that position, so that the turbulent boundary layer behaves an an entity.

Hence, the label laminar or turbulent is selected on the basis of how the state of shear on the surface is being propagated or transmitted away from the surface to the outer flow.

The growth of a boundary layer on a flat plate in a wind tunnel airstream may alter the properties of the airstream in several ways. Besides potential changes of the free stream which are dependent on the boundary layer displacement thickness, it is also possible for the boundary layer to have a more subtle influence on the free stream flow. As the boundary layer grows, turbulent air is being removed from the main stream and either has its turbulent energy dissipated when the plate boundary layer is laminar, or, in the usual case, has it increased if the plate boundary layer is turbulent. In either case, the removal of a layer of turbulent air from the main stream may affect the main stream in the following way.

The wind tunnel air is turbulent, and if it is also non-uniform, then turbulent mixing will cause a progressive alteration of the mean velocity distribution and the turbulence of the air as it passes through the test section. The removal of a layer of test section air must necessarily change the course of the turbulent mixing processes. In the usual wind tunnel case, these effects are negligible since a serious attempt is usually made to achieve uniform flow in the test section. In the flow about the cone-cylinder model used in these experiments, where the outer portion of the complete shear layer at a particular position constitutes the "free stream" for the boundary layer, these effects have had to be considered.

Once the boundary layer at a particular position has been identified as being laminar or turbulent in the local sense defined above, then the determination of the local friction, and heat transfer, requires a knowledge of the history and development of the entire shear layer near the model surface.

In this report evidence has been presented to show that along a model surface the boundary layer may be successively laminar, turbulent, laminar, and turbulent again. It was found that with a laminar boundary layer at the base of the cone, the boundary layer on the beginning of the cylinder was also laminar, but that the strong pressure drop at the shoulder had a lasting effect on the subsequent boundary layer development. For a relatively large distance downstream of the pressure drop, it was not sufficient

to describe the boundary layer properties in terms of the local Mach Number just outside of the boundary layer, but rather, the history of the flow had to be considered.

When the boundary layer was turbulent at the cone base, the result of the strong pressure drop was to allow the growth of a laminar boundary layer starting at the beginning of the cylinder. This new laminar boundary layer subsequently underwent transition to a turbulent boundary layer a short distance back on the cylinder. The recovery factors along the cylinder were found to depend on the local laminar or turbulent state of the boundary layer and also upon the history and development of the shear layer near the model surface. These two cases are portrayed in Figure 35.

The second transition from laminar to turbulent flow which occurs on the cylinder of the cone-cylinder model is believed to be controlled by the high turbulence level of the "free stream" for the new laminar boundary layer starting at the beginning of the cylinder. The experimental data are compared with existing low-speed correlations for laminar-turbulent transition in highly turbulent free streams. Further, a compressible analogue for Taylor's turbulence parameter is derived and it is found that at least for the present experiments the error in using low-speed turbulent boundary layer data and the low-speed correlation data should not be large.

While these experiments are at supersonic speeds, the same phenomena would be expected to occur at low speeds given suitable conditions. For instance, wind tunnel contractions have a strong pressure drop and as a result, although the boundary layer in the settling section is turbulent, the boundary layer on the nozzle wall may be laminar.

Joseph Sternberg

JOSEPH STERNBERG

ACKNOWLEDGMENT

The author wishes to thank Professor F. H. Clauser for his stimulating interest and for his persistent encouragement in bringing this research to fruition.

Preliminary experiments (using a wooden model) on the effect of the corner expansion on the temperature recovery factors were made in association with Mr. B. des Clers. Recovery temperature variations qualitatively similar to those shown herein were obtained, but the situation was confused by the large heat transfer in the model resulting from its construction, and from our inability, at that time, to satisfactorily reproduce the recovery factor levels on successive tests. The lucite model was designed to greatly lessen the model heat transfer.

The author wishes to thank Miss Carol Sande for her substantial help in transcribing the manuscript and in proofreading the report.

APPENDIX

APPLICATIONS TO WIND TUNNEL CONTRACTIONS

In an ordinary wind tunnel contraction section, the conditions of the linear theory are not satisfied anywhere in the contraction. Viscous dissipation is important and there is a continuous readjustment of the turbulent energy in the contraction since anisotropic flows, left to their own devices, tend to become isotropic.

Ribner and Tucker have compared the results of their analysis with available experiments by accounting for viscous dissipation in an approximate way. The changes in the contraction are considered to be a step by step process, where for each step there is a change of energy associated with the stream deformation and a change of energy due to viscous dissipation. In most of the experiments, turbulent intensity measurements were made in the settling section and in the test section. Surprisingly enough, the experiments are in reasonably good agreement with the calculations. However, MacPhail[22] made measurements on the axis all along the contraction. While the ratio of the lateral turbulent intensity at the test section to that in the settling section is not too far from the prediction, the lateral velocity ratios along the contraction are much larger than predicted, and are, in fact, larger than would be obtained neglecting viscous decay. MacPhail also made some measurements in a channel of approximately constant velocity where the cross-section was gradually changed from a high narrow rectangle to a low wide rectangle of the same area. Again the development of the turbulent velocity components does not seem to be predictable on the basis of fluid element deformation. In addition to unpredicted variations of the turbulence intensity in the deforming section, there seems to be an oscillatory exchange of energy between the fluctuation components in the fixed section following the deformation. MacPhail suggests that some sort of gyroscopic action may be involved so that the initial change of orientation of the vorticity vector is not that predicted by Taylor's linear theory. In this concept, the vortex cores exhibit some of the characteristics of solid bodies.

Some comments can be made on MacPhail's suggestion that a gyroscopic action may be present. For solid bodies, a precessional motion of a rotating body is maintained by an external couple, since the precessional motion involves a time rate of change of angular momentum of the rotating body. The mean motion in a wind tunnel contraction (neglecting the wall boundary layer) is represented by an irrotational solution. This means that the fluid element deformations imparted by the contraction do not change the angular momentum of the fluid elements. Therefore, the fluid in the vortex core should not precess at least in the conventional gyroscopic sense. If MacPhail's measurements are correct and the vortices turn in a way not predicted by the fluid deformation theory, then possibly an explanation of the measurements should require consideration of secondary flow in the vortex cores as they pass through the contraction.

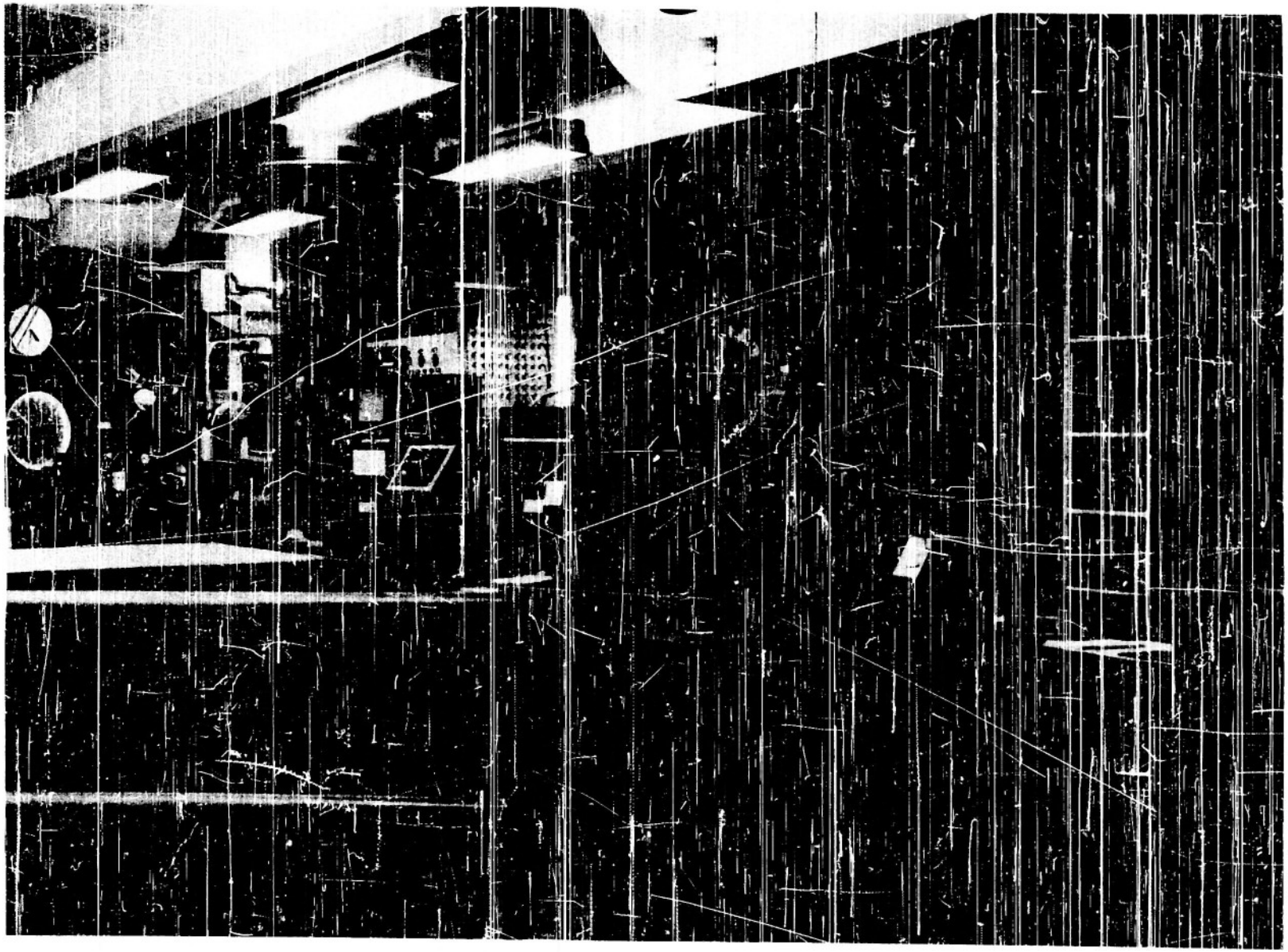

FIG. 1. View of Flexible Nozzle Tunnel

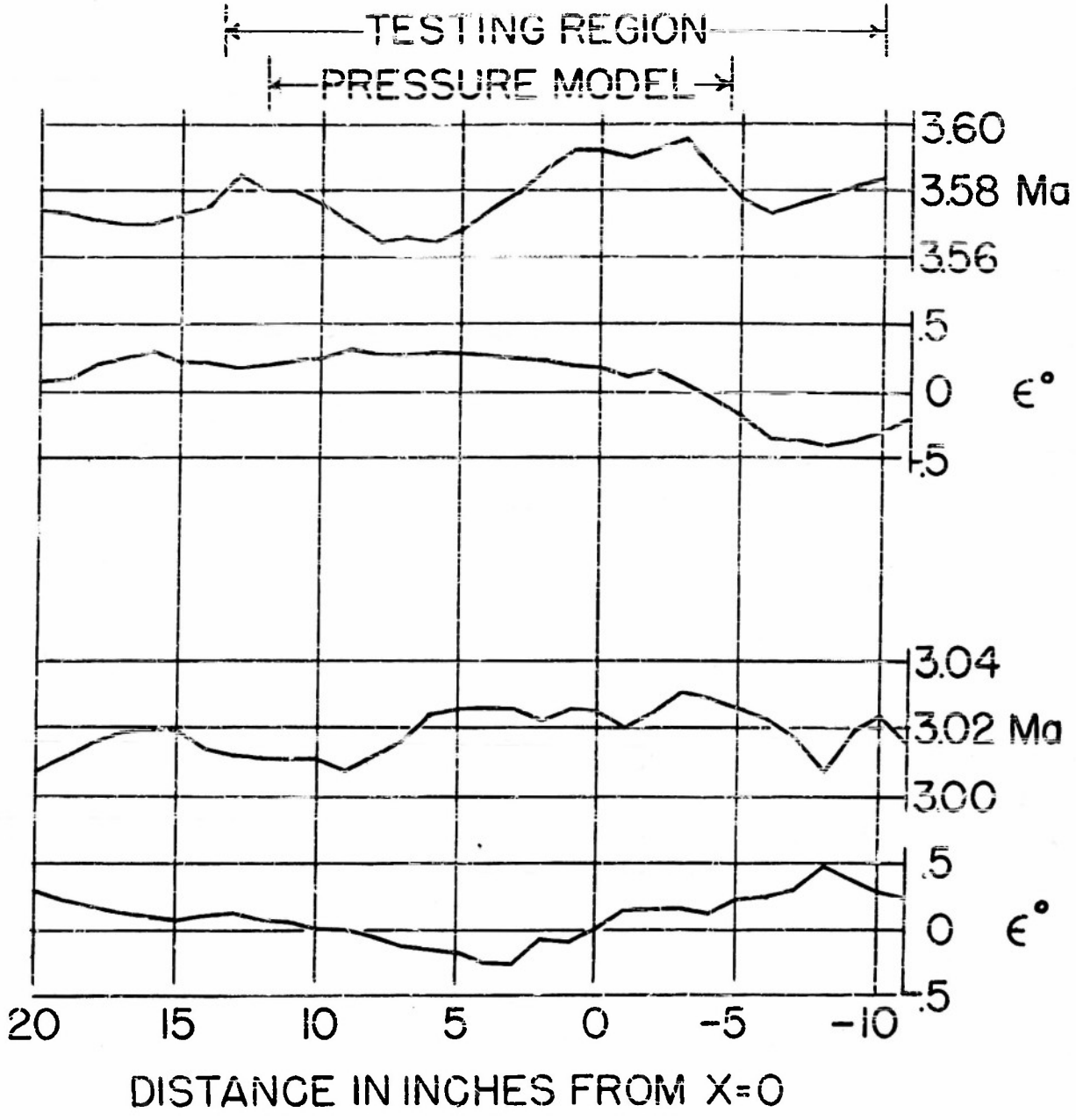

FIG. 2. Flow Distribution in Test Nozzles

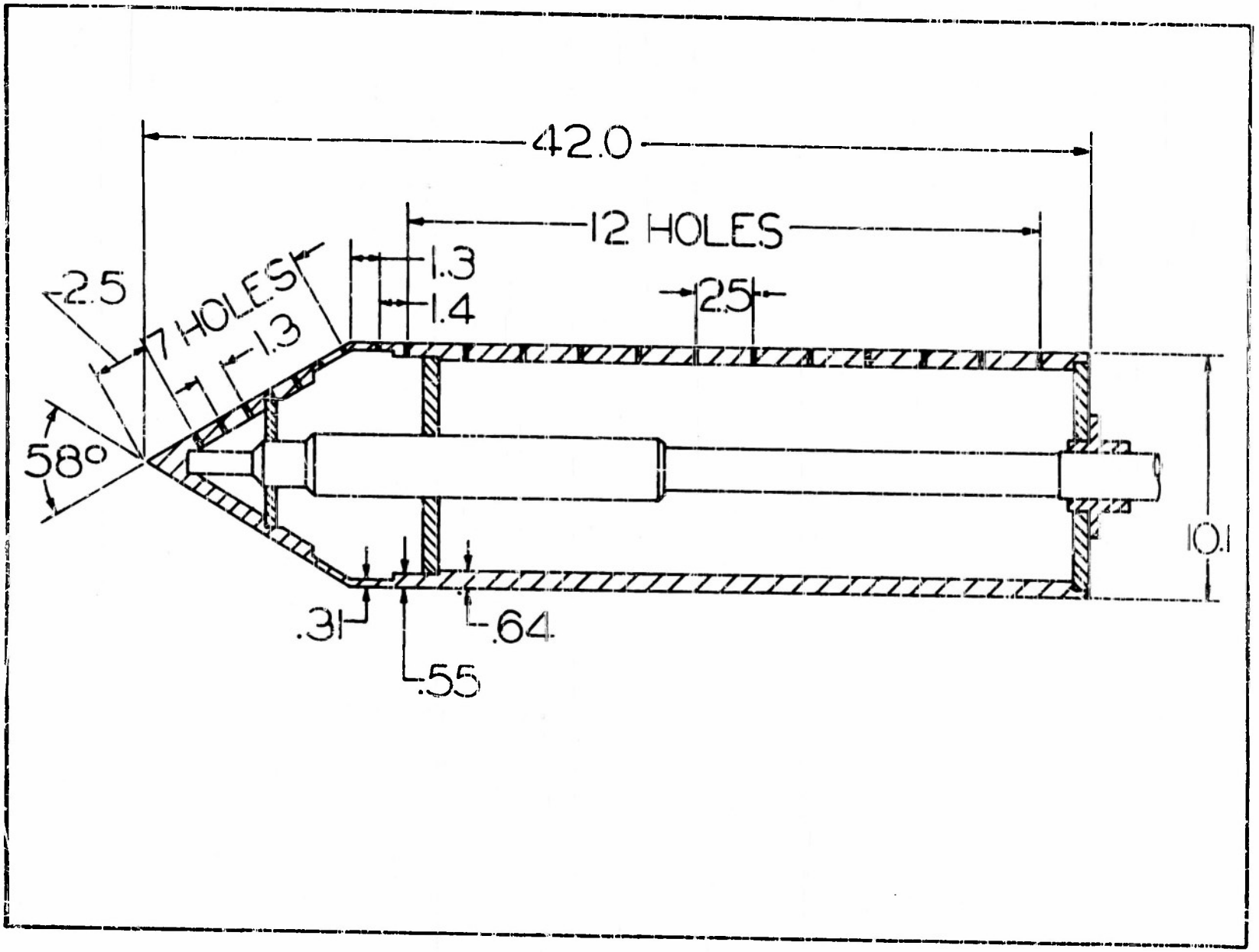

FIG. 3. Temperature Recovery Cone Cylinder Model

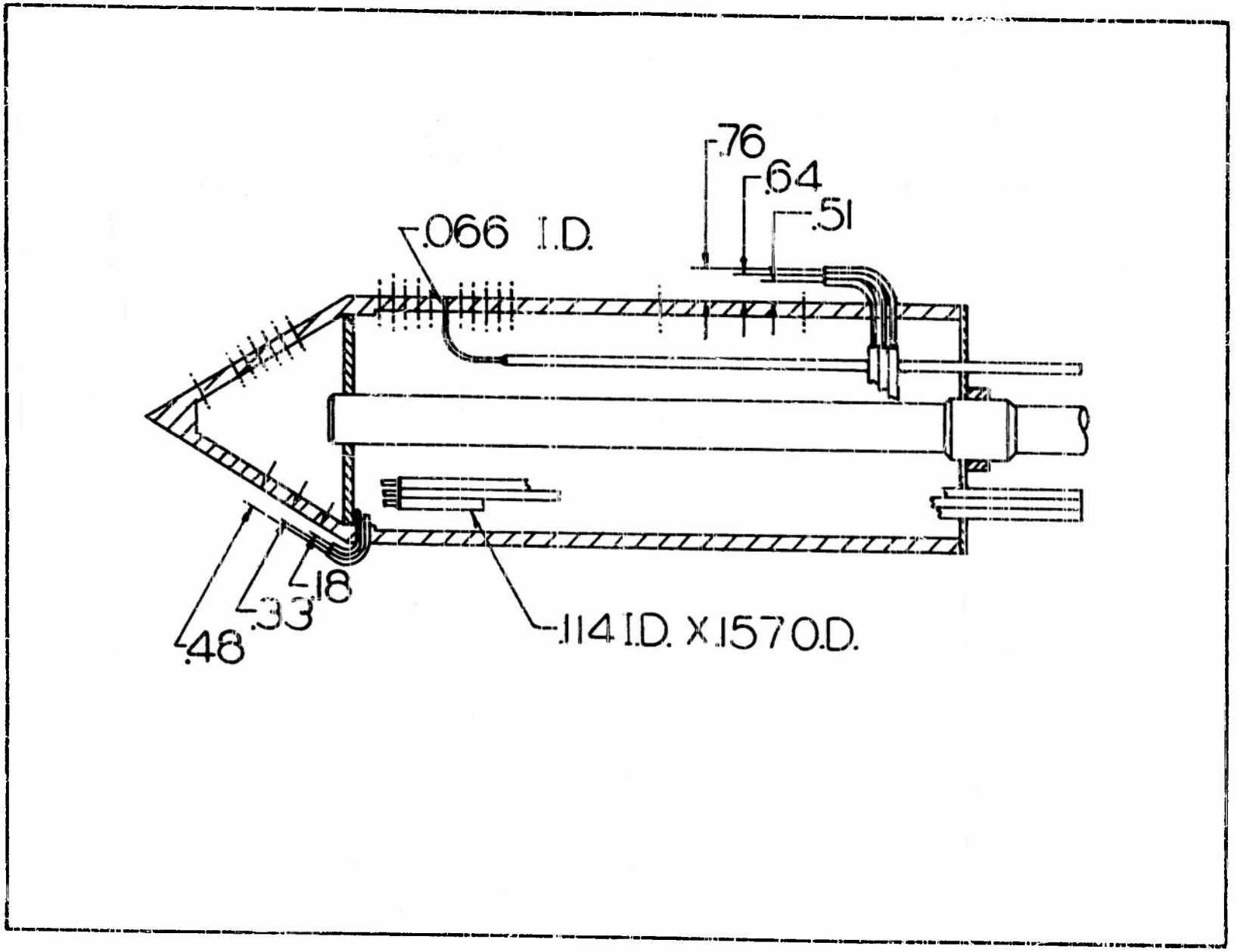

FIG. 4. Cone Cylinder Pressure Model

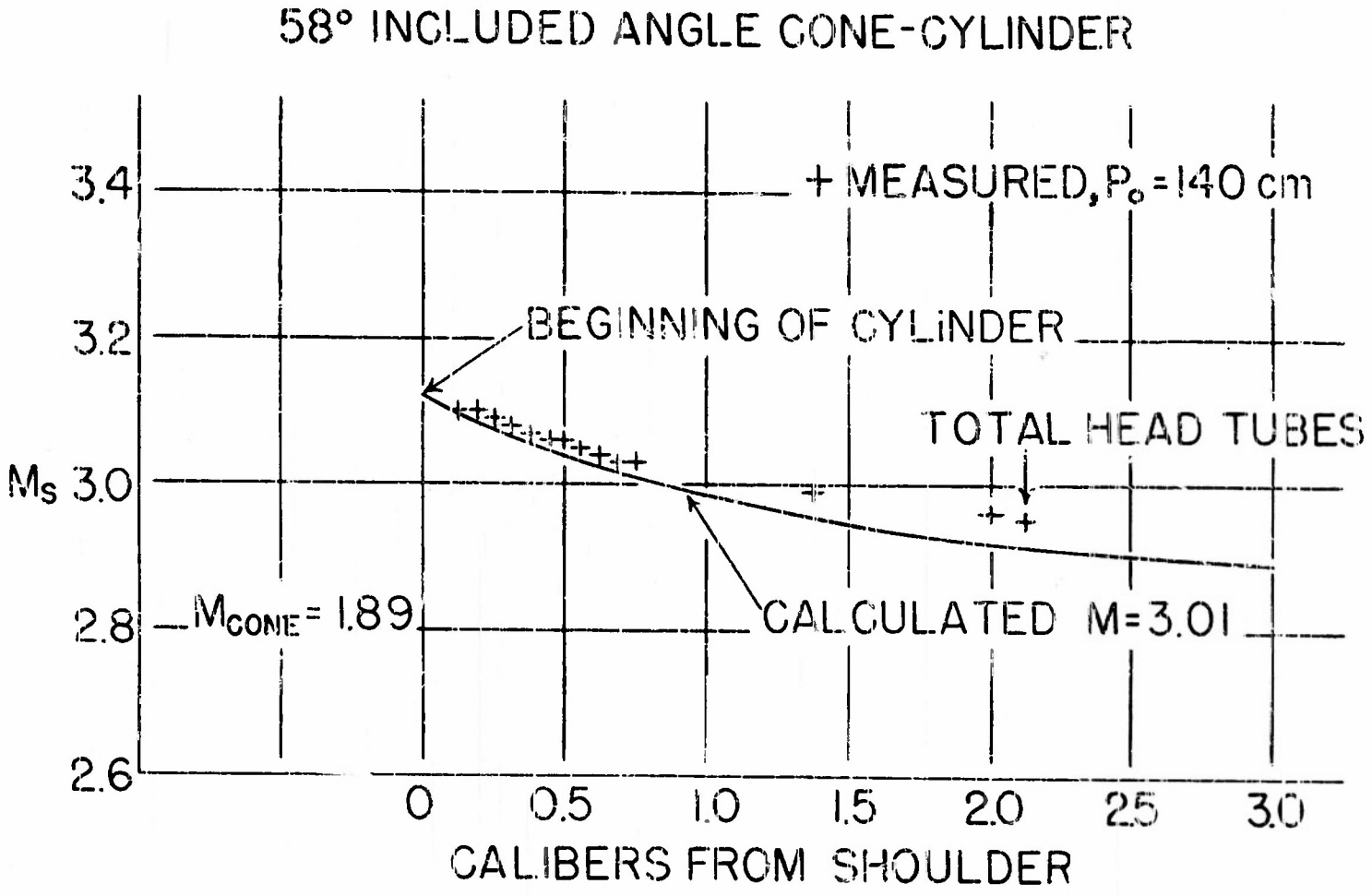

FIG. 5. Surface M Distribution at M = 3.02

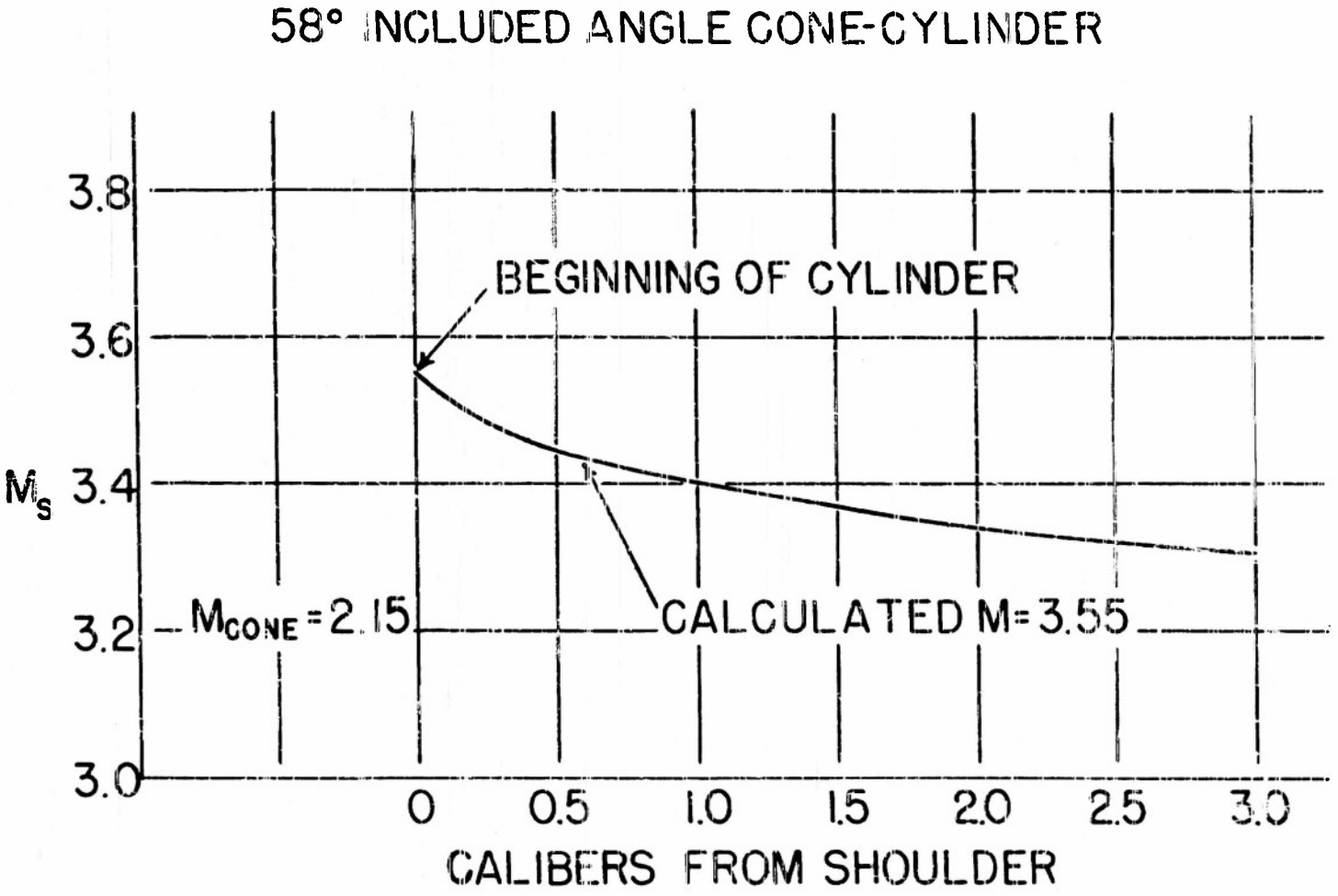

FIG. 6. Surface M Distribution at M = 3.55

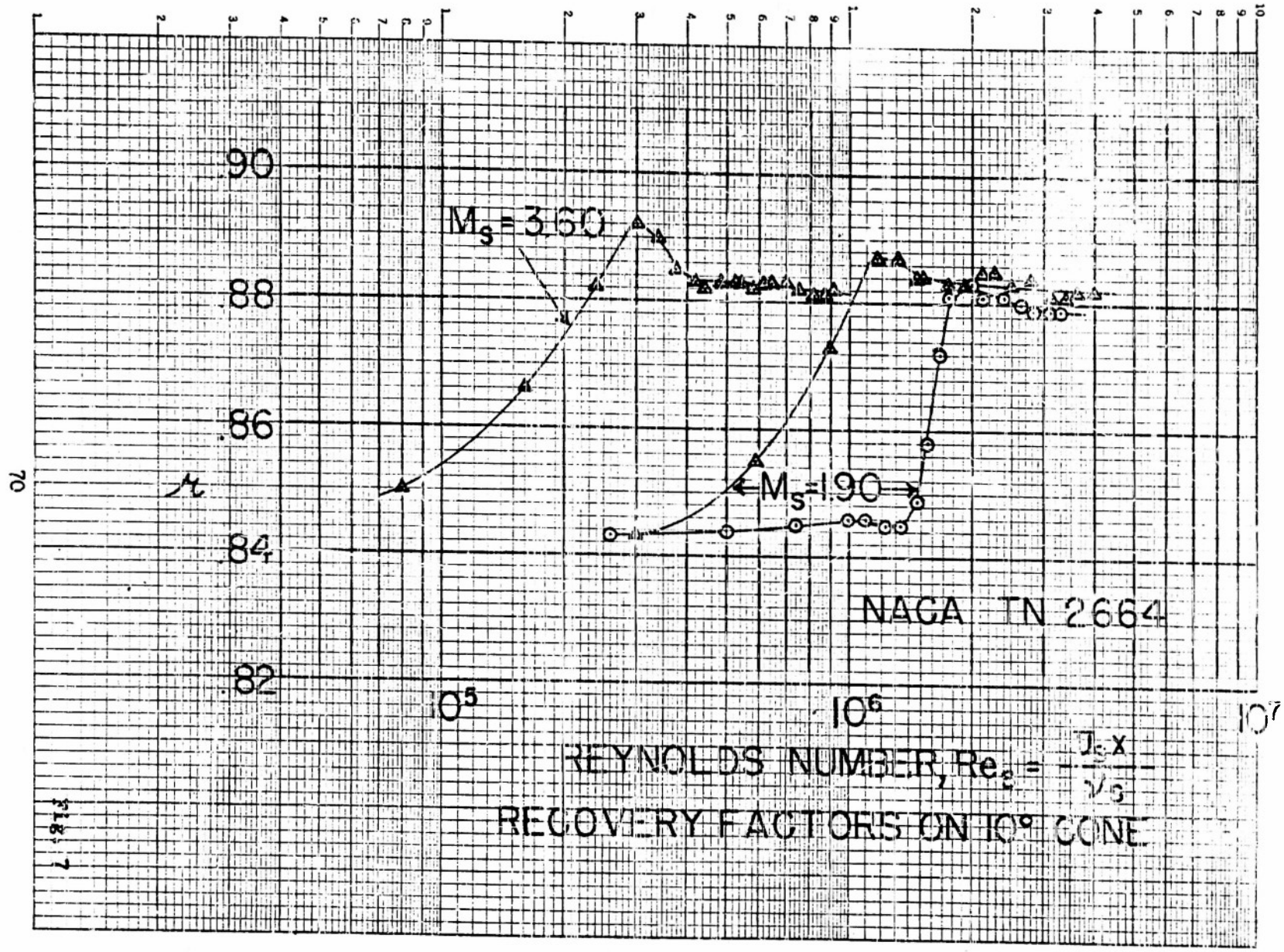

Laminar, Transitional, and Turbulent Temperature Recovery Factors

FIG. 8. Shadowgraph at P_o = 140 cm. - Cone M = 3.02

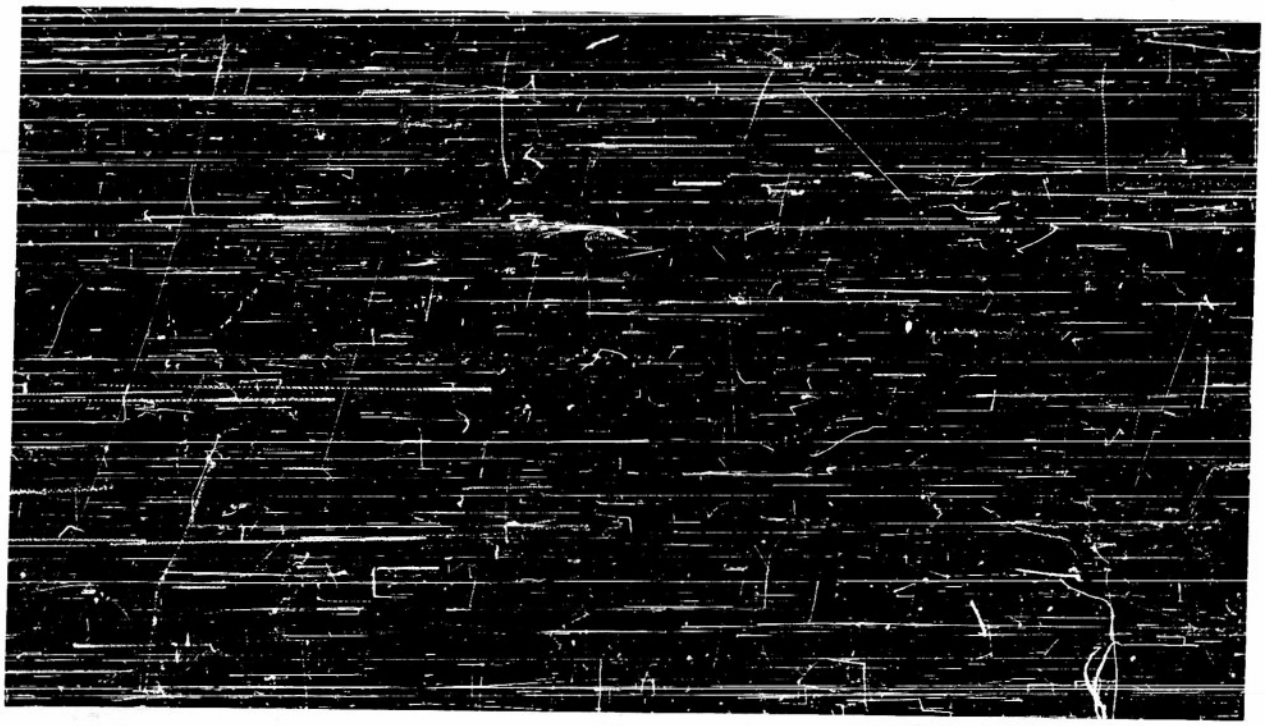

FIG. 9. Shadowgraph at P_o = 140 cm. - M = 3.02 Transition on Cylinder

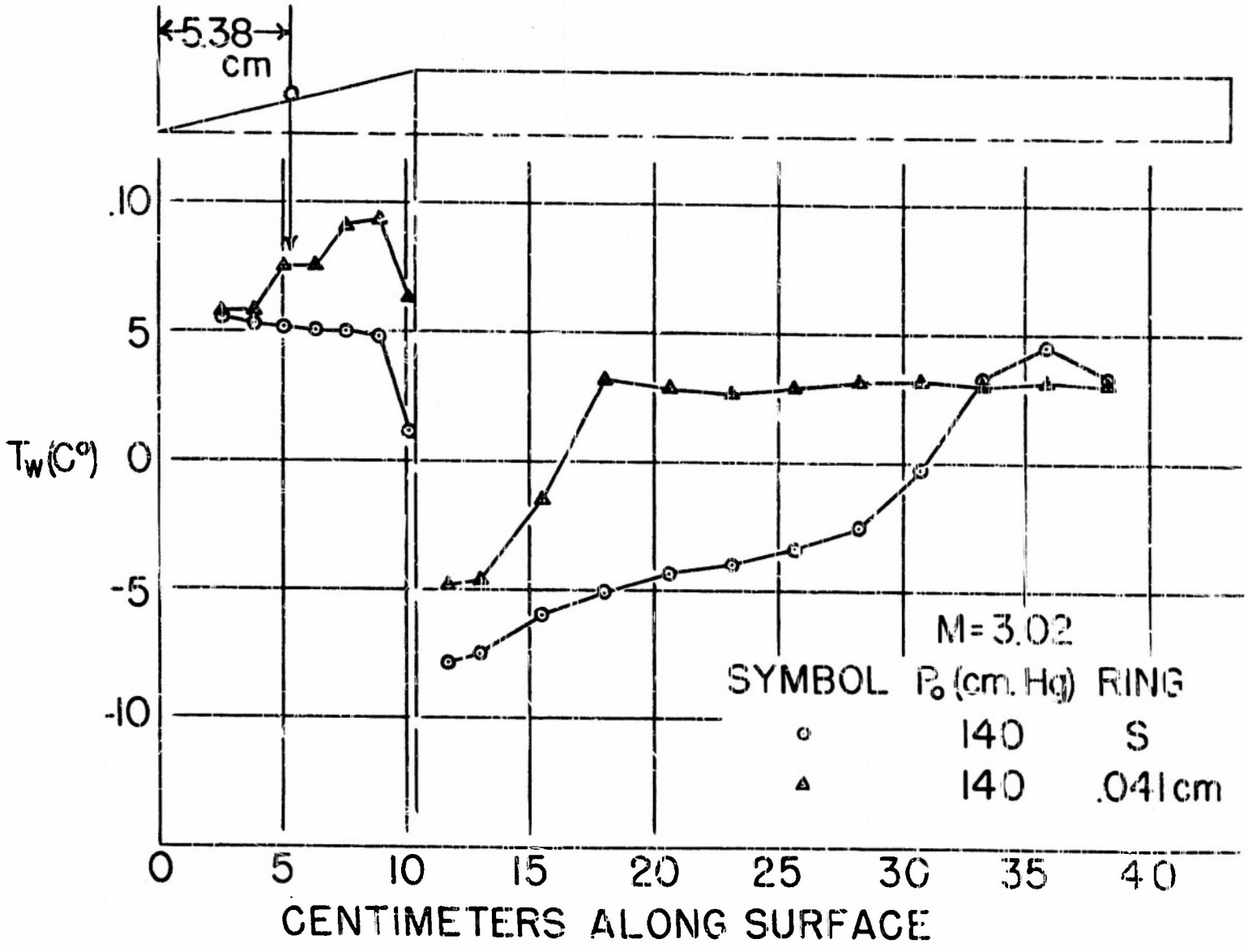

FIG. 10. Surface Temperatures at M = 3.02

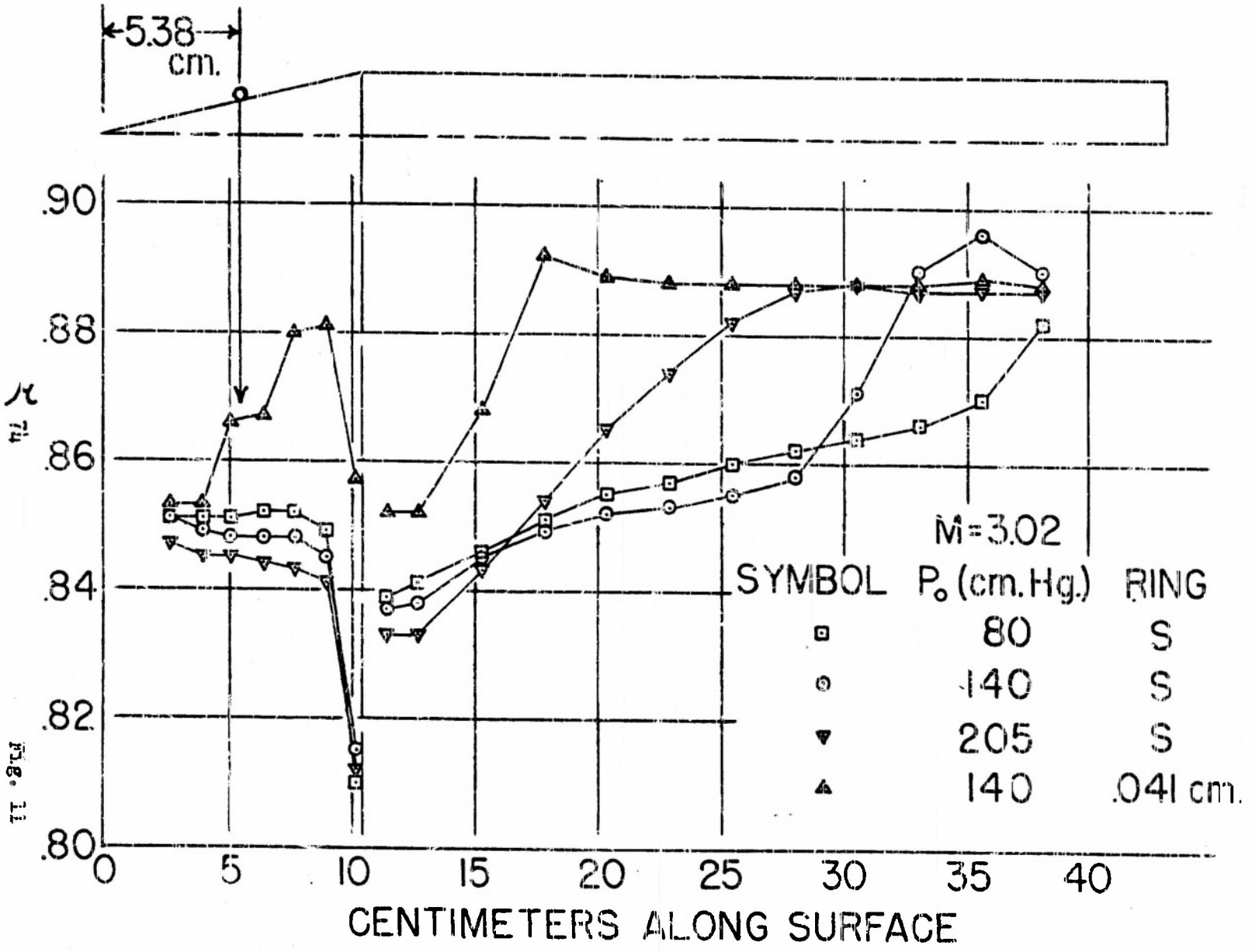

Fig. 11

Temperature Recovery Factors at M = 3.02 Smooth and Rough

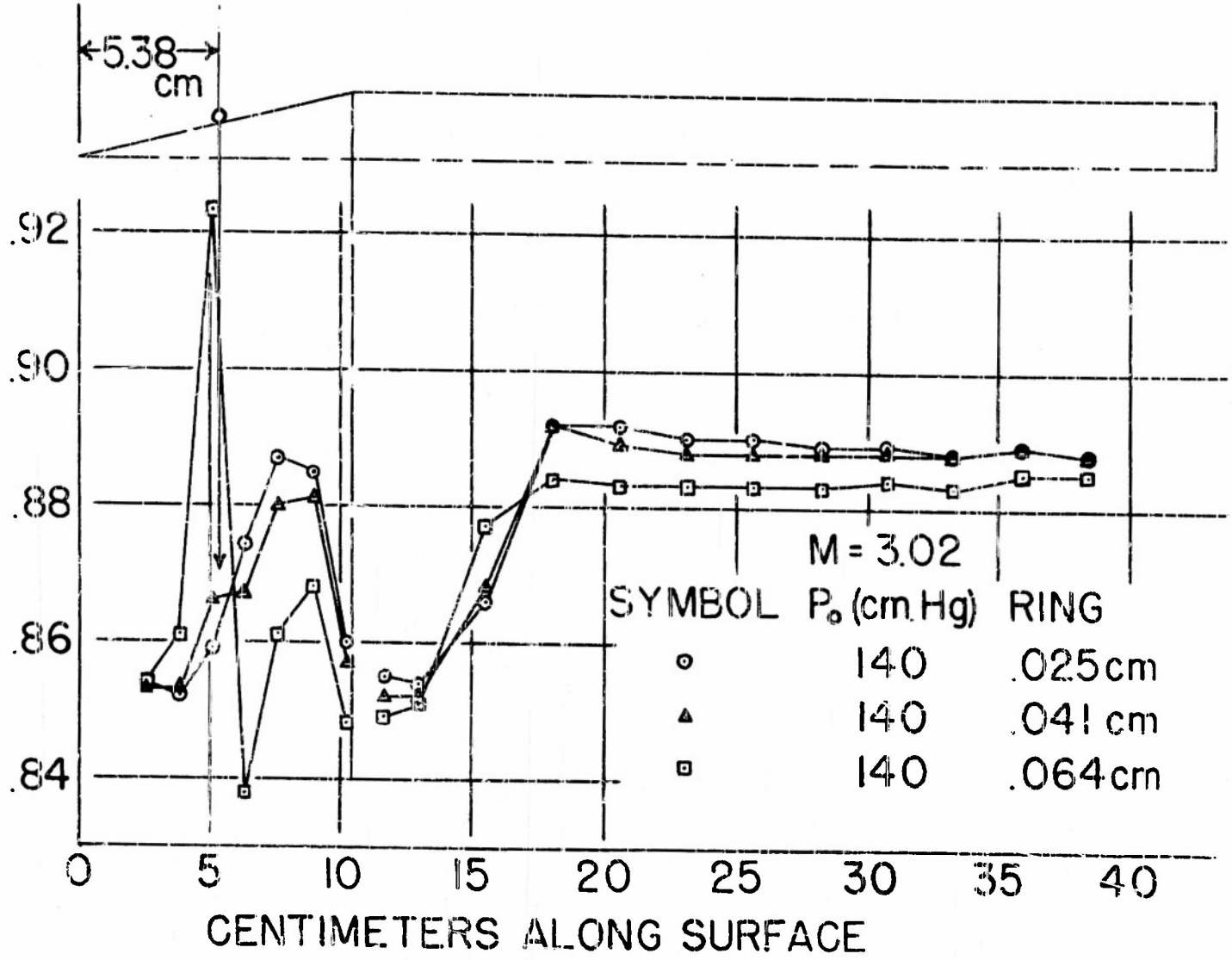

FIG. 12. Temperature Recovery Factors at M = 3.02

FIG. 13 (a). Shadowgraphs with Wire Trips M = 3.02 P_o = 140 cm. (a) Trip - .025 cm.

FIG. 13 (b). Shadowgraphs with Wire Trips M = 3.02 P_o = 140 cm. (b) Trip - .041 cm.

FIG. 13 (c). Shadowgraphs with Wire Trips M - 3.02 P_o = 140 cm. (c) Trip - .064 cm.

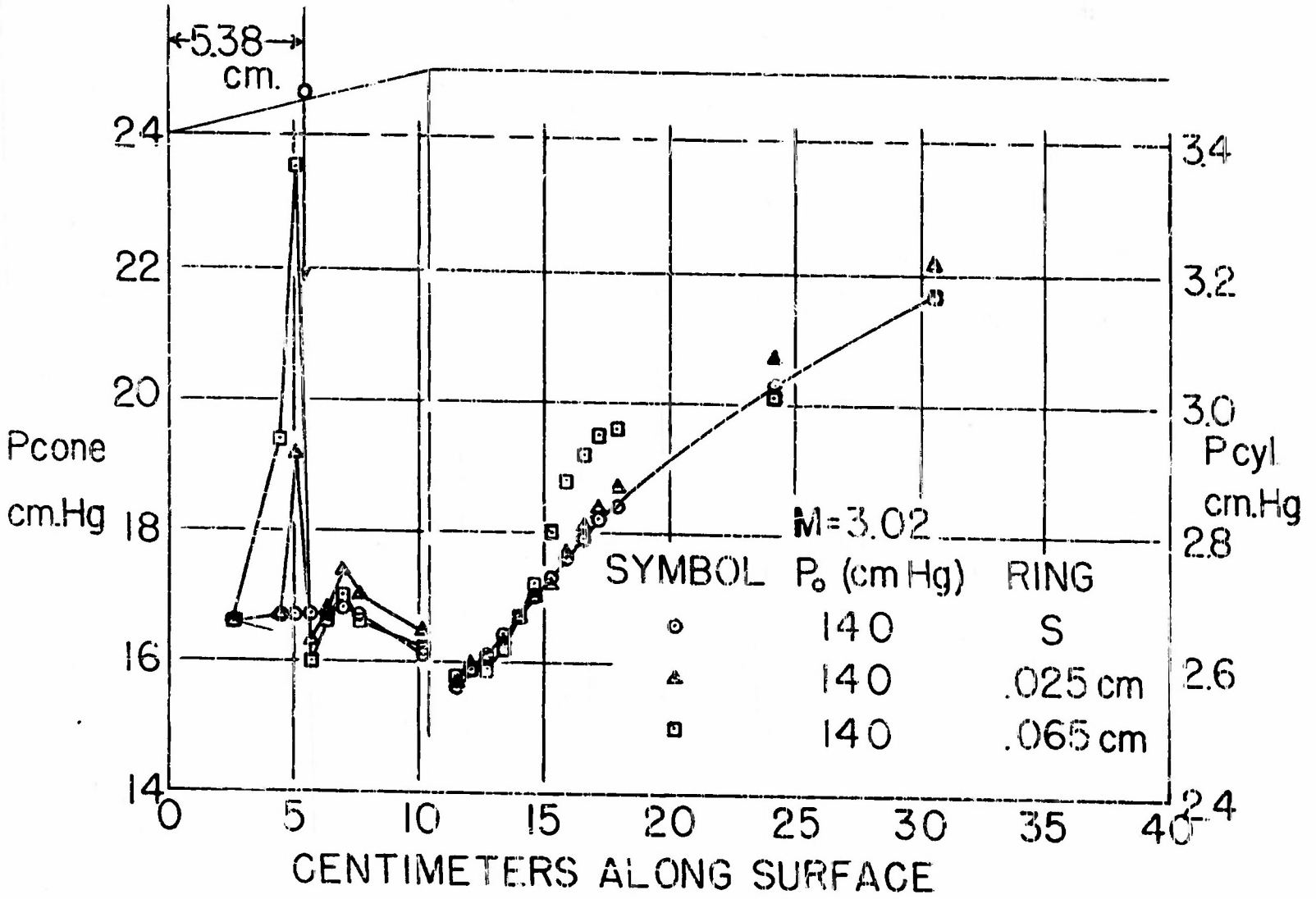

FIG. 14. Static Pressures with and without Trips

FIG. 15. Shadowgraph on Cylinder M = 3.02 , .041 cm. wire trip P_O = 140 cm.

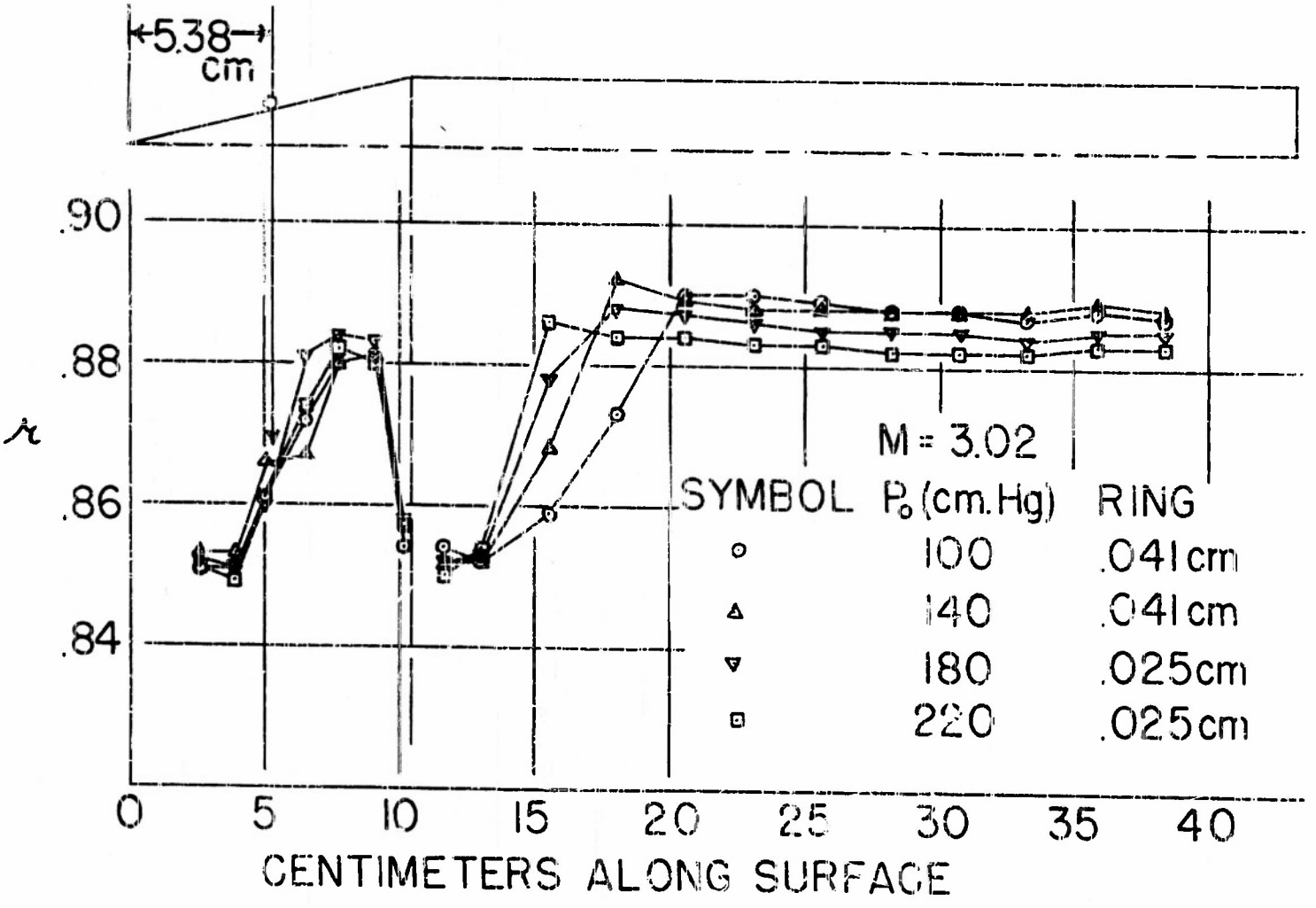

FIG. 16. Temperature Recovery Factors M = 3.02 Various Pressure Levels

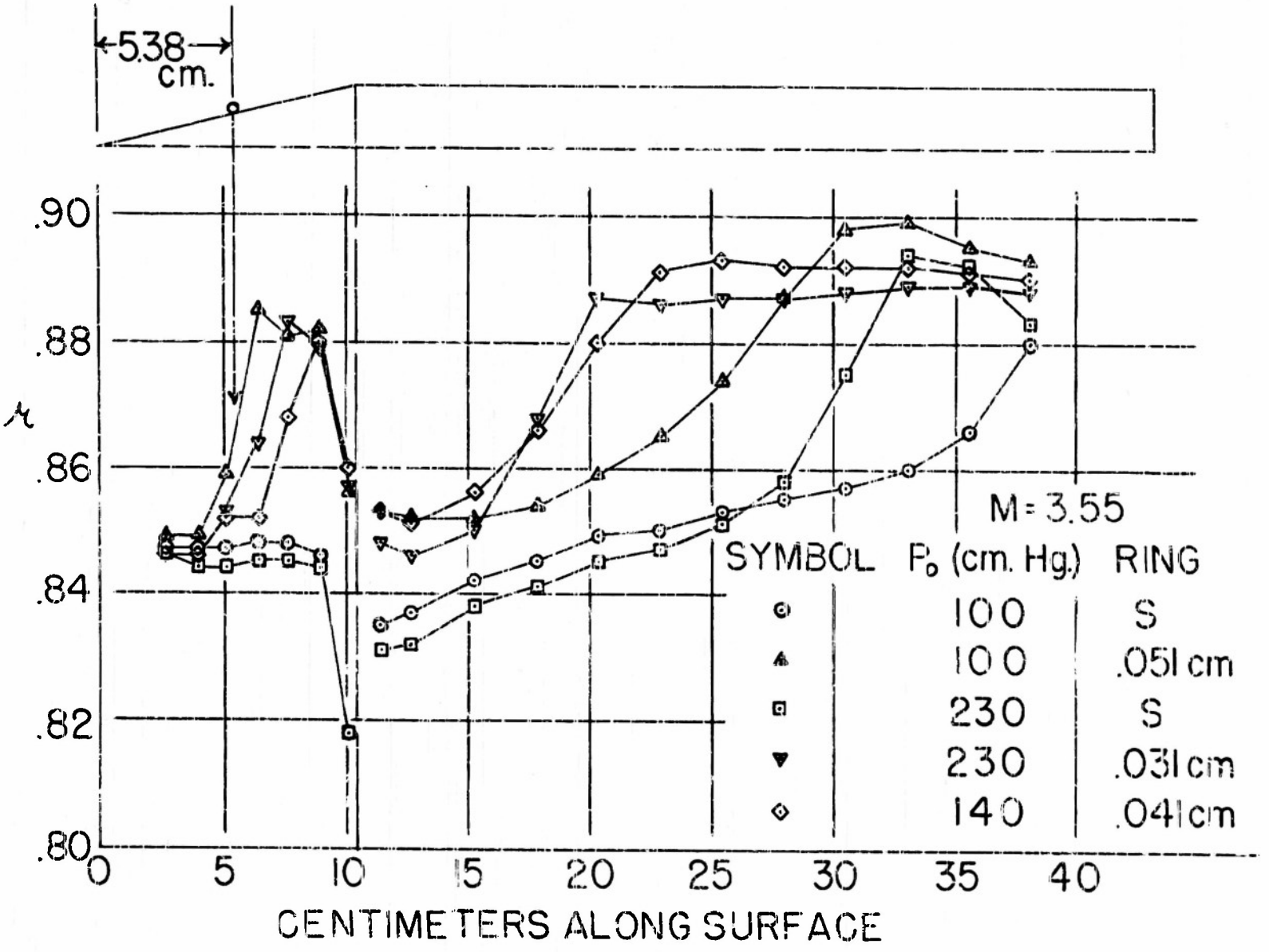

FIG. 17. Temperature Recovery Factors M = 3.55 Various Pressure Levels

FIG. 18 (a). Shadowgraph of New Laminar Boundary Layer P_o = 180 cm. - M = 3.02 (a) on cone

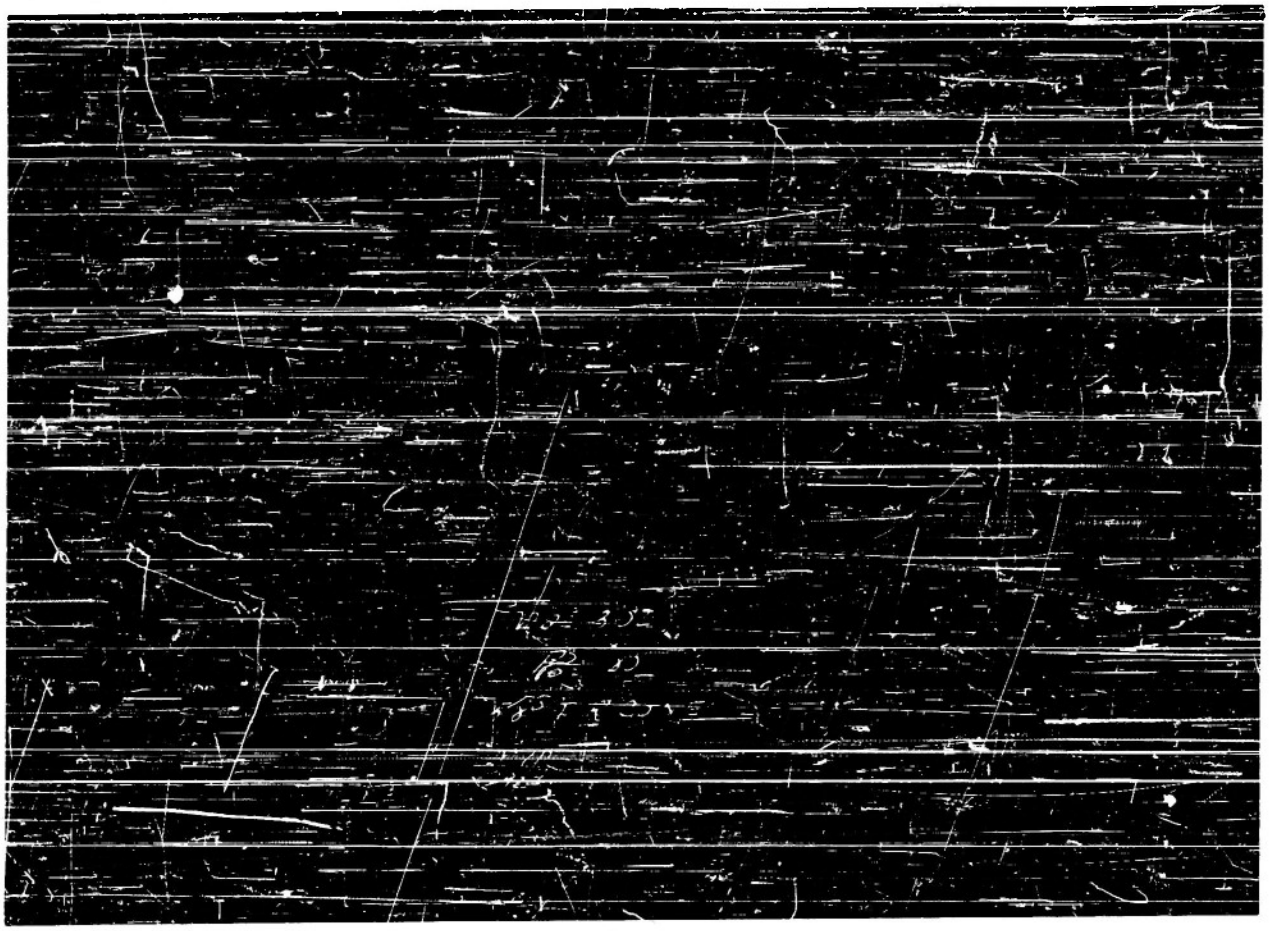

FIG. 18 (b). Shadowgraph of New Laminar Boundary Layer P_o = 180 cm. - M = 3.02 (b) on cylinder

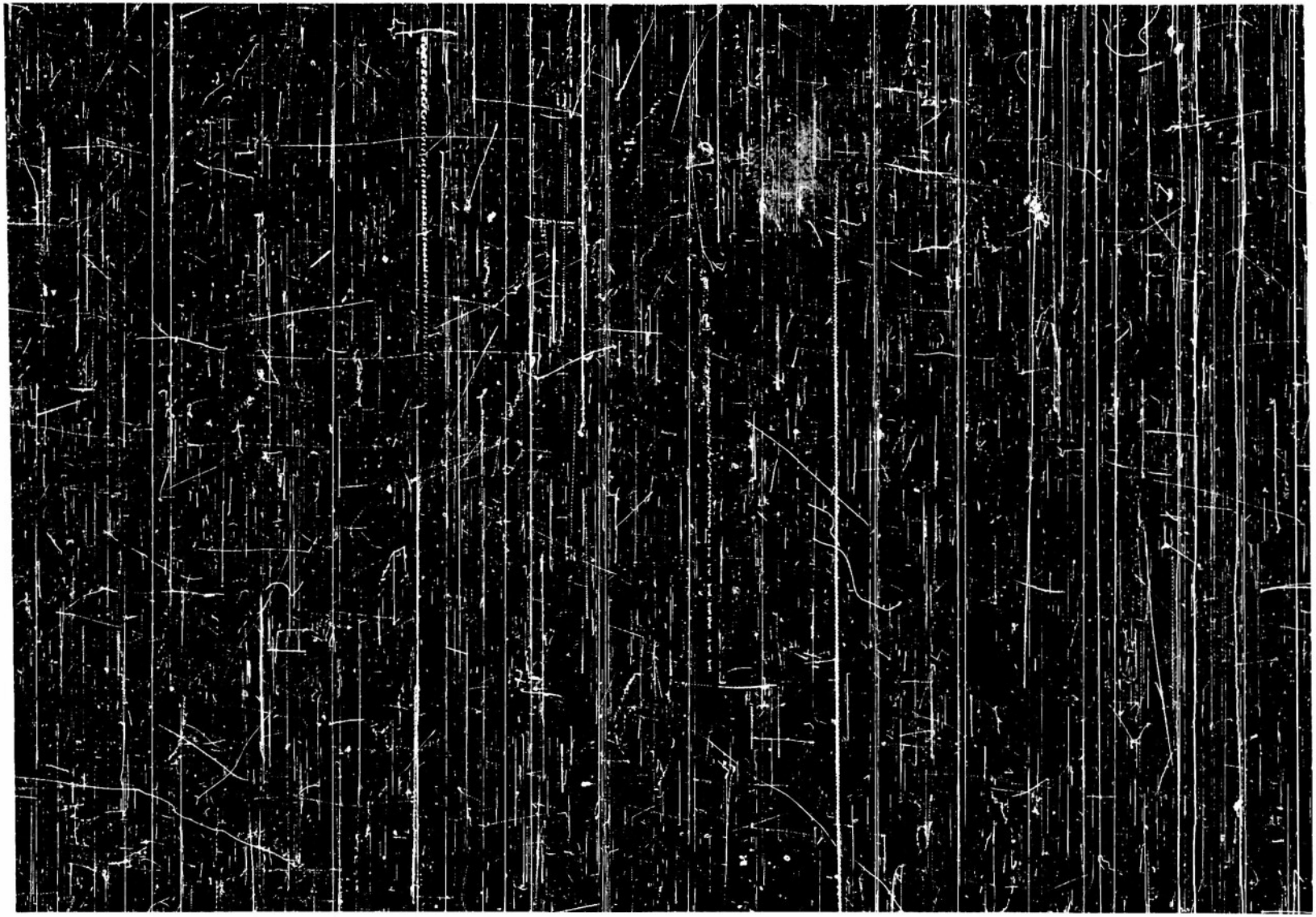

FIG. 19. Shadowgraph of 20° Cone Showing Wavy Laminar Boundary Layer

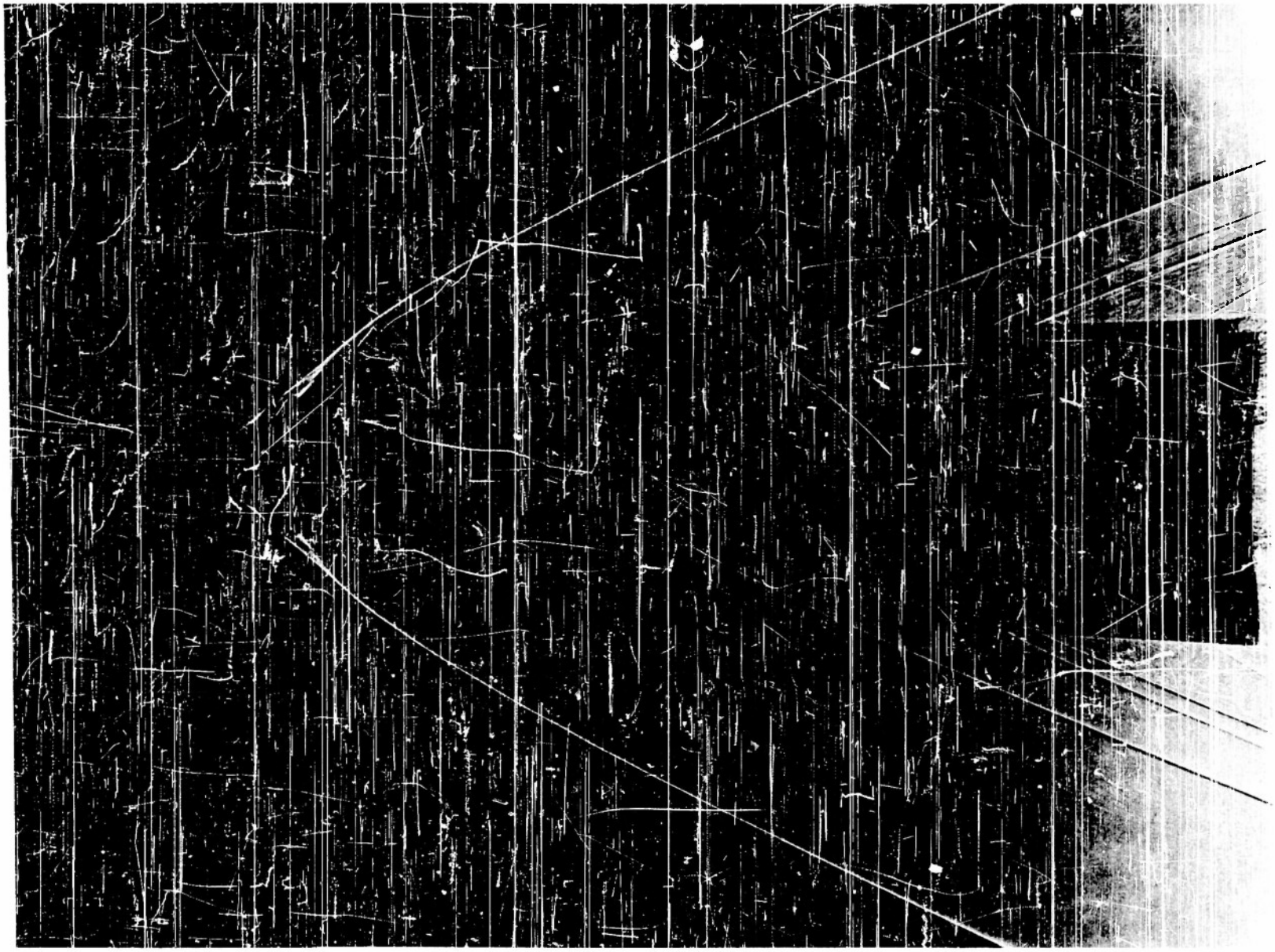

FIG. 20. Shadowgraph of 20 mm. Free Flight Cone Cylinder Model

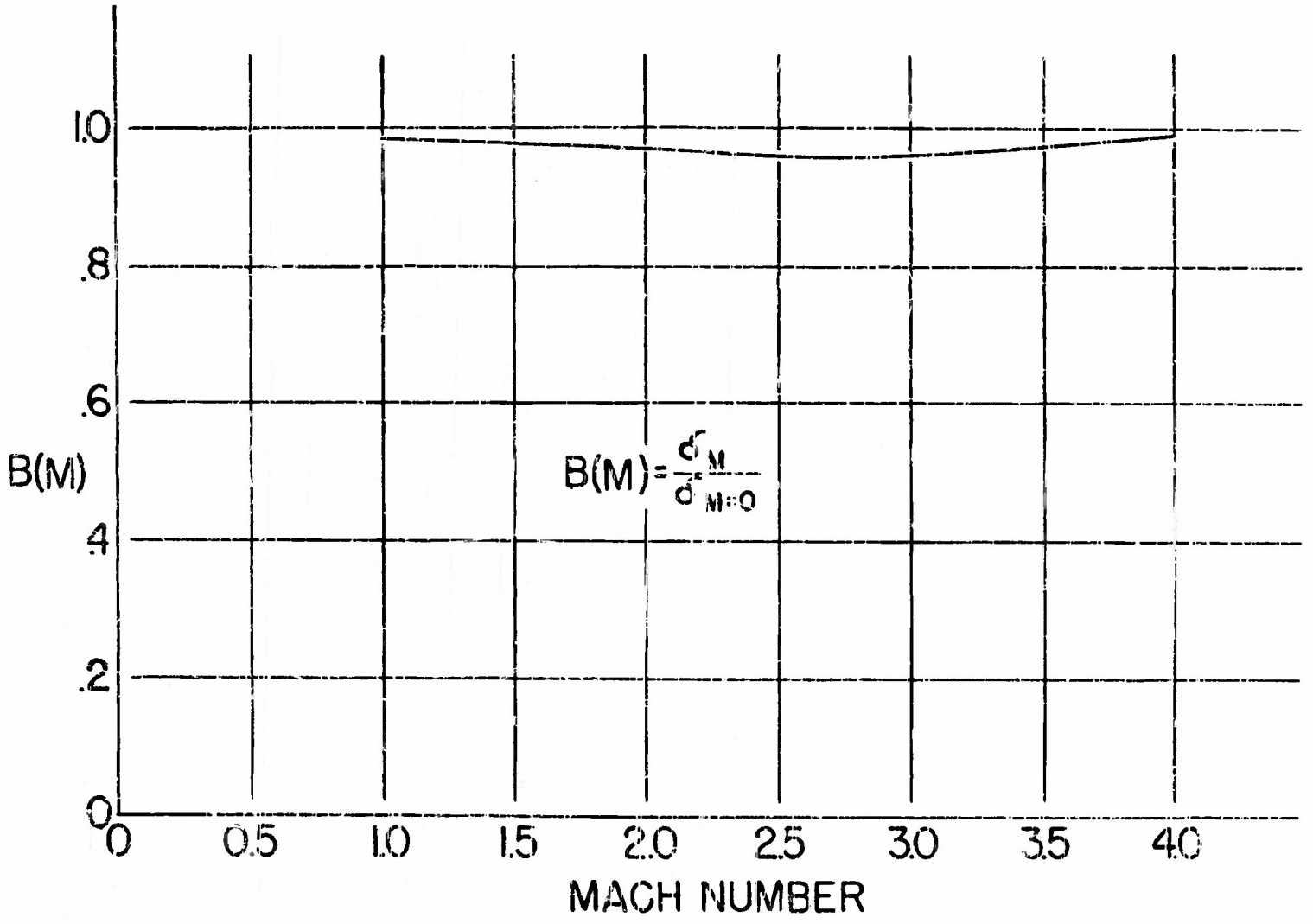

FIG. 21. Compressible Turbulent Boundary Layer Thickness

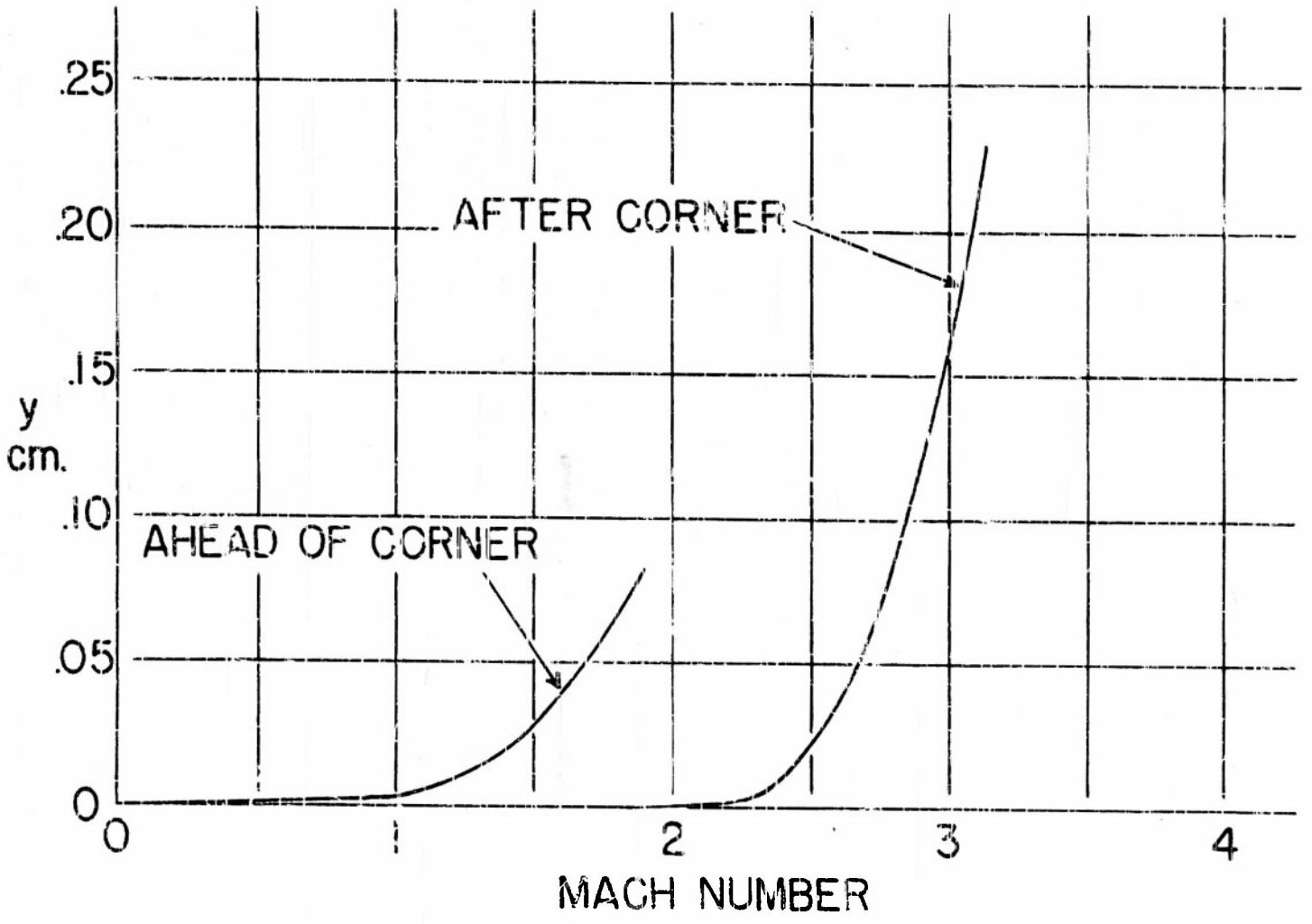

FIG. 22. Effect of Corner on Turbulent Boundary Layer

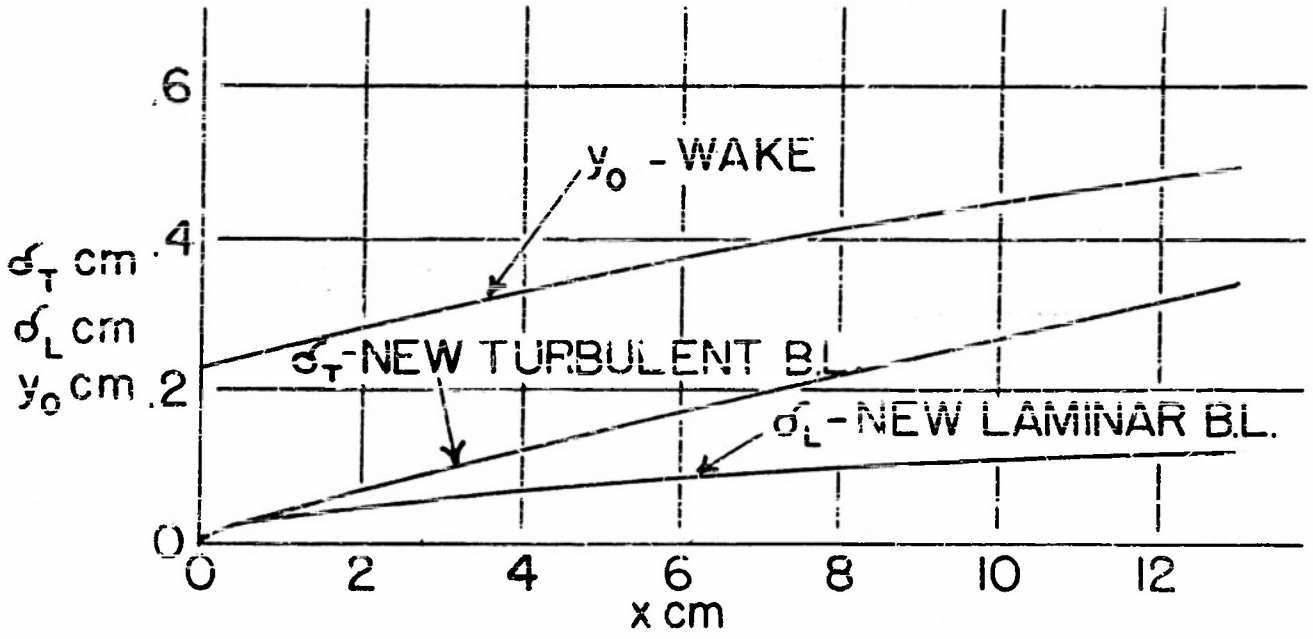

TURBULENT AHEAD OF CORNER

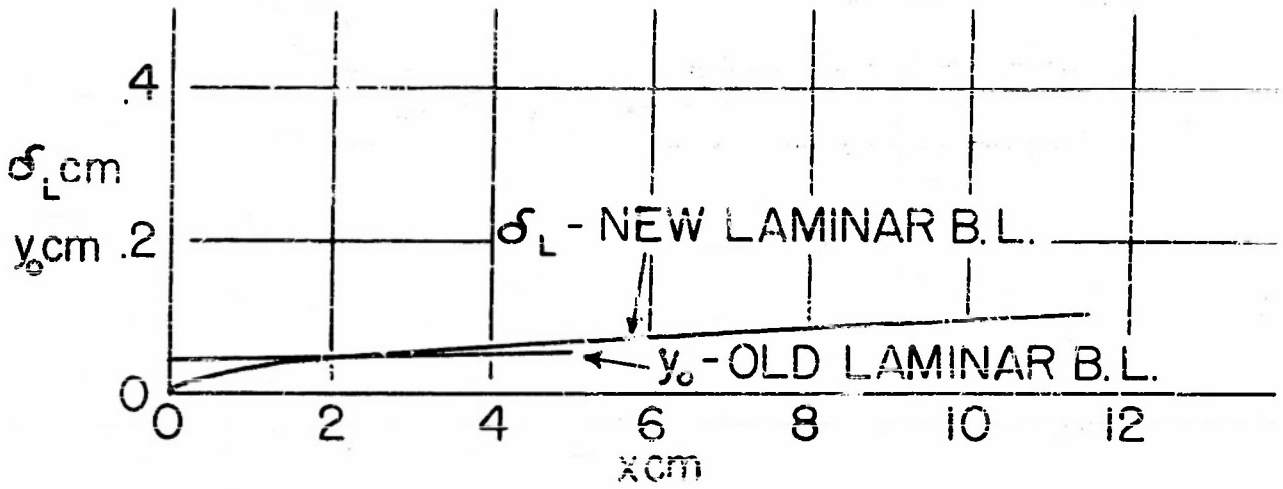

LAMINAR AHEAD OF CORNER

FIG. 23. New Laminar and Turbulent Boundary Layer Growth

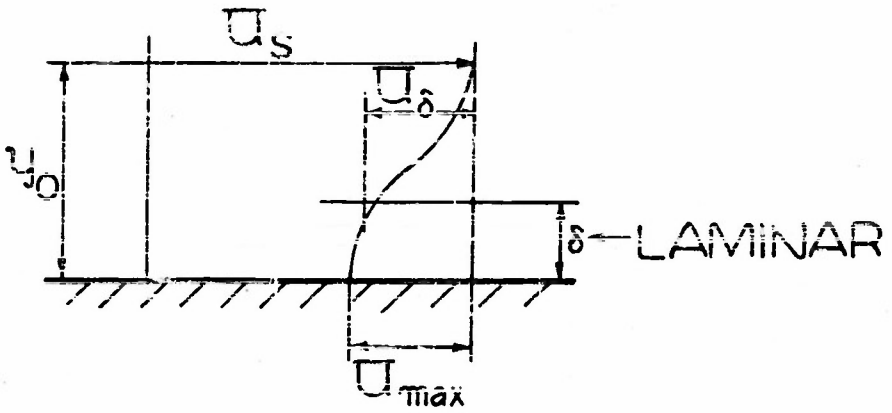

$$y'_0 + \delta \approx y_0$$

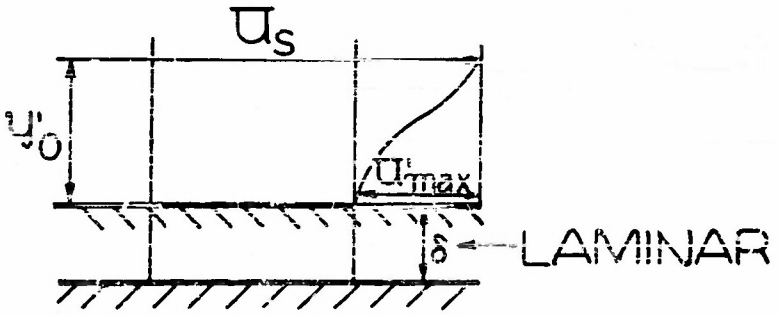

$$U_\delta \approx U'_{max}$$

GROWTH OF EFFECTIVE WAKE

Fig. 24

Growth of Eifective Wake

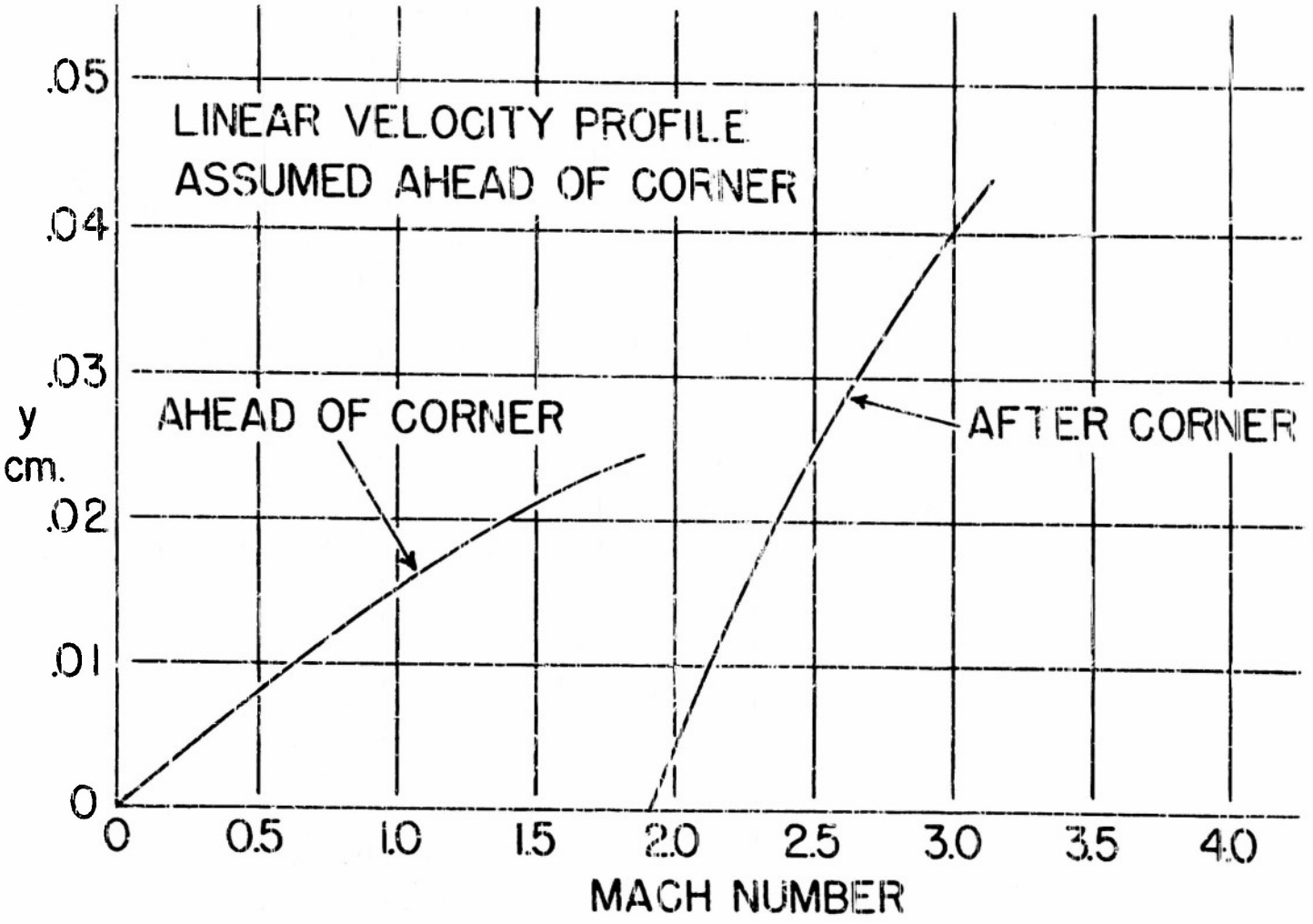

FIG. 25. Effect of Corner on Laminar Boundary Layer

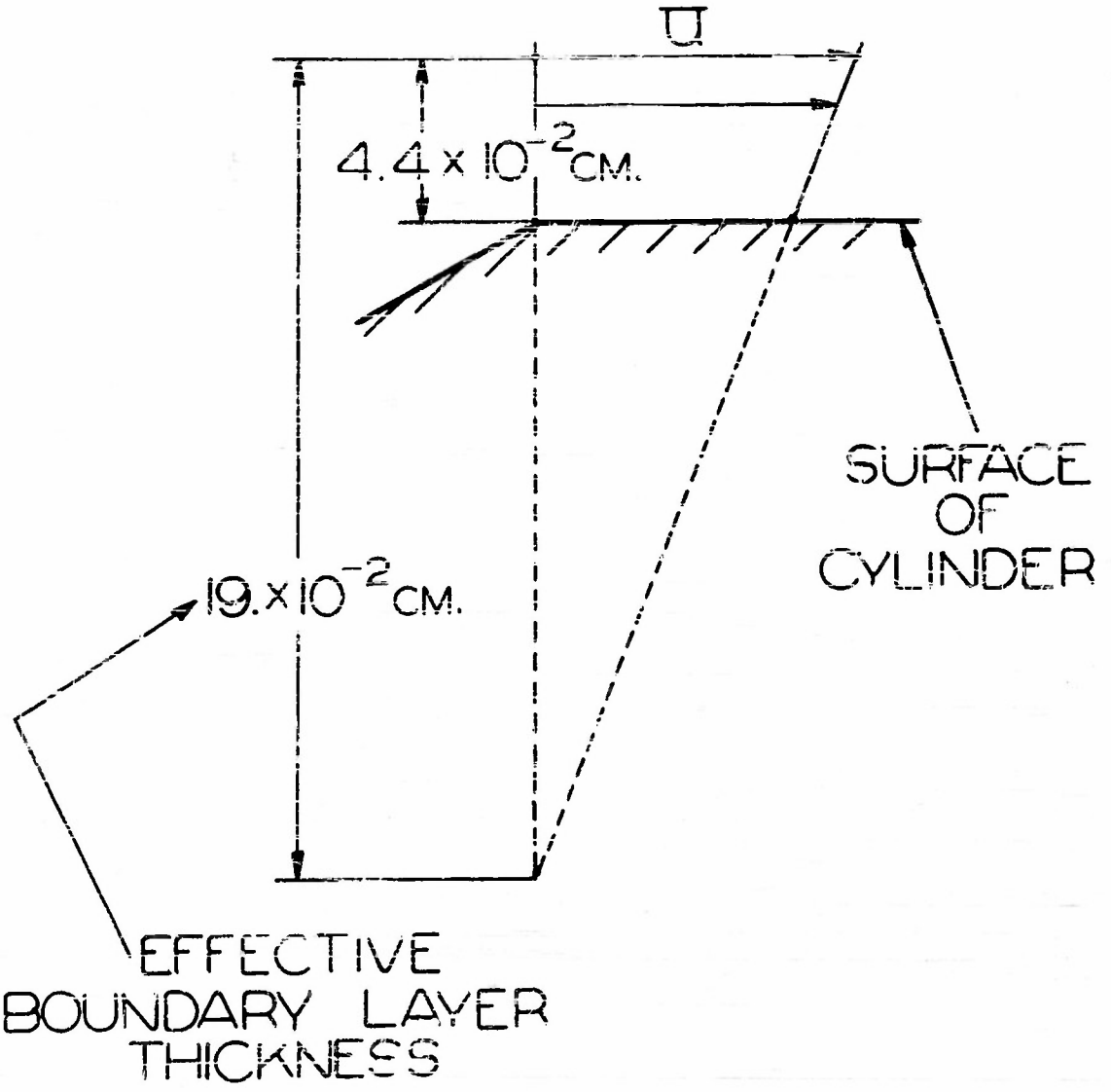

FIG. 26. Old Shear Layer After Corner

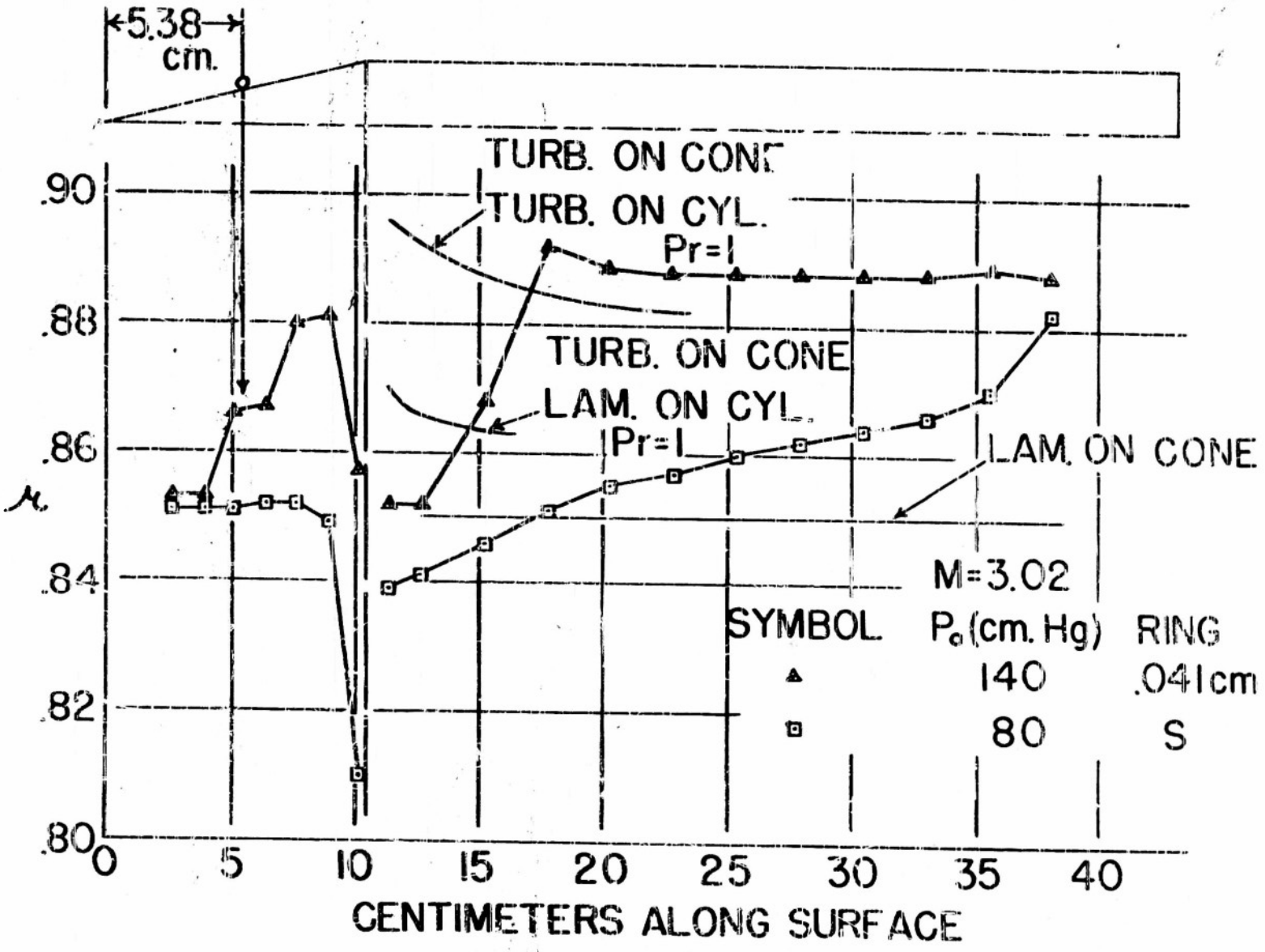

FIG. 27. Comparison of Estimated and Experimental Temperature Recovery Factors on Cylinder

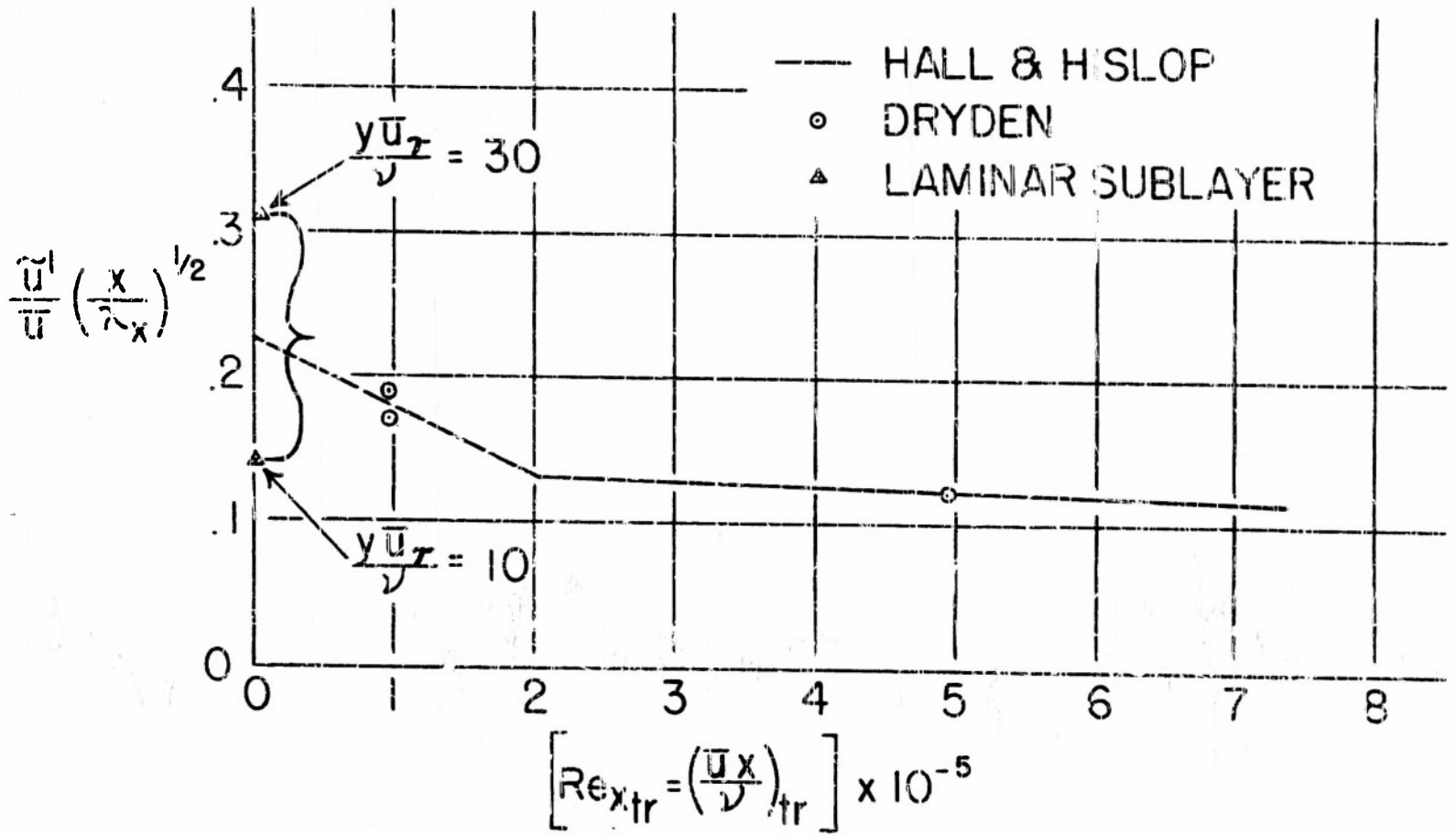

FIG. 28. Low Speed Correlation Curve for Transition by Strong Turbulence

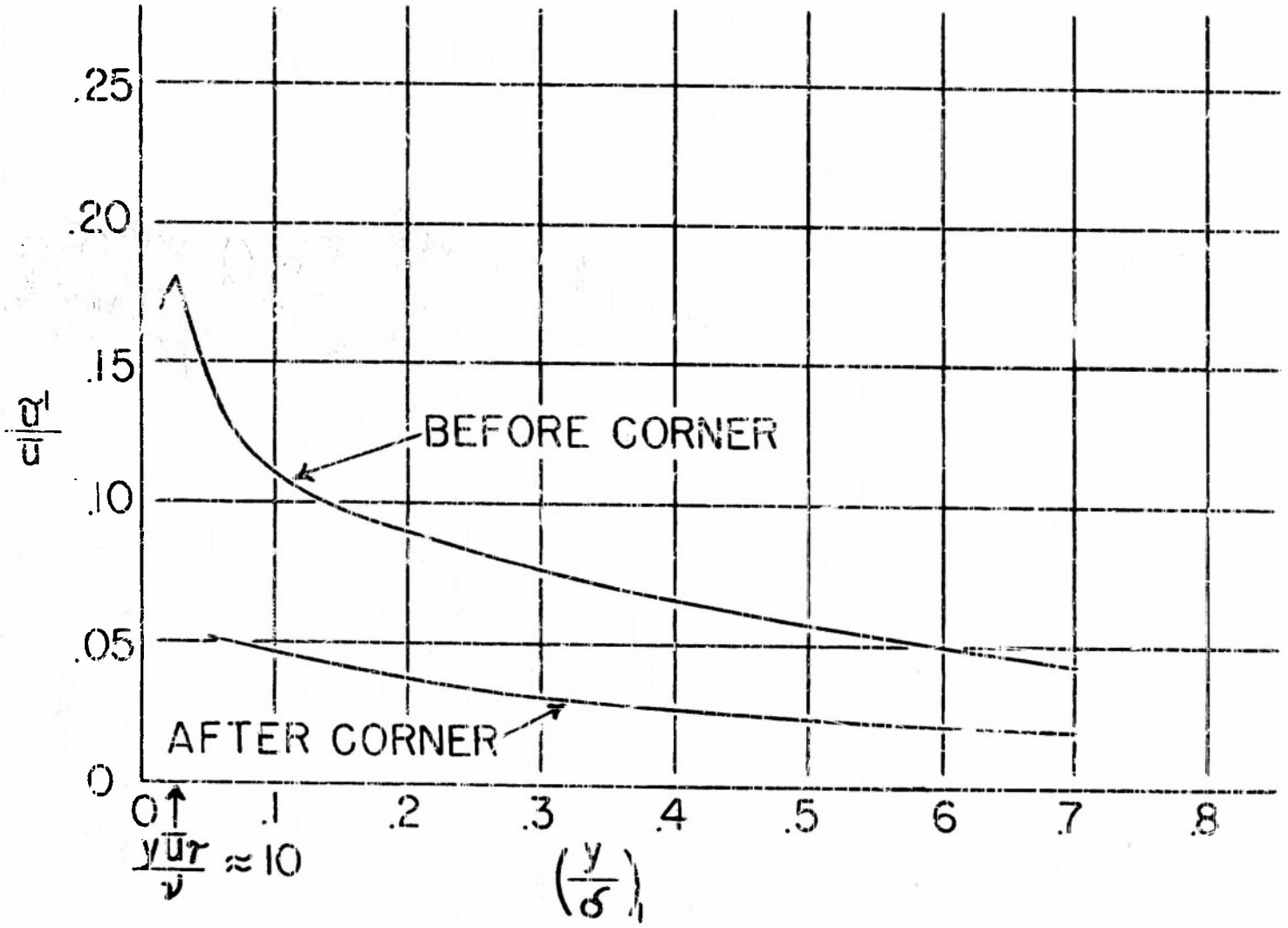

FIG. 29. Fluctuation Level Before and After Corner

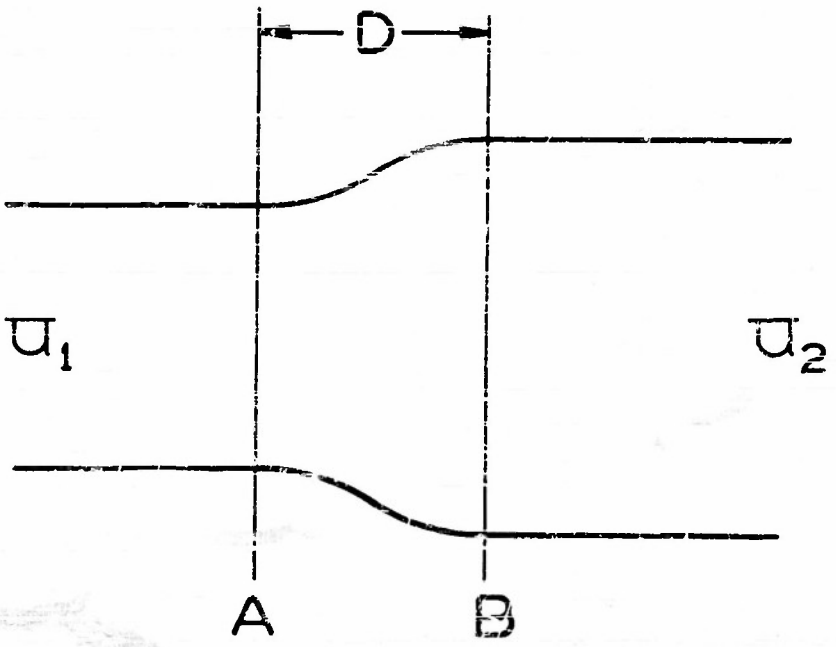

FIG. 30. Streamtube Contraction

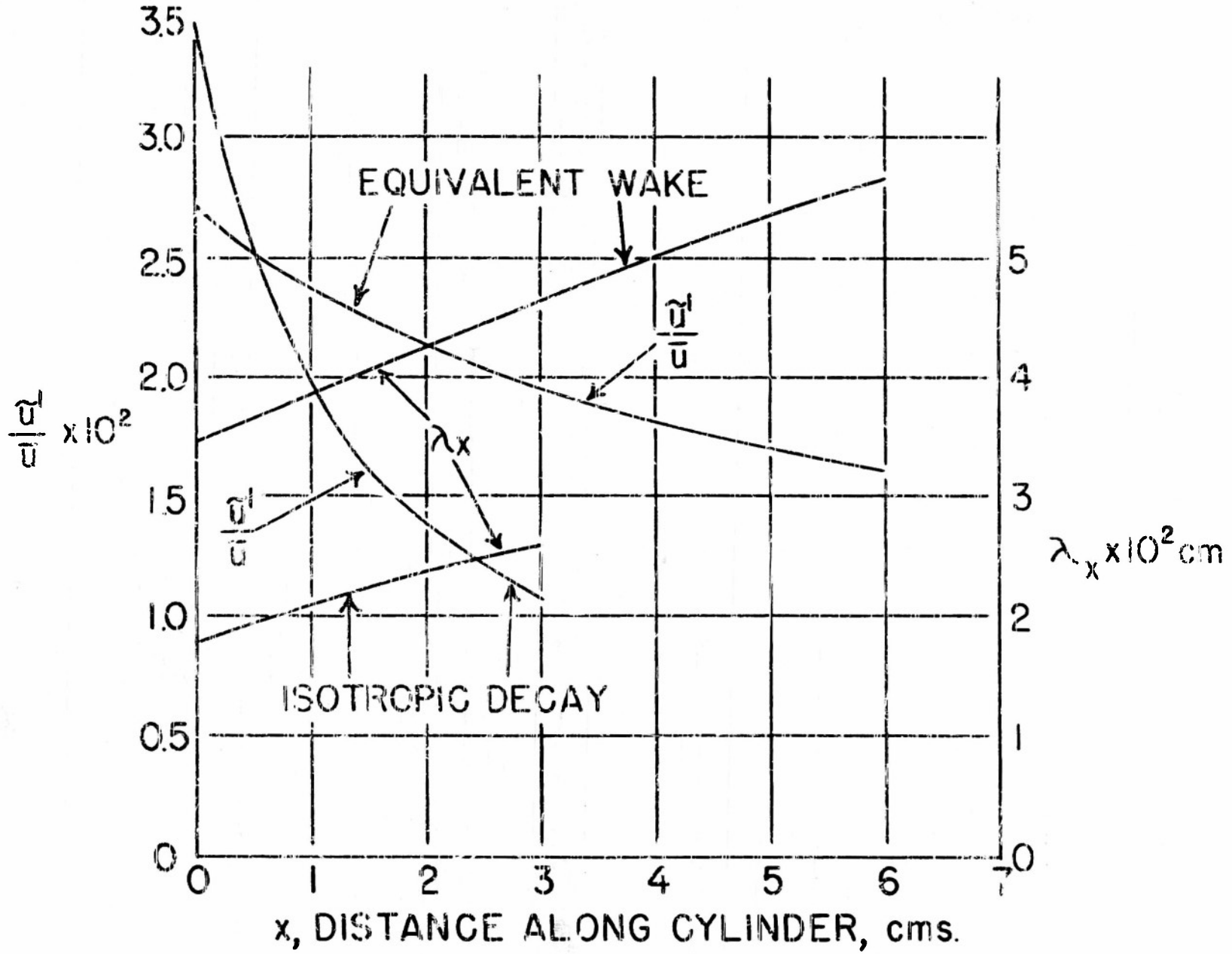

FIG. 31. Turbulence Levels and Microscales Along Cylinder

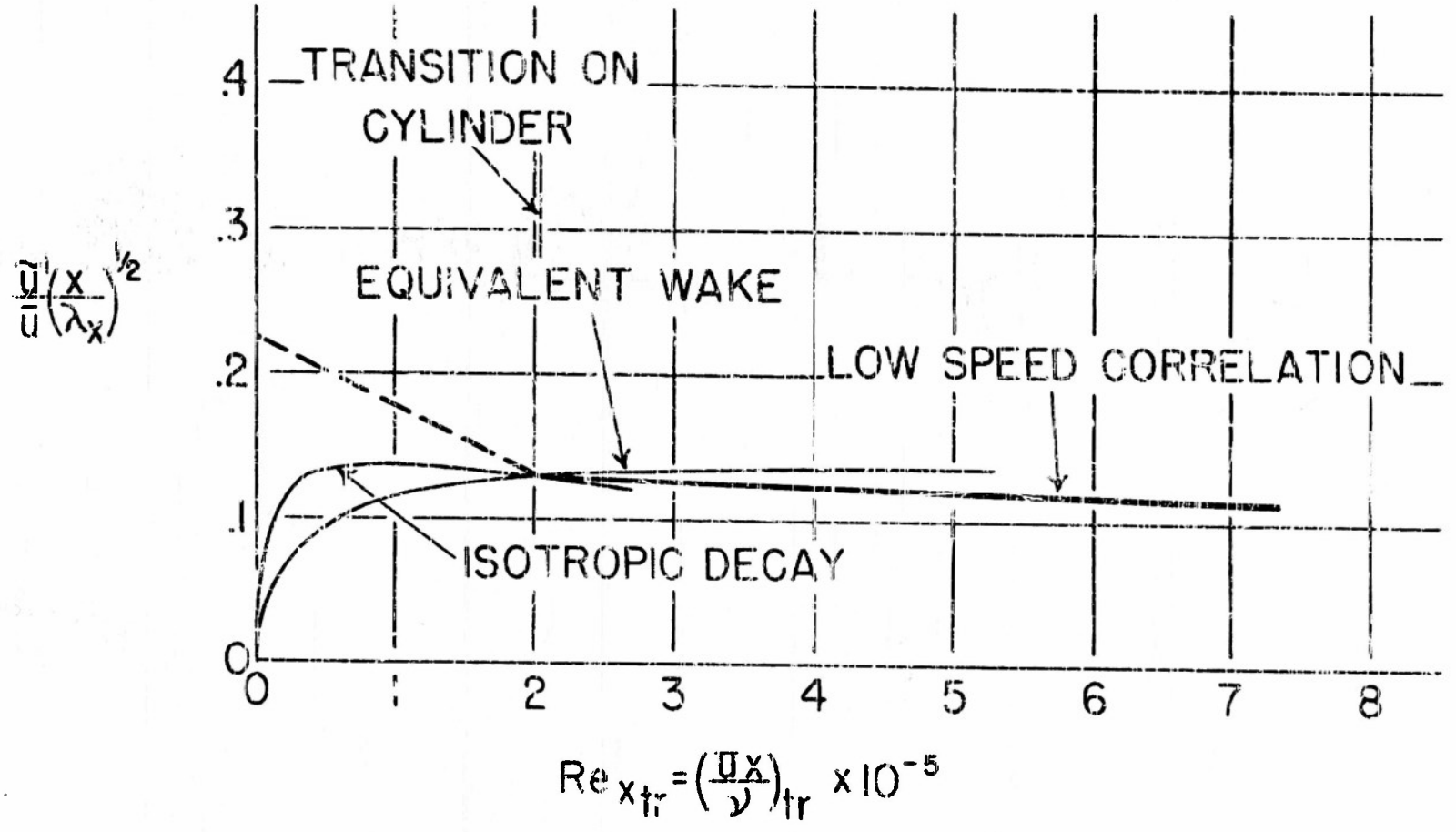

FIG. 32. Turbulence Parameters Along Cylinder

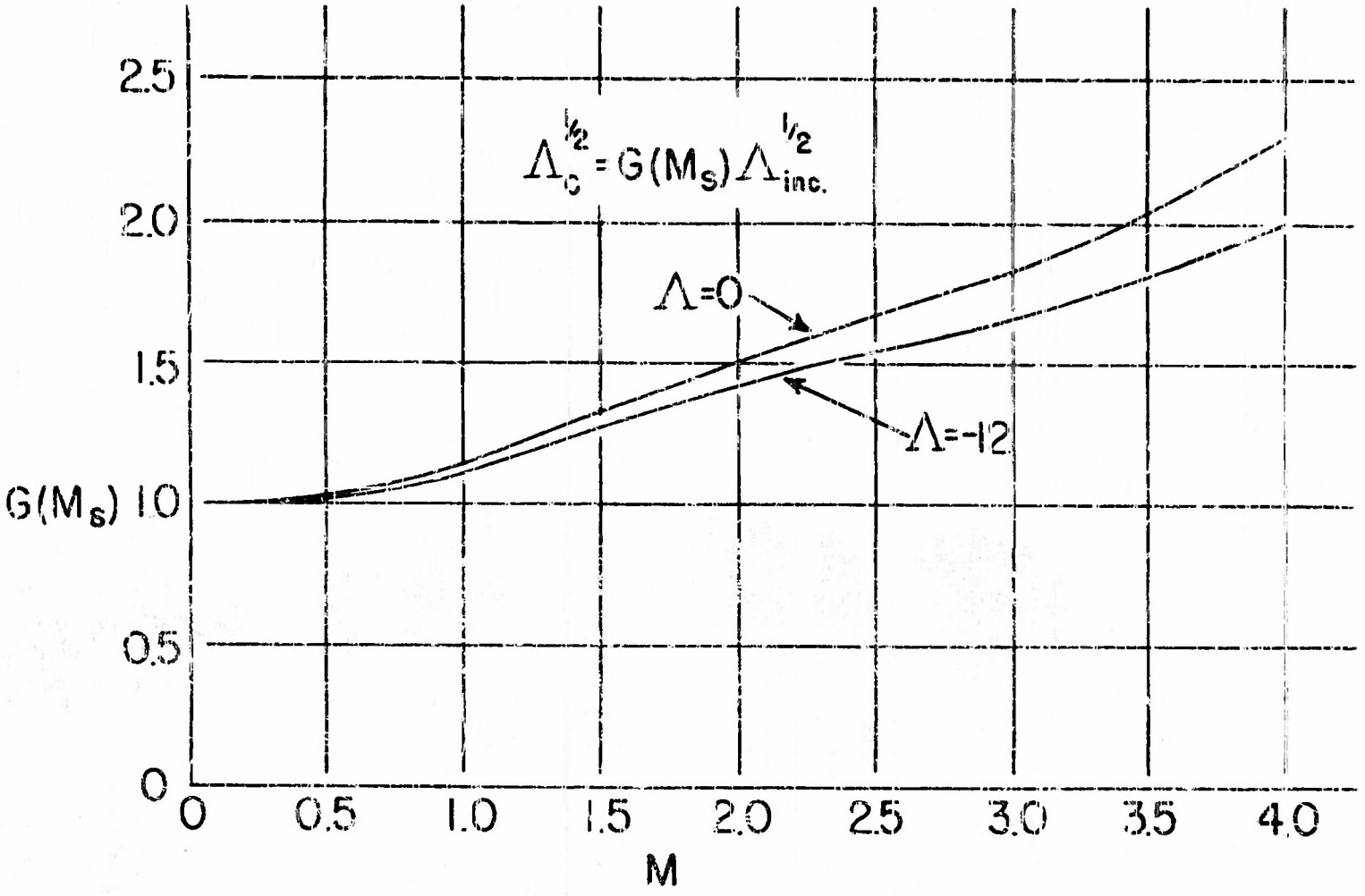

FIG. 33. Effect of Compressibility on Transition Turbulence Parameter

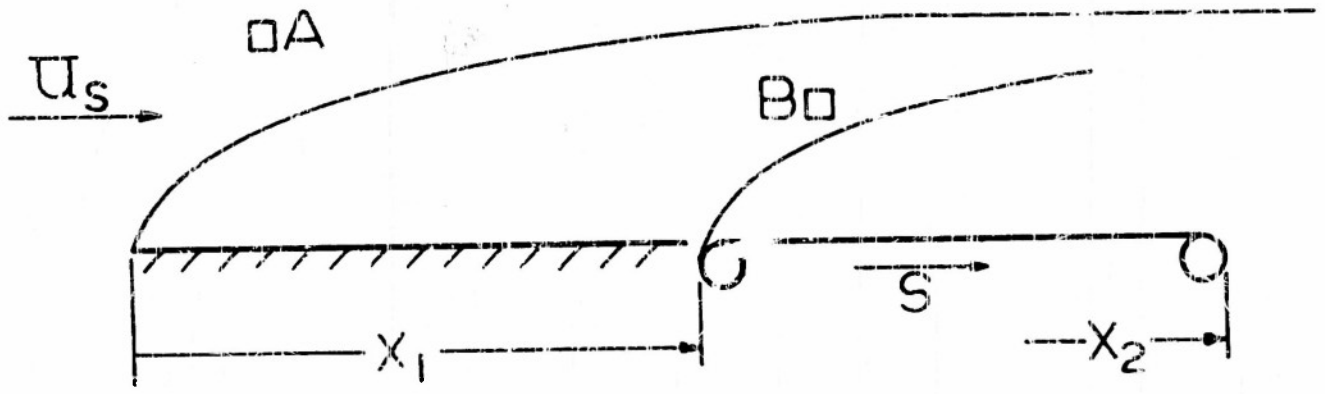

FIG. 34. Laminar Boundary Layer within Laminar Boundary Layer

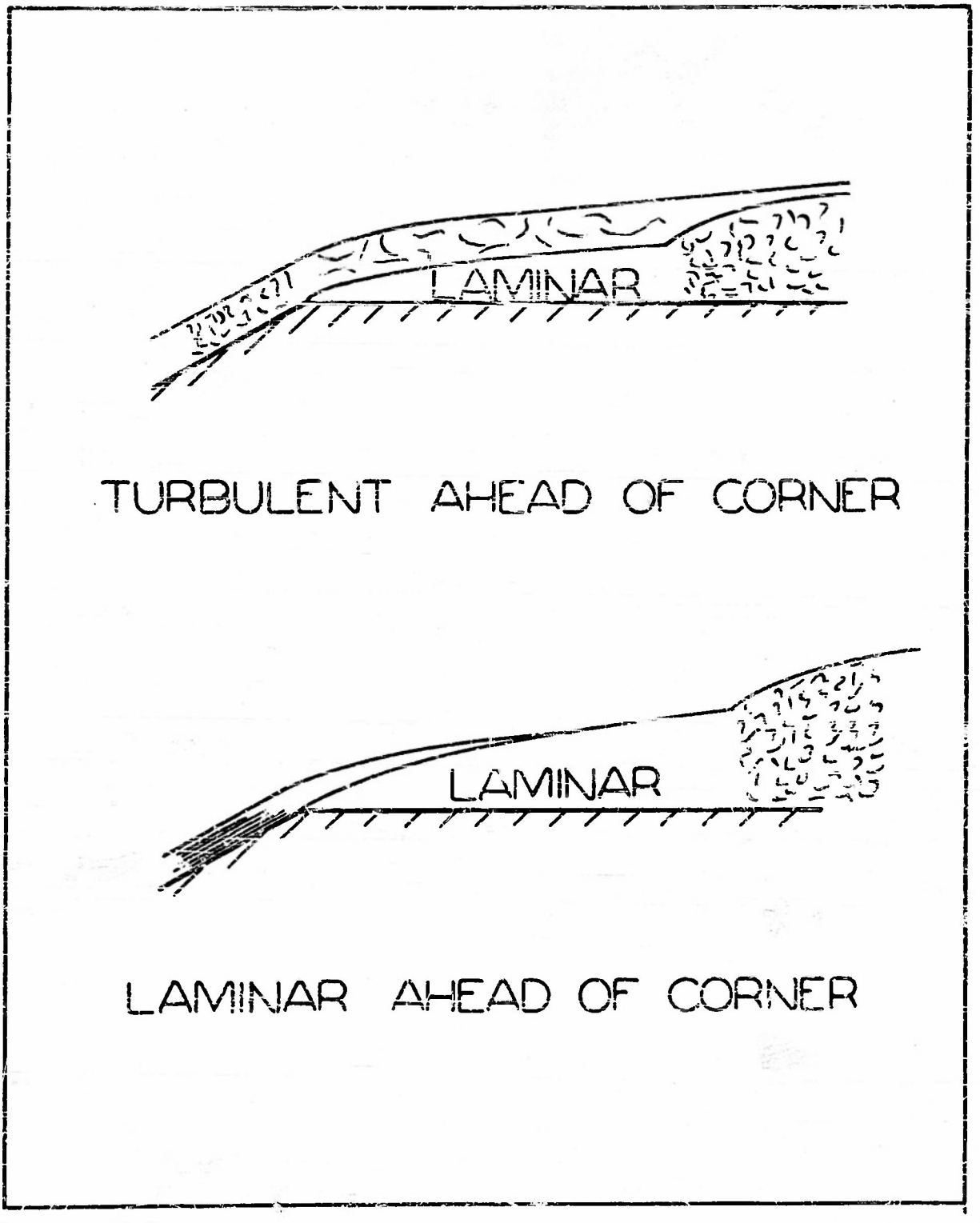

FIG. 35. Observed Boundary Layer Flows

REFERENCES

1. Clippinger, R. F., Cloos, J. H., Carter, W. C. - "Tables of Supersonic Flows about Cone Cylinders". Part I. Surface Data. Ballistic Research Laboratories Report 729.

2. Dryden, Hugh L. - "Review of Published Data on the Effect of Roughness on Transition from Laminar to Turbulent Flow." Presented at 21st Annual Meeting of the Institute of the Aeronautical Sciences - Preprint No. 390.

3. Kovasznay, Leslie S. G. - "Turbulence in Supersonic Flow". Journal of Aeronautical Sciences. October 1953.

4. Klebanoff, P. S., Diehl, Z. W. - "Some Features of Artificially Thickened Fully Developed Turbulent Boundary Layers with Zero Pressure Gradient". NACA TN 2475.

5. Townsend, A. A. - "The Structure of the Turbulent Boundary Layer". Proceedings of the Cambridge Philosophical Society. Vol. 47, Pt. 2.

6. Klebanoff, P. S. - "Characteristics of Turbulence in a Boundary Layer with Zero Pressure Gradient". NACA TN. 3178, 1954.

7. Goldstein, S. Modern Developments in Fluid Dynamics. Vol. I.

8. Townsend, A. A. "Measurements in the Turbulent Wake of a Cylinder". Proceedings of the Royal Society. Series A, Vol. 190. September 1947.

9. Van Dreist, E. R. - "Investigation of the Laminar Boundary Layer in Compressible Fluids Using the Crocco Method". North American Aviation Report AL-1183.

10. Taylor, G. I. - "Statistical Theory of Turbulence". Proceedings of the Royal Society of London. Series A, Vol. 156. 1936.

11. Fage, A. and Preston, J. H. - "On Transition from Laminar to Turbulent Flow in the Boundary Layer". Proceedings of Royal Society of London. Series A, Vol. 178.

12. Hall, A. A. and Hislop, G. S. - "Experiments on the Transition of the Laminar Boundary Layer on a Flat Plate". Reports and Memoranda, Aeronautical Research Council. No. 1847. August 1938.

13. Dryden, Hugh L. - "Air Flow in the Boundary Layer Near a Plate". NACA Report No. 562.

14. Laufer, J. - "The Structure of Turbulence in Fully Developed Pipe Flow". NACA TN 2954. June 1953.

15. Laufer, J. - "Investigation of Turbulent Flow in a Two-Dimensional Channel". NACA TN 2123.

16. Dryden, Hugh L. - "A Review of the Statistical Theory of Turbulence". Quarterly of Applied Mathematics. Volume 1, No. 1. 1943.

17. Prandtl, L. - "Attaining a Steady Air Stream in Wind Tunnels". NACA TN 726.

18. Taylor, G. I. - "Turbulence in a Contracting Stream". ZAMM. February 1935.

19. Ribner, H. S. and Tucker, M. - "Spectrum of Turbulence in a Contracting Stream". NACA TN 2606.

20. Tucker, Maurice. - "Combined Effect of Damping Screens and Stream Convergence on Turbulence". NACA TN 2896.

21. Lamb, Horace. Hydrodynamics.

22. MacPhail, D. C. - "Turbulence Changes in Contracting and Distorted Passages". British Ministry of Supply. Aeronautical Research Council. Reports and Memoranda 2437.

23. Corrsin, Stanley. - "Effect of Wind Tunnel Nozzle on Steady Flow Non-uniformities". Journal of Aeronautical Sciences. Readers-Forum. February 1952.

24. Dorodnitsyn, A. "Laminar Boundary Layer in Compressible Fluid". Comptes Rendus. Vol. XXXIV. 1942.

25. Stine, H. A., and Scherrer, R. "Experimental Investigation of the Turbulent-Boundary-Layer Temperature Recovery Factor on Bodies of Revolution at Mach Numbers from 2.0 to 3.8."

26. Des Clers, B., and Sternberg, J. "On Boundary Layer Temperature Recovery Factors." Readers Forum. J. Ae. Sciences. September 1952.

DISTRIBUTION LIST

No. of Copies	Organization
6	Chief of Ordnance Department of the Army Washington 25, D. C. Attn: ORDTB - Bal Sec
10	British - ORDTB for distribution
5	Canadian Joint Staff - ORDTB for distribution Of Interest to: Prof. G. N. Patterson University of Toronto Institute of Aerophysics Toronto, Canada
4	Chief, Bureau of Ordnance Department of the Navy Washington 25, D. C. Attn: Re3
4	ASTIA Reference Center Technical Information Div. Library of Congress Washington 25, D. C.
2	Commander Naval Proving Ground Dahlgren, Virginia
1	Chief of Naval Research Department of the Navy Washington 25, D. C. Attn: Code 463
1	Commanding Officer Naval Ordnance Laboratory Corona, California Attn: Documents Librarian
4	Chief, Bureau of Aeronautics Department of the Navy Washington 25, D. C. Attn: TD-4

No. of Copies	Organization
3	Commander Naval Ordnance Laboratory White Oak Silver Spring, Maryland Attn: Library, Room 1-333 Of Interest to: Dr. R. E. Wilson Dr. H. Kurzweg
2	Commanding Officer and Director Naval Research Laboratory Washington 25, D. C. Attn: Code 2021
2	Commander Naval Ordnance Test Station Inyokern P. O. China Lake, California Attn: Technical Library
1	Superintendent U. S. Naval Postgraduate School Monterey, California
1	Commanding Officer and Director David W. Taylor Model Basin Washington 7, D. C. Attn: Mrs. Betty C. Craven, Aerodynamics Laboratory
1	Chief of Staff United States Air Force Washington 25, D. C. Attn: DCS/D, AFDRD-AC-33
1	Commander Arnold Engineering Development Center Tullahoma, Tennessee Attn: Deputy Chief of Staff, Operations

DISTRIBUTION LIST

No. of Copies	Organization
15	Commander Wright Air Development Center Wright-Patterson Air Force Base Ohio Attn: WCACD
1	Commander Air Research and Development Command P. O. Box 1[illegible]5 Baltimore 3, Maryland Attn: Major Zubon
2	Director, Project RAND Department of the Air Force 1700 Main Street Santa Monica, California Of Interest to: Dr. Carl Gazley Missiles Division
5	Director Armed Services Technical Information Agency Document Service Center Knott Building Dayton 2, Ohio Attn: DSC - SA
2	Central Intelligence Agency 2430 E Street, N. W. Washington 25, D. C. Attn: Liaison Division, OCD
3	Director National Advisory Committee for Aeronautics 1724 F Street, N. W. Washington 25, D. C. Attn: Division Research Information
1	Director National Bureau of Standards Washington 25, D. C. Attn: Dr. G. B. Schubauer, Chief, Aerodynamics Section
1	National Advisory Committee for Aeronautics Langley Aeronautical Laboratory Langley Field, Virginia Attn: Mr. John Stack
1	National Advisory Committee for Aeronautics Lewis Flight Propulsion Laboratory 21000 Brookpark Road Cleveland 11, Ohio Attn: Dr. John C. Evvard
1	National Advisory Committee for Aeronautics Ames Aeronautical Laboratory Moffett Field, California Attn: Mr. H. Julian Allen, High Speed Research Div.
1	Commanding Officer Frankford Arsenal Philadelphia 37, Pennsylvania
3	Commanding Officer Picatinny Arsenal Dover, New Jersey Attn: Technical Division
3	Commanding General Redstone Arsenal Huntsville, Alabama Attn: Technical Library

DISTRIBUTION LIST

No. of Copies	Organization
1	Director, JPL Ordnance Corps Installation Department of the Army 4800 Oak Grove Drive Pasadena 2, California Attn: Mr. Frank Goddard, Wind Tunnel Division
1	Aerophysics Development Corp. P. O. Box 657 Pacific Palisades, California Attn: Dr. William Bollay
2	Applied Physics Laboratory Johns Hopkins University Silver Spring, Maryland Attn: Mr. George L. Seielstad
1	Aerojet-General Corp. Azusa, California Attn: Mr. M. T. Grenier Librarian
1	Aro, Incorporated Tullahoma, Tennessee Attn: Mr. Ronald Smelt, Gas Dynamics Facility
1	Bell Aircraft Corporation P. O. Box 1 Buffalo 5, New York Attn: Miss Dorothy F. Zeman Chief Librarian
1	Bell Telephone Laboratories, Inc. Whippany, New Jersey Attn: W. H. C. Higgins
1	Bendix Aviation Corp. Research Laboratory 4855 Fourth Avenue Detroit 1, Michigan Attn: Dr. Harmer Selvidge
1	Boeing Airplane Company Seattle 14, Washington Attn: Mr. R. H. Nelson
1	Bendix Products Division Bendix Aviation Corporation 400 S. Beiger Street Mishawaka, Indiana Attn: Mr. W. C. Shuttle
1	Consolidated Vultee Aircraft Corp. Pomona Division Pomona, California Attn: Lilly O'Dessa Haugh Engineering Librarian
1	Consolidated Vultee Aircraft Corp. San Diego 12, California Attn: Mrs. Dora B. Burke
1	Cornell Aeronautical Lab. Inc. Buffalo, New York Attn: Miss Elma T. Evans Librarian
1	Chrysler Corporation Engineering Division Missile Branch P. O. Box 2628 Detroit 31, Michigan Attn: Mr. J. E. Charipar Supervisor Dept. of Tech. Information
1	Consolidated Vultee Aircraft Corp. Fort Worth Division Fort Worth, Texas Attn: Mr. K. G. Brown Engineering Librarian

DISTRIBUTION LIST

No. of Copies	Organization
1	Chance Vought Aircraft, Inc. P. O. Box 5907 Dallas, Texas Attn: Mr. P. C. Moran
1	Consolidated Vultee Aircraft Corp. Ordnance Aerophysics Laboratory Daingerfield, Texas Attn: Mr. J. E. Arnold
1	Capehart-Farnsworth Corp. Fort Wayne, Indiana Attn: Mrs. Margaret D. Moyer
1	California Institute of Technology Guggenheim Aeronautical Laboratory Pasadena 4, California Attn: Dr. Hans W. Liepmann
1	Douglas Aircraft Co. 3000 Ocean Park Boulevard Santa Monica, California Attn: Mrs. E. F. Burton
1	Eastman Kodak Co. Navy Ordnance Division Rochester 4, New York Attn: Dr. Robert Trotter
1	Fairchild Engine and Airplane Corp. Guided Missiles Division Wyandanch, L. I., New York Attn: Mr. R. E. Jacobs
1	General Electric Company Project HERMES Schenectady, New York Attn: Mr. J. C. Hoffman
1	Glenn L. Martin Company Baltimore 3, Maryland Attn: Mrs. Mary Ezzo
1	Goodyear Aircraft Corporation Akron 15, Ohio Attn: Dr. Karl Arnstein
1	Hughes Aircraft Company Florence Avenue at Teal Street Culver City, California Attn: Miss Mary Jo Case
1	Johns Hopkins University Institute for Coop. Research 4810 Roland Avenue Baltimore, Maryland Attn: Dr. E. R. C. Miles Project THOR
1	M. W. Kellogg Company Foot of Danforth Ave. Jersey City 3, New Jersey Attn: Miss E. M. Hedley
1	Lockheed Aircraft Corporation Missile Systems Division Plant B-1 Burbank, California Attn: Mr. J. H. Culver
1	Massachusetts Institute of Technology Department of Mechanical Engineering Cambridge, Massachusetts Attn: Professor Joseph Kaye
1	McDonnell Aircraft Corporation P. O. Box 516 St. Louis 3, Missouri Attn: Dr. B. G. Brombarg

DISTRIBUTION LIST

No. of Copies	Organization
1	Marquardt Aircraft Company 7801 Hayvenhurst Avenue Van Nuys, California Attn: Mr. R. E. Marquardt
1	Northrop Aircraft, Inc. Hawthorne, California Attn: Mrs. E. S. Francis Librarian
2	North American Aviation, Inc. 12214 Lakewood Boulevard Downey, California Attn: Aerophysics Library
1	Purdue University Lafayette, Indiana Attn: Dr. M. J. Zucrow
1	Princeton University Forrestal Research Center Library Project SQUID Princeton, New Jersey Attn: Mr. M. H. Smith
1	Princeton University Department of Aeronautics Princeton, New Jersey Attn: Professor Seymour Bogdonoff
1	Polytechnic Institute of Brooklyn 99 Livingston Street Brooklyn 2, New York Attn: Dr. Antonio Ferri
1	Reeves Instrument Corporation 215 E. 91st Street New York 28, New York Attn: Dr. L. Bauer
1	Raytheon Manufacturing Co. Missile and Radar Division P. O. Box 398 Bedford, Massachusetts Attn: Mr. R. G. Ling
1	Radioplane Corporation Metropolitan Airport Van Nuys, California Attn: Mr. Ferris M. Smith
1	Ryan Aeronautical Co. Lindbergh Field San Diego 12, California Attn: Mr. W. T. Immenschuh
1	Republic Aviation Corp. Military Contract Department Farmingdale, L. I., New York Attn: Dr. William O'Donnell
1	Sylvania Electric Products, Inc. 208-20 Willets Point Blvd. Bayside, L. I., New York Attn: Mrs. Rose L. Cassidy Document Custodian
1	Sandia Corporation Sandia Base P. O. Box 5800 Albuquerque, New Mexico Attn: Mrs. Wynne K. Cox
1	Sperry Gyroscope Company Division of the Sperry Corp. Great Neck, L. I., New York Attn: Mrs. Florence W. Turnbull Librarian
1	Sanders Associates, Inc. 137 Canal Street Nashua, New Hampshire Attn: Mr. R. C. Sanders

DISTRIBUTION LIST

No. of Copies	Organization
1	Vitro Corp. of America Silver Spring Laboratory 962 Wayne Avenue Silver Spring, Maryland Attn: Miss C. Marion Jaques Librarian
1	Wright Aeronautical Division Curtiss-Wright Corp. Wood-Ridge, New Jersey Attn: Sales Dept. (Govt.)
1	University of Maryland Institute for Fluid Dynamics and Applied Mathematics College Park, Maryland Attn: Dr. C. C. Chang
1	University of Michigan Department of Aeronautics Ann Arbor, Michigan Attn: Dr. Mahinder Uberoi
1	University of Virginia Physics Department Charlottesville, Virginia Attn: Mr. J. W. Beams
1	University of Southern California Engineering Center Los Angeles 7, California Attn: Mr. H. R. Saffell Director
1	University of Texas Defense Research Laboratory P. O. Box 8029, Univ. State Austin, Texas Attn: Dr. C. P. Boner

No. of Copies	Organization
1	University of Mic[illegible] Willow Run Resear[illegible] Willow Run Airpor[illegible] Ypsilanti, Michiga[illegible] Attn: Mr. J. E. Cr[illegible]
1	Dr. H. L. Dryden Director of Aeronau[illegible] Research National Advisory Co[illegible] for Aeronautics 1724 F. Street, N[illegible] Washington 25, D. C.
1	Professor Howard W[illegible] Engineering and Appli[illegible] Science Department Harvard University Cambridge 38, Massachu[illegible]
1	Professor Clark B. Mi[illegible] Director, Guggenheim Aeronautical Laborat[illegible] 1500 Normandy Drive California Institute o[illegible] Technology Pasadena 4, Californi[illegible]
1	Dr. Francis H. Clau[illegible] Department of Aeronau[illegible] Johns Hopkins Univers[illegible] Baltimore 18, Maryla[illegible]

UNCLASSIFIED